

FORSCHUNGSZENTRUM ROSSENDORF



WISSENSCHAFTLICH-TECHNISCHE BERICHTE

**FZR-343**

Mai 2002

**Annual Report 2001**  
**Institute of Radiochemistry**

**Editor:** Prof. Dr. Th. Fanghänel

**Editorial staff:** Prof. Dr. G. Bernhard  
Dr. H.-J. Engelmann

# Preface

The Institute of Radiochemistry (IRC), one of the five institutes of the Forschungszentrum Rossendorf (FZR) performs basic and applied research in the fields of radiochemistry and radioecology. Main goal is the quantification of the interaction and mobility of radionuclides in the geo- and biosphere. Because of their high radiotoxicity and long half-life the actinides are of special interest. Among the actinides uranium and its manifold interactions plays a major role in the institute's research activities. In addition the interactions of some important long-lived fission and decay products are studied.

More than 60 scientists, technicians and PhD students are employed in the Institute of Radiochemistry. The research is focused on understanding the fundamental processes relevant for the behavior of radionuclides in the environment. Main topics are:

- Aquatic chemistry
- Radionuclide interaction with mineral surfaces
- Radionuclide interaction with biological materials (bacteria and plants)
- Modeling the radionuclide transport
- Development of spectroscopic speciation methods

We accomplished many new scientific results in the past year, which are presented in this Annual Report. Among them only a very few can be highlighted in this preface.

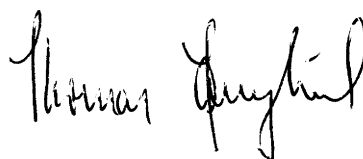
Further progress was achieved in understanding the interaction mechanism of actinides with mineral surfaces. The sorption of Cm(III) in trace concentration on calcite as well as its incorporation into the calcite bulk structure has been studied by Time-Resolved Laser Fluorescence Spectroscopy (TRLFS). The results clearly demonstrate the formation of two different Cm(III) species with different coordination environment.

The further development of our mineral-specific database RES<sup>3</sup>T for surface complexation has achieved considerable progress. It is now accessible for a broad user community. Many new features have been implemented and the number of evaluated data sets has been increased considerably.

Numerous measurements on actinide samples performed at our beam-line ROBL at the ESRF in Grenoble have provided us with a much better understanding of the structure and bonding of actinides in aqueous solution, sorbed on mineral surfaces and colloids or bonded to organic matter like humic or fulvic acids. Only a few examples can be highlighted here. The structure and bond distances of aqueous Am(III) and Cm(III) have been determined by EXAFS spectroscopy. It was shown by EXAFS that U(VI) is sorbed as a bi-dentate complex via aluminol groups on montmorillonite. For the first time the structure of Pu(III) humate complexes have been studied by EXAFS and XANES spectroscopy.

The institute organized together with Forschungszentrum Karlsruhe, Institut für Nukleare Entsorgung (INE), and Paul Scherrer Institut (PSI) the 8<sup>th</sup> International Conference on Chemistry and Migration Behaviour of Actinides and Fission Products in the Geosphere MIGRATION-01 in Bregenz, Austria with about 270 participants from 24 nations.

I would like to express many thanks to our numerous national and international research partners, visitors and collaborators. Special thanks are due to the Executive Board of the Forschungszentrum Rossendorf, the Ministry of Science and Arts of the State of Saxony, the Federal Ministry of Education and Research of Germany, the Federal Ministry of Economics and Technology of Germany, the Deutsche Forschungsgemeinschaft, the Bundesamt für Strahlenschutz, the European Commission and other organizations for their support of our research and last, but not least, to the staff and guests of the IRC for performing excellent research and administration.



Prof. Dr. Thomas Fanghänel

# CONTENTS

## I. SCIENTIFIC CONTRIBUTIONS

### 1. AQUATIC CHEMISTRY OF ACTINIDES/RADIONUCLIDES

Complex Formation in the System Uranium(VI) - Alpha-Substituted Carboxylic Acids Studied by TRLFS Part I: Glycolic and Alpha-Hydroxyisobutyric Acid at pH 2 H. Moll, G. Geipel, G. Bernhard, Th. Fanghänel, I. Grenthe	1
Complex Formation in the System Uranium(VI) - Alpha-Substituted Carboxylic Acids Studied by TRLFS Part II: Alpha-Aminoisobutyric Acid at pH 3 H. Moll, G. Geipel, G. Bernhard, Th. Fanghänel, I. Grenthe	2
Complex Formation in the System Uranium(VI) - Alpha-Substituted Carboxylic Acids Studied by TRLFS Part III: Alpha-Aminoisobutyric Acid at pH 4 H. Moll, G. Geipel, G. Bernhard, Th. Fanghänel, I. Grenthe	3
Uranium(VI) Complexation by Alpha-Substituted Carboxylic Acids Studied by EXAFS H. Moll, T. Reich, G. Geipel, C. Hennig, H. Funke, A. Roßberg, Th. Fanghänel, I. Grenthe	4
Complex Formation of Uranium(IV) with Arsenate G. Geipel, G. Bernhard	5
Formation Constants of Uranium(IV) Dihydrogen Arsenate Complexes - Extrapolation to Infinite Dilution G. Geipel, G. Bernhard	6
Complex Formation of Uranium(VI) with 2,3-Dihydroxybenzoic Acid Studied by Time-Resolved Laser-Induced Fluorescence Spectroscopy with Ultrashort Laserpulses (fs-TRLFS) G. Geipel, G. Bernhard	7
Complex Formation of Neptunium(V) with 2,3-Dihydroxybenzoic Acid Studied by Time-Resolved Laser-Induced Fluorescence Spectroscopy with Ultrashort Laserpulses (fs-TRLFS) G. Geipel, G. Bernhard	8
Complex Formation of Uranium(VI) with Organic Ligands Studied by fs-TRLFS Part I: Benzoic Acid D. Vulpius, G. Geipel, L. Baraniak, G. Bernhard, Th. Fanghänel	9
Complex Formation of Uranium(VI) with Organic Ligands Studied by fs-TRLFS Part II: Vanillic Acid D. Vulpius, G. Geipel, L. Baraniak, G. Bernhard, Th. Fanghänel	10
Complex Formation of Uranium(VI) with Glucose 1-Phosphate A. Koban, G. Geipel, G. Bernhard	11
Complex Formation of Uranium(VI) with Glutathione A. Günther, G. Geipel, G. Bernhard	12
Synthesis and Characterization of Humic Acids with Distinct Redox Capacities S. Sachs, K.H. Heise, G. Bernhard	13
NIR Spectroscopic Study of the Neptunium(V) Complexation by Humic Acids with Different Functionalities S. Sachs, K.H. Heise, G. Bernhard	14
Plutonium(III) Humate Complexation Studied by XAFS Spectroscopy K. Schmeide, S. Sachs, T. Reich, C. Hennig, H. Funke, A. Roßberg, G. Geipel, K.H. Heise, G. Bernhard	15
Complex Formation of Uranium(VI) with Lignin Degradation Products D. Vulpius, L. Baraniak, G. Bernhard, Th. Fanghänel	16

Redox Reactions in Flooded Uranium Mines Caused by Natural Wood Degradation A. Abraham, L. Baraniak, G. Bernhard	17
Complexation of Curium(III) by Glycolic Acid: TRLFS Studies Th. Stumpf, Th. Fanghänel, I. Farkas, I. Grenthe	18
Thermochromatographic Volatility Studies of Plutonium Oxides S. Hübener, S. Taut, A. Vahle, Th. Fanghänel	19
Chemical Investigation of Hassium (Hs, Z = 108) A. Vahle	20
<b>2. INTERACTION OF ACTINIDES/RADIONUCLIDES WITH SURFACES OF ROCKS, MINERALS AND COLLOIDS</b>	
Sorption of U(VI) on Granite: Comparison of Experimental and Predicted U(VI) Sorption Data T. Arnold, E. Krawczyk-Bärsch, G. Bernhard	21
Neptunium(V) Sorption onto Granite and its Mineral Constituents in the Absence and Presence of Humic Acid K. Schmeide, K.H. Heise, G. Bernhard	22
Ferrihydrite Formation During the Dissolution of Chlorite and its Effect on the Sorption Behavior of U(VI) E. Krawczyk-Bärsch, T. Arnold, F. Brandt, D. Bosbach, G. Bernhard	23
Sorption of Uranium(VI) onto Schwertmannite - EXAFS Investigations M. Walter, T. Arnold, H. Funke, T. Reich, G. Bernhard	24
Using Spectroscopic Evidence by EXAFS to Model the Sorption of Uranyl(VI) on Schwertmannite T. Arnold, M. Walter, G. Bernhard	25
EXAFS Investigation on Uranyl Sorbed onto Montmorillonite C. Hennig, T. Reich, H. Funke, A. Roßberg, R. Dähn, A. Scheidegger	26
Time-Resolved Laser Fluorescence Spectroscopy (TRLFS): Investigations of the Interaction of Cm(III) with Ferrihydrite S. Stumpf, Th. Stumpf, Th. Fanghänel, J.I. Kim	27
Time-Resolved Laser Fluorescence Spectroscopy (TRLFS) Study of the Interaction of Trivalent Actinides (Curium(III)) with Calcite Th. Stumpf, Th. Fanghänel	28
Inner-Sphere, Outer-Sphere and Ternary Surface Complexes: A TRLFS Study of the Sorption Process of Europium(III) onto Smectite Th. Stumpf, Th. Fanghänel, A. Bauer, F. Coppin, J.I. Kim	29
The Impact of Water Chemistry on U(VI) Scavenging by Flooding Water Colloids (Königstein Uranium Mine) H. Zänker, W. Richter	30
Colloid Investigations of Acid Rock Drainage Solution From an Abandoned Zn-Pb-Ag Mine by Ultrafiltration and PCS Measurements W. Richter, H. Zänker	31
Correction of Sorption Data of <sup>234</sup> U Contaminated with <sup>232</sup> U C. Nebelung	32
Separation of Uranium(VI) from Aqueous Solution by Textile Bound Calix[6]arenes K. Schmeide, K. Jansen, D. Keil, K.H. Heise, G. Bernhard	33
<b>3. INTERACTION OF ACTINIDES/RADIONUCLIDES WITH BIOLOGICAL SYSTEMS</b>	
Comparative Analysis of Bacteria in Uranium Mining Wastes T. Tzvetkova, K. Flemming, S. Selenska-Pobell	35

Partial Analysis of the Central Domain of the <i>Bacillus sphaericus</i> JG-A12 S-Layer Protein M. Schnorpfel, J. Raff, K. Flemming, S. Selenska-Pobell	36
Biosorption of Uranium and Copper by <i>Bacillus sphaericus</i> JG-A12 Cells, Spores and S-Layer Proteins Embedded in Sol-Gel Ceramics J. Raff, U. Soltmann, S. Matys, H. Boettcher, W. Pompe, S. Selenska-Pobell	37
Characterization of the Uranium(VI) Complexes Formed by the Cells of Three <i>A. ferrooxidans</i> Eco- Types Using Time-Resolved Laser-Induced Fluorescence Spectroscopy (TRLFS) M. Merroun, G. Geipel, S. Selenska-Pobell	38
Cellular Localization of Uranium Accumulated by <i>A. ferrooxidans</i> Cells Using Transmission Electron Microscopy and Energy-Dispersive X-Ray Analysis M. Merroun, S. Selenska-Pobell	39
FT-IR Studies of the Photoreactions of Phytochrome Assembled with Isotopic Labeled Chromophores H. Foerstendorf, W. Gärtner, F. Siebert	40
<b>4. MODELING OF RADIONUCLIDE TRANSPORT</b>	
Integration of the Metal Ion Charge Neutralization Model for Humic Acid Complexation into the Geochemical Speciation Code EQ3/6 V. Brendler	41
Further Developments of the RES <sup>3</sup> T Sorption Database V. Brendler	42
Modeling Gypsum Dissolution in a Column Experiment: Comparison of Two Reactive Transport Codes J. Mibus, R. Kuchler	43
<b>5. DEVELOPMENT OF NANOSCOPIC METHODS</b>	
Wavelet Analysis of EXAFS Data – First Studies H. Funke, M. Chukalina	45
Progress Report on the Regularisation Method for EXAFS Data Analysis M. Kunicke, H. Funke, T. Reich, Yu.A. Babanov	46
EXAFS Analysis of Uranium Speciation in Plants Using the Difference Technique A. Roßberg, T. Reich, A. Günther, G. Bernhard	47
Radium Determination after Chemical Separation and by Analysing Liquid Scintillation Spectra - A Comparison L. Baraniak, C. Nebelung, M. Thieme	48
Establishment of a Laboratory for Spectroscopic Investigation of Radioactive Samples at the ELBE - FEL Facility. Intentions and Perspectives H. Foerstendorf, H. Friedrich, K.H. Heise	49
The Use of Thermal Optical Detection by FEL-IR Measurement of Solutions K.H. Heise, R. Nicolai, W. Seidel, A. Schamlott, J.-M. Ortega, F. Glotin, R. Prazeres	50
An X-Ray Absorption Spectroelectrochemical Cell for Radioactive Solutions D. Rettig, S. Herrmann, F. Mitschke, V. Brendler, G. Geipel, T. Reich, W. Vonau, G. Bernhard	51
<b>II. PUBLICATIONS, PATENTS, LECTURES AND POSTERS</b>	53
<b>III. SEMINARS, CONFERENCES AND WORKSHOPS</b>	65
<b>IV. PERSONNEL</b>	69
<b>V. ACKNOWLEDGMENTS</b>	71

# **I. SCIENTIFIC CONTRIBUTIONS**

## **Aquatic Chemistry of Actinides/Radionuclides**

# COMPLEX FORMATION IN THE SYSTEM URANIUM(VI) – ALPHA-SUBSTITUTED CARBOXYLIC ACIDS STUDIED BY TRLFS; PART I: GLYCOLIC AND ALPHA-HYDROXYISOBUTYRIC ACID AT pH 2

H. Moll, G. Geipel, G. Bernhard, Th. Fanghänel, I. Grenthe<sup>1</sup>

<sup>1</sup> Department of Chemistry, Inorganic Chemistry, The Royal Institute of Technology, Stockholm, Sweden

We observed a very strong quenching of the U(VI) fluorescence in these systems that can be quantitatively described by the Stern-Volmer equation. The following stability constants were determined: a) for the glycolate system  $\log \beta_{1:1} = 2.52 \pm 0.20$ , b) for the  $\alpha$ -hydroxyisobutyrate system  $\log \beta_{1:1} = 3.40 \pm 0.21$ .

The goal of this study is to explore the fluorescence properties of U(VI) complexes with glycolate and  $\alpha$ -hydroxyisobutyrate in aqueous solution. In particular, we wanted to test whether the slow ligand exchange between complex and free ligand observed by Szabó and Grenthe [1] affects the fluorescence lifetime and fluorescence intensity or not.

The TRLFS spectra were recorded at  $22 \pm 1^\circ\text{C}$  using a pulsed Nd:YAG laser system (Spectron Laser Systems, SL 400 Series, Rugby, UK). The excitation wavelength of the uranyl fluorescence was 266 nm using a laser energy of 150 – 250  $\mu\text{J}$ . The fluorescence signal was measured in time-resolved mode with discrimination of the signal against the laser pulse. The spectral intensity from 450 to 580 nm was obtained by integration using the codes Origin 5.0 and PeakFit 5.0 (Microcal Software Inc., USA). The data were processed as a function of the ligand concentration at a total concentration of U(VI) equal to  $7 \times 10^{-5}$  M in test solutions at pH=2.

Fig. 1 depicts the TRLFS spectra of uranium(VI) as a function of the total  $\alpha$ -hydroxyisobutyric acid concentration.

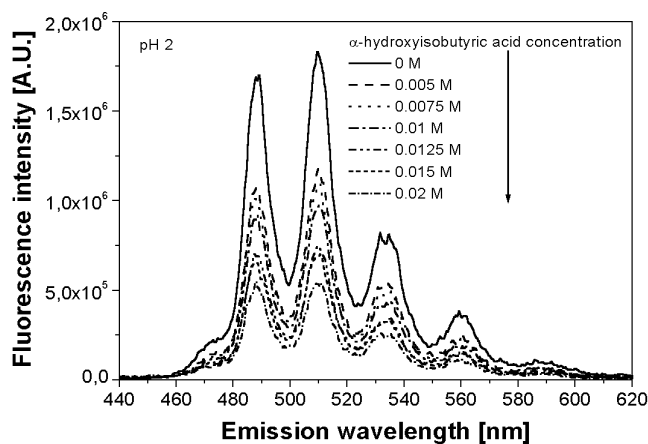


Fig. 1: TRLFS spectra of uranium(VI) as a function of the  $\alpha$ -hydroxyisobutyric acid concentration at pH=2.

The experiments with glycolic acid (not shown here) yielded similar results. In the spectra of both systems, we noticed a decrease in the fluorescence intensity with increasing ligand concentration. At the same time there was no detectable emission from the complexes present. The fluorescence decay was mono-exponential in all samples, with decreasing lifetime at increasing ligand concentration (Fig. 2). This behavior is typical for dynamic and static fluorescence quenching due to the complex formation and can be described quantitatively using a Stern-Volmer plot.

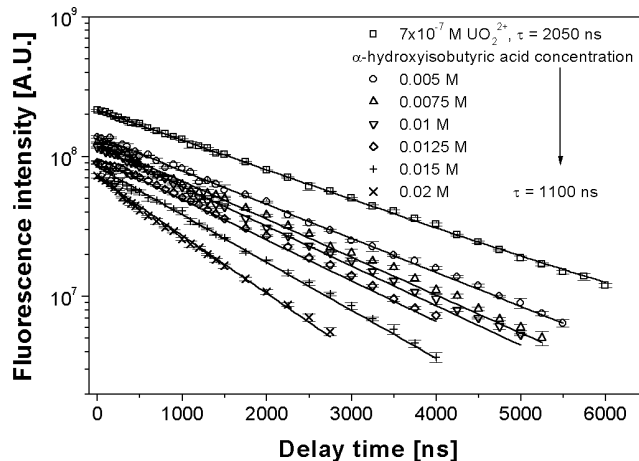


Fig. 2: Mono-exponential fluorescence decay (integrated signal from 450 to 580 nm) measured in the  $\alpha$ -hydroxyisobutyrate system at pH=2.

The quenching constant for the glycolate and  $\alpha$ -hydroxyisobutyrate systems at pH 2 was determined to be 26 and  $41 \text{ M}^{-1}$ , respectively. By using the data from the quenching experiments, it was possible to calculate the fluorescence intensity of  $\text{UO}_2^{2+}(\text{aq})$  if no dynamic quenching due to the quencher takes place. These fluorescence intensities were used to determine the concentration of  $\text{UO}_2^{2+}(\text{aq})$  in the test solutions. Finally we could calculate the equilibrium constants for reaction (1) with glycolate and  $\alpha$ -hydroxyisobutyrate [2].



The stability constants: a) for the glycolate system  $\log \beta_{1:1} = 2.52 \pm 0.20$  and b) for the  $\alpha$ -hydroxyisobutyrate system  $\log \beta_{1:1} = 3.40 \pm 0.21$  are in fair agreement with the UV-vis findings and the literature [1-4]. As fluorescence emission spectra of the individual species are not detectable, it was not possible to test whether the slow ligand exchange between complex and free ligand results in a longer fluorescence lifetime and higher fluorescence intensity, or not.

## Acknowledgements

The studies were funded by the European Union (EU) under contract number HPMF-CT-1999-00342.

## References

- /1/ Szabó, Z. et al., Inorg. Chem. **39**, 5036 (2000)
- /2/ Moll, H. et al., Radiochim. Acta, submitted (2002)
- /3/ Magnon, L. et al., Gazz. Chim. Ital. **104**, 967 (1974)
- /4/ Moll, H. et al., Report FZR-318 (2001) p. 2, 3

# COMPLEX FORMATION IN THE SYSTEM URANIUM(VI) – ALPHA-SUBSTITUTED CARBOXYLIC ACIDS STUDIED BY TRLFS; PART II: ALPHA-AMINOISOBUTYRIC ACID AT pH 3

H. Moll, G. Geipel, G. Bernhard, Th. Fanghänel, I. Grenthe<sup>1</sup>

<sup>1</sup> Department of Chemistry, Inorganic Chemistry, The Royal Institute of Technology, Stockholm, Sweden

An increase of the fluorescence intensity connected with a red shift of the fluorescence emission spectra was observed. Fluorescence lifetimes and spectra were obtained for  $\text{UO}_2^{2+}$  and  $\text{UO}_2[\text{NH}_3\text{C}(\text{CH}_3)_2\text{COO}]^{2+}$ . The complex formation constant was found to be  $\log \beta_{1:1} = 1.30 \pm 0.10$ .

The solution coordination chemistry of U(VI) with  $\alpha$ -aminoisobutyric acid is less understood compared to the  $\alpha$ -hydroxyacids. There is only one study reporting a formation constant of a 1:1 species of uranyl with  $\alpha$ -aminoisobutyric acid at pH range of 2-3.5 /1/.

The TRLFS spectra were recorded as a function of the ligand concentration at a total concentration of U(VI) equal to  $7 \times 10^{-5}$  M in test solutions at pH=3.

Fig. 1 depicts the TRLFS spectra of uranium(VI) as a function of the total  $\alpha$ -aminoisobutyric acid concentration at pH=3.

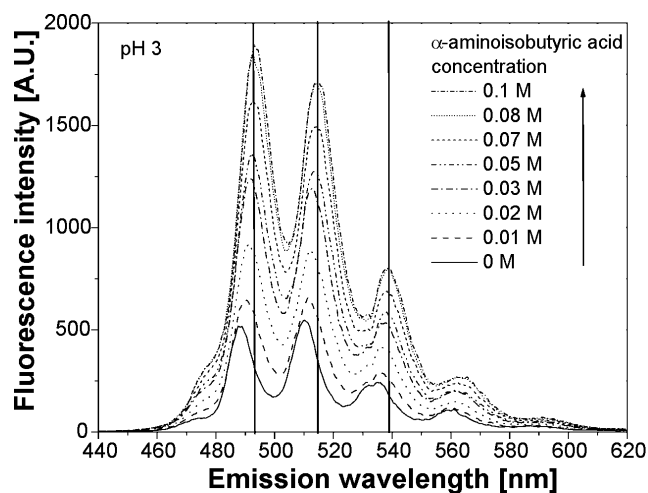


Fig. 1: TRLFS spectra of uranium(VI) as a function of the  $\alpha$ -aminoisobutyric acid concentration at pH=3.

A change of the substituent in  $\alpha$  position from  $-\text{OH}$  to  $-\text{NH}_3^+$ , as in  $\alpha$ -aminoisobutyric acid, results in major changes both in the U(VI) complex formation reactions and in the spectroscopic properties of the complexes formed. The fluorescence spectra of U(VI) -  $\alpha$ -aminoisobutyrate show a red shift of about 6 nm compared to the uranyl ion. We observed increased fluorescence with increasing ligand concentration. The spectra of solutions containing 0.01 to 0.1 M  $\alpha$ -aminoisobutyrate at pH 3 showed bi-exponential fluorescence decay indicating a mixture of two species. The lifetimes are  $1600 \pm 300$  ns and  $330 \pm 80$  ns, respectively. The longer lifetime is typical for the free uranyl ion. The shorter lifetime can be assigned to the complex,  $\text{UO}_2[\text{NH}_3\text{C}(\text{CH}_3)_2\text{COO}]^{2+}$ . To the knowledge of the authors, lifetimes of uranyl- $\alpha$ -aminoisobutyrate complexes have not been published before.

Since the fluorescence lifetimes of  $\text{UO}_2^{2+}(\text{aq})$  and  $\text{UO}_2[\text{NH}_3\text{C}(\text{CH}_3)_2\text{COO}]^{2+}$  are significantly different, their individual fluorescence spectra can be determined from the composite spectrum using conventional peak deconvolution (method of least squares). The main fluorescence bands of the complex

$\text{UO}_2[\text{NH}_3\text{C}(\text{CH}_3)_2\text{COO}]^{2+}$  are centered at 477, 494, 516, 540, 565, and 594 nm.

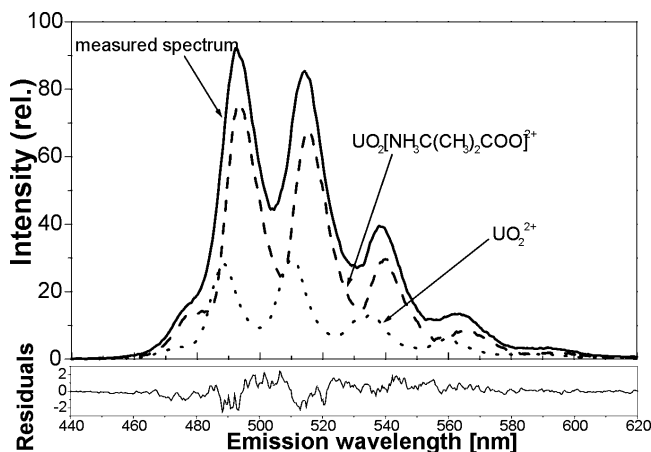


Fig. 2: Results of the peak deconvolution of the measured TRLFS spectra for a solution containing 0.08 M  $\alpha$ -aminoisobutyric acid at pH=3.

A ratio of 1:20 was determined for the intensities of the integral fluorescence signals between 450 and 580 nm for the free uranyl ion and the 1:1 complex. Due to the different lifetimes of the two species, the concentrations of  $\text{UO}_2^{2+}(\text{aq})$  and  $\text{UO}_2[\text{NH}_3\text{C}(\text{CH}_3)_2\text{COO}]^{2+}$  can be extracted from the intensity data, and used to determine the stability constant for the reaction:



The linear function has a slope of  $1.01 \pm 0.06$  and an intercept  $\log \beta_{1:1} = 1.30 \pm 0.10$ , confirming that Eqn.(1) is the predominant reaction. The value of the stability constant is in fair agreement with the UV-vis findings /2/. This equilibrium constant is more than six orders of magnitude smaller than the value reported by Rangaraj and Ramanujam,  $\log \beta = 7.72$  /1/. The reason for the discrepancy is that these authors have not taken into account the formation of complexes with the "zwitter-ion",  $^+\text{NH}_3\text{C}(\text{CH}_3)_2\text{COO}^-$ . Species such as  $\text{UO}_2[\text{NH}_2\text{C}(\text{CH}_3)_2\text{COO}]^+$  containing an U-N bonded ligand are important only at pH > 7 as reported for glycine /3/.

## Acknowledgements

The studies were funded by the European Union (EU) under contract number HPMF-CT-1999-00342.

## References

- /1/ Rangaraj, K., et al., J. Inorg. Nucl. Chem. **39**, 489 (1977)
- /2/ Moll, H. et al., Radiochim. Acta, submitted (2002)
- /3/ Szabó, Z., et al., Inorg. Chem. **39**, 5036 (2000)

# COMPLEX FORMATION IN THE SYSTEM URANIUM(VI) – ALPHA-SUBSTITUTED CARBOXYLIC ACIDS STUDIED BY TRLFS; PART III: ALPHA-AMINOISOBUTYRIC ACID AT pH 4

H. Moll, G. Geipel, G. Bernhard, Th. Fanghänel, I. Grenthe<sup>1</sup>

<sup>1</sup> Department of Chemistry, Inorganic Chemistry, The Royal Institute of Technology, Stockholm, Sweden

At higher ligand concentrations a 1:2 complex between  $\text{UO}_2^{2+}$  and  $\alpha$ -aminoisobutyric acid was observed at pH 4. Fluorescence lifetimes and spectra were obtained for  $\text{UO}_2[\text{NH}_3\text{C}(\text{CH}_3)_2\text{COO}]_2^{2+}$ . The complex formation constant was found to be  $\log \beta_{1:2} = 2.07 \pm 0.25$ .

In continuation of our studies concerning the complex formation of uranyl with alpha-substituted carboxylic acids, we investigated the uranyl-alpha-aminoisobutyrate system at pH 4.

Fig. 1 depicts the TRLFS spectra of uranium(VI) as a function of the total alpha-aminoisobutyric acid concentration at pH=4.

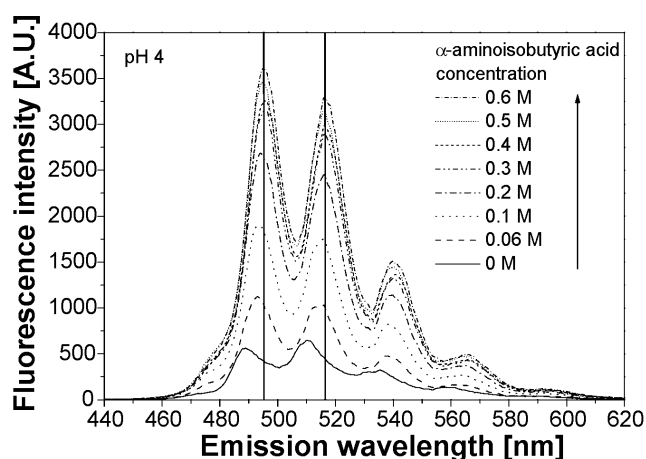


Fig. 1: TRLFS spectra of uranium(VI) as a function of the alpha-aminoisobutyric acid concentration at pH=4.

We found again an increased fluorescence intensity with increasing ligand concentrations. The TRLFS spectra show a little larger red shift of the emission bands of about 7 nm compared to the measurements at pH 3. The measurements were made at much higher total concentrations of the ligand, and we found evidence for the formation of a second complex, most likely  $\text{UO}_2[\text{NH}_3\text{C}(\text{CH}_3)_2\text{COO}]_2^{2+}$ .

The time-resolved fluorescence spectra showed a bi-exponential fluorescence decay with lifetimes of  $1560 \pm 300$  ns and  $330 \pm 80$  ns, respectively. The intensity of the fluorescence spectrum of the species with the longer lifetime increases with increasing ligand concentration. This is a strong indication that it is not due to  $\text{UO}_2^{2+}$  (aq), which has the same lifetime, but to a new species, presumably  $\text{UO}_2[\text{NH}_3\text{C}(\text{CH}_3)_2\text{COO}]_2^{2+}$ . The species with the shorter lifetime is  $\text{UO}_2[\text{NH}_3\text{C}(\text{CH}_3)_2\text{COO}]^{2+}$ . For comparison, we also measured the fluorescence spectra and the lifetimes of a test solution at pH 4 that did not contain any organic ligand; the measured lifetimes  $1720 \pm 50$  ns and  $11700 \pm 500$  ns, correspond to the species  $\text{UO}_2^{2+}$  (aq) and  $(\text{UO}_2)_2(\text{OH})_2^{2+}$ . In all test solutions containing  $\alpha$ -aminoisobutyric acid, the long fluorescence lifetime could not be detected indicating that hydrolysis of U(VI) is negligible.

The deconvolution of the composite spectrum of a test solution containing 0.4 M  $\alpha$ -aminoisobutyric acid at pH 4 is shown in Fig. 2. The main fluorescence bands of the  $\text{UO}_2[\text{NH}_3\text{C}(\text{CH}_3)_2\text{COO}]_2^{2+}$ -complex are centered at 483, 496, 517, 541, 565, and 594 nm.

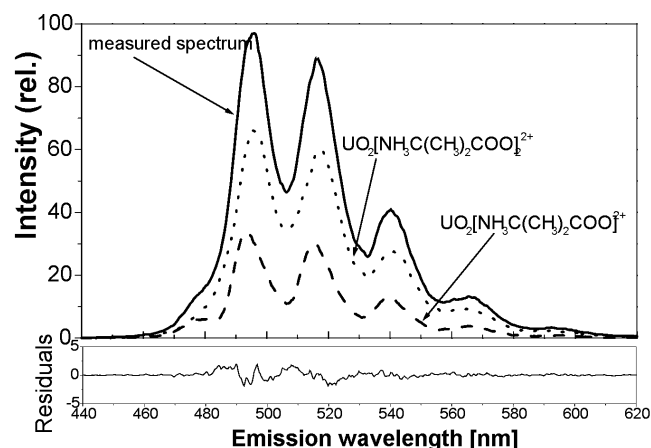
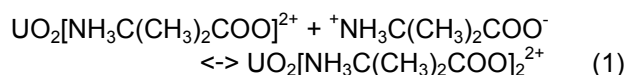
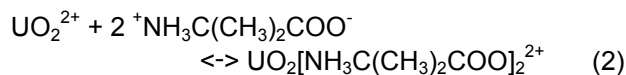


Fig. 2: Results of the peak deconvolution of the measured TRLFS spectra for a solution containing 0.4 M  $\alpha$ -aminoisobutyric acid at pH 4.

The stepwise equilibrium constant,  $\log K = 0.77 \pm 0.10$  for the formation of  $\text{UO}_2[\text{NH}_3\text{C}(\text{CH}_3)_2\text{COO}]_2^{2+}$  according to:



was obtained in the same way as described in /1/. Using the equilibrium constant,  $\log \beta_{1:1} = 1.30$ , for the formation of the 1:1 complex, we obtain for



the equilibrium constant  $\log \beta_{1:2} = 2.07 \pm 0.25$ . This value is in fair agreement with the UV-vis results /1/. The existence of a 1:2 species is supported by the isolation of such a complex in solid state.

## Acknowledgements

The studies were funded by the European Union (EU) under contract number HPMF-CT-1999-00342.

## References

/1/ Moll, H. et al., Radiochim. Acta, submitted (2002)

# URANIUM(VI) COMPLEXATION BY ALPHA-SUBSTITUTED CARBOXYLIC ACIDS STUDIED BY EXAFS

H. Moll, T. Reich, G. Geipel, C. Hennig, H. Funke, A. Roßberg, Th. Fanghänel, I. Grenthe<sup>1</sup>

<sup>1</sup> Department of Chemistry, Inorganic Chemistry, The Royal Institute of Technology, Stockholm, Sweden

A decrease in the U-O<sub>eq</sub> distance to 2.36–2.37 Å at pH values > 5 shows the formation of a chelate complex due to the deprotonation of the α-OH-group of the ligand. In the glycolate system in the pH range 5.5 to 11, the EXAFS data showed evidence of U-U interaction at 3.81 Å indicating the formation of dimeric species.

Organic ligands having a α-OH-group can form chelates even at low pH. EXAFS is a challenging technique to explore structural changes in the atomic surrounding of the uranyl center as a consequence from this process.

The EXAFS data were recorded at the Rossendorf Beamline (ROBL) at the ESRF in Grenoble /1/. The transmission spectra were measured at room temperature using a water-cooled Si(111) double-crystal monochromator of fixed-exit type (E = 5 - 35 keV). For energy calibration of the sample spectra, the K-edge spectrum (17038 eV) from an Y foil was recorded simultaneously. Three spectra for each sample were recorded and then averaged. The data were treated using the EXAFSPAK suite of programs /2/.

Figure 1 depicts the EXAFS spectra and the corresponding Fourier transforms (FT) measured for the uranyl-glycolate-system.

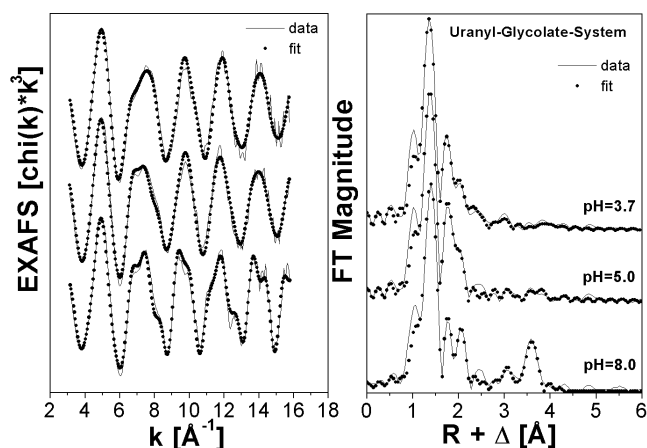


Fig. 1: Raw U L<sub>III</sub>-edge k<sup>3</sup>-weighted EXAFS spectra and corresponding Fourier transforms measured in the uranyl glycolate system including the best theoretical fits.

The bond lengths and coordination numbers obtained are summarized in Table 1. The U-O<sub>eq</sub> distance is an indicator for the coordination mode of carboxylate ligands to the uranyl center /3/. For sample A at pH 3.7 we measured an U-O<sub>eq</sub> distance of 2.38 Å. This value is shorter than expected for a bidentate coordination of the carboxylic group via both of the carboxylate oxygens. An additional indicator of unidentate coordination is the absence of U-C distances around 2.90 Å.

In contrast to the glycolate system, we observed a longer U-O<sub>eq</sub> bond distance of 2.43 Å and an U-C interaction at 2.87 Å at pH 4 (sample D) in the α-hydroxyisobutyrate system. Furthermore, we found evidence for a multiple scattering path, presumably U-C-C, at 4.4 Å. This implies a dominant bidentate coordination of the α-hydroxyisobutyric acid. This is supported by the U-O<sub>eq</sub> distance of 2.45 Å measured in

the uranyl-β-hydroxybutyrate system at pH 6 (not shown here). These U-O<sub>eq</sub> distances are typical for bidentate coordinated COO<sup>-</sup>-groups, as indicated by the presence of an U-C contribution at 2.87 Å.

Sample	Shell	N	σ <sup>2</sup> (Å <sup>2</sup> )	R (Å)
A 0.01M U(VI), 1M H <sub>2</sub> Gly, pH=3.7 (80% UO <sub>2</sub> (Hgly) <sub>3</sub> )	U-O <sub>ax</sub>	2f	0.0014	1.78
	U-O <sub>eq</sub>	5.4	0.0124	2.38
B 0.02M U(VI), 0.25M H <sub>2</sub> Gly, pH=5.0 (80% UO <sub>2</sub> (Gly) <sub>2</sub> <sup>2-</sup> )	U-O <sub>ax</sub>	2f	0.0015	1.79
	U-O <sub>eq1</sub>	4.8	0.0098	2.37
	U-C	1.5	0.0035	3.24
C 0.02M U(VI), 0.25M H <sub>2</sub> Gly, pH=8 (92% UO <sub>2</sub> (Gly) <sub>2</sub> <sup>2-</sup> )*	U-O <sub>ax</sub>	2f	1.80	0.0015
	U-O <sub>eq</sub>	5.5	2.37	0.0150
	U-C	1.7	3.25	0.0046
	U-U	1.4	3.81	0.0037
D 0.01M U(VI), 0.6M H <sub>2</sub> IBA, pH=4.0 (92% UO <sub>2</sub> (HIBA) <sub>3</sub> )	U-O <sub>ax</sub>	2f	0.0017	1.78
	U-O <sub>eq</sub>	5.4	0.0115	2.43
	U-C	2.7	0.0082	2.89
E 0.01M U(VI), 0.6M H <sub>2</sub> IBA, pH=6.5 (82% UO <sub>2</sub> (IBA) <sub>2</sub> <sup>2-</sup> )	U-O <sub>ax</sub>	2f	0.0014	1.79
	U-O <sub>eq</sub>	4.7	0.0137	2.37
	U-C	1.8	0.0020	3.25
F 0.01M U(VI), 0.6M H <sub>2</sub> IBA, pH=8 (98% UO <sub>2</sub> (IBA) <sub>2</sub> <sup>2-</sup> )	U-O <sub>ax</sub>	2f	0.0012	1.80
	U-O <sub>eq</sub>	4.4	0.0127	2.36
	U-C	2.6	0.0023	3.25

Tab. 1: Summary of the EXAFS structural parameters. \*: possibly [(UO<sub>2</sub>)<sub>2</sub>(Gly)<sub>4</sub>]<sup>4-</sup>. H<sub>2</sub>Gly: glycolic acid, H<sub>2</sub>IBA: α-hydroxyisobutyric acid, f: fixed during the fit.

The U-O<sub>eq</sub> distance, 2.36 – 2.37 Å, measured in the near neutral and alkaline pH region (samples B, E, and F) is a strong indication for the formation of chelate complexes due to the deprotonation of the α-OH-group of the ligand. Roßberg et al. reported similar structural parameters for the chelate complex of uranyl with 2-hydroxyphenol /4/.

In contrast to the α-hydroxyisobutyrate system, the EXAFS data from the glycolate system in the pH range 5.5 to 11 contain a feature at 3.81 Å which could be fit as an U-U interaction. This implies the formation of a dimer, most likely similar to [(UO<sub>2</sub>)<sub>2</sub>(OCH<sub>2</sub>COO)<sub>2</sub>F<sub>4</sub>]<sup>4-</sup> /5/, where the oxo-group is bridging the two uranium atoms and where the fluorides are replaced by a chelated (OCH<sub>2</sub>COO)<sup>2-</sup>.

## Acknowledgements

The studies were funded by the European Union (EU) under contract number HPMF-CT-1999-00342.

## References

- 1/ Reich, T. et al., Radiochim. Acta **88**, 633 (2000)
- 2/ George, G.N., Pickering, I.J., "EXAFSPAK", SSRL, Stanford, CA, USA (1995)
- 3/ Denecke, M. et al., Radiochim. Acta **79**, 151 (1997)
- 4/ Roßberg, A. et al., Radiochim. Acta **88**, 593 (2000)
- 5/ Farkas, I. et al., Acta Chem. Scand. **53**, 1009 (1999)

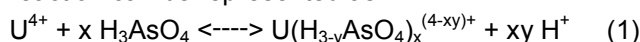
# COMPLEX FORMATION OF URANIUM(IV) WITH ARSENATE

G. Geipel, G. Bernhard

We studied the complex formation of uranium(IV) with arsenate in acid solution using UV-vis and laser-induced photoacoustic spectroscopy at various ionic strengths. We found a one to one complex formation between uranium and arsenic acid. During the complex forming reaction one hydrogen ion was released from arsenic acid.

Complexation of uranium(VI) with various inorganic ligands is well known [1]. Under reducing conditions uranium(IV) is the stable oxidation state. We continued to study complex formation with various inorganic ligands by determining the complex formation of uranium(IV) with arsenate. To obtain the formation constant and the stoichiometry, three parameters had to be varied i) the ionic strength, ii) the concentration of phosphoric acid and iii) the concentration of hydrogen ions.

The measurements were carried out at  $1 \times 10^{-4}$  M and  $5 \times 10^{-4}$  M uranium. The concentration of arsenic acid varied between 0 and  $1 \times 10^{-2}$  M. The concentration of hydrogen ions was kept constant in a range from 0.1M to 2 M. As shown in [2] the complex forming reaction can be represented as



After rearranging and transforming the mass action law in logarithmic form it becomes

$$\log \frac{[U(H_{3-y}AsO_4)_x^{(4-xy)+}]}{[U^{4+}]} = \log K + x \log [H_3AsO_4] - xy \log [H^+] \quad (2)$$

At a constant hydrogen ion concentration the right side of Equation (2) can be simplified to be

$$\log K' = \log K - xy \log [H^+] \quad (3)$$

Fig. 1 shows a series of UV-vis measurements in the uranium(IV)-arsenate system as examples. The spectra as a function of arsenic acid are changed. The absorption maxima of the formed complex are found to be 645.1 nm and 662.9 nm. Two isosbestic points were detected at 661.0 nm and 667.5 nm.

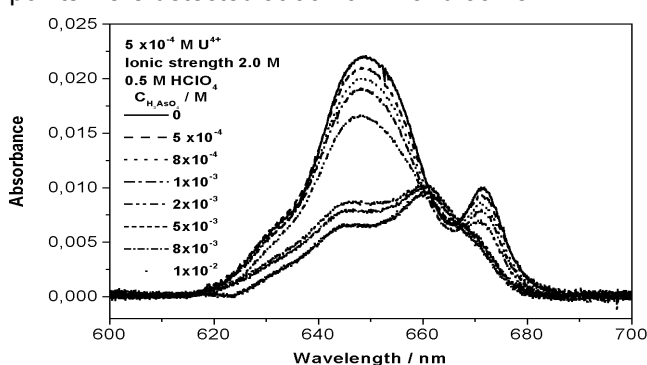


Fig.1: UV-vis spectra of uranium(IV) as function of the concentration of arsenic acid

The validation of complex formation is shown in Fig. 2. By plotting the  $\log([complex]/[U^{4+}])$  vs. the  $\log[H_3AsO_4]$ , we obtain the stoichiometry of the complex reaction from the slope. The value  $x$  is found to be  $1.08 \pm 0.10$ , which clearly shows a 1:1 complex formation. From the intersection we obtain the formation constant at a fixed hydrogen ion concentration of 0.25 M to be  $\log K' = 3.29 \pm 0.27$ .

In a second step experiments were carried out at various hydrogen ion concentrations. By plotting  $\log K'$  vs.  $\log[H^+]$  we determined the number of hydrogen ions released during the complex forming reaction. From the slope analysis and the intersection we ob-

tained the formation constant at the selected ionic strength.

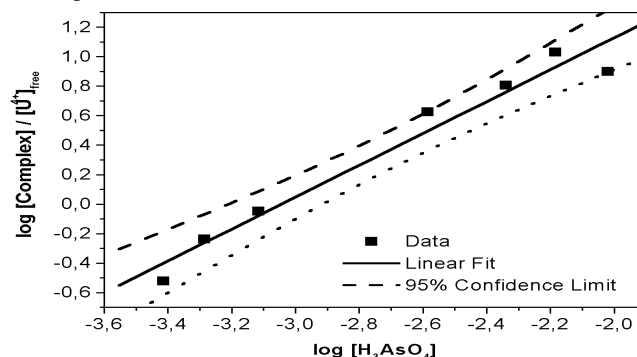


Fig.2: Slope analysis of the complex formation in 0.25 M HClO<sub>4</sub> solution at an ionic strength of 0.5 M

This is shown, for example, in Fig. 3 for an ionic strength of 2 M. We found a slope of  $-1.03 \pm 0.19$ . This means that one hydrogen ion is released during the first complex formation step. The formation constant was calculated to be  $\log K = 2.24 \pm 0.06$ .

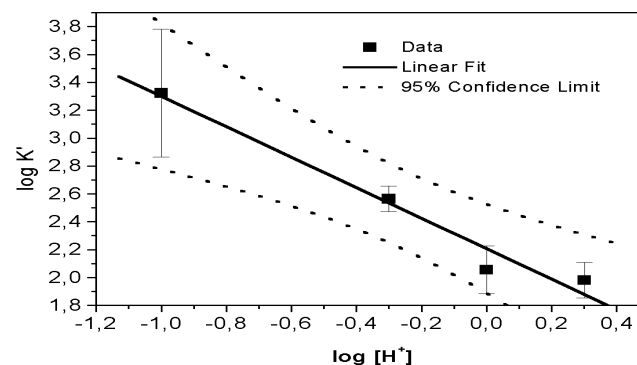


Fig.3: Slope analysis of the complex formation at an ionic strength of 2M

The results of all experiments are summarized in Tab. 1.

Ionic strength /M	log K	Slope analysis H <sub>3</sub> AsO <sub>4</sub>	Slope analysis H <sup>+</sup>
2	2.24 ± 0.06	1.05 ± 0.17	-1.03 ± 0.19
1.5	2.22 ± 0.10	1.03 ± 0.06	-1.31 ± 0.48
1	1.95 ± 0.08	1.01 ± 0.07	-1.31 ± 0.16
0.75	2.31 ± 0.14	1.37 ± 0.21	-
0.5	2.16 ± 0.06	1.14 ± 0.05	-1.40 ± 0.25
0.1	2.18 ± 0.14	0.93 ± 0.17	

Tab. 1: Calculated data for the complex formation of uranium(IV) with arsenate

## References

- [1/] Grenthe, J., Fuger, R.J., Lemire, A.B., Muller, C., Nguyen-Trung, Wanner, H., *Chemical Thermodynamics of Uranium*, 1st ed., Elsevier Science Publishers, Amsterdam, 1992
- [2/] Geipel, G., Bernhard, G., Report FZR 285 (2000) p. 2-4

# FORMATION CONSTANTS OF URANIUM(IV) DIHYDROGEN ARSENATE COMPLEXES - EXTRAPOLATION TO INFINITE DILUTION

G. Geipel, G. Bernhard

We reported on the determination of the complex formation constants of uranium(IV) with arsenic acid at various ionic strengths. We used these data to extrapolate to infinite dilution. Including the protonation constant of arsenic acid at infinite dilution, the formation constant was derived to be  $\log \beta_{121}^0 = 23.94 \pm 0.13$ .

With dihydrogen phosphate and dihydrogen arsenate uranium(IV) forms complexes in strong acid solutions /1,2/. Fig. 1 compares the UV-vis spectra of these complexes with the UV-vis spectrum of the uranium(IV) ion. The spectra of these two complexes can be clearly distinguished from the uranium(IV)-ion.

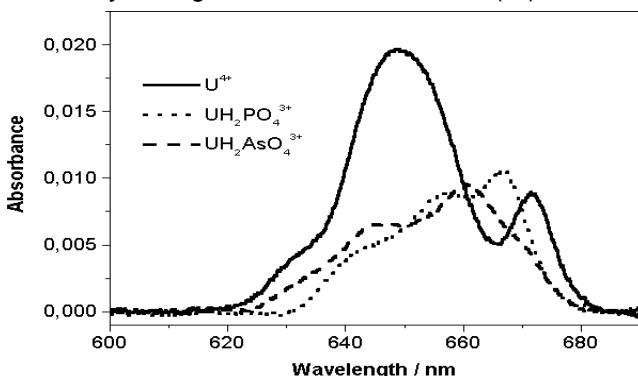


Fig. 1: Comparison of UV-vis Spectra of Uranium(IV)

For the phosphate complex the absorption band of the uranium band at 671.7 nm shows a blue shift to 667.0 nm. For the arsenate complex the absorption band shifts to 662.9 nm. By contrast the absorption bands of uranium(IV) at 629.5 nm and 649.1 nm show a red shift.

To extrapolate the complex formation constant at infinite dilution we used the SIT theory:

$$\log KJ - \Delta z^2 D = \log K^0 - \Delta \epsilon J \quad (1)$$

Using the charges of the species in solution, we calculated  $\Delta z^2 = -6$ .  $D$  is a function of the ionic strength:

$$D = \frac{0.5093\sqrt{J}}{1 + 1.5\sqrt{J}} \quad (2)$$

Adding the product of  $\Delta z^2 D(J)$  to the formation constants at the various ionic strengths we obtain an expression which should be a linear function of ionic strength. The slope represents the sum of the specific interaction coefficients. The intersection is equal to the formation constant at infinite dilution.

Ionic strength M	Ionic strength mol/kg	$\log K_J$	$D(J)$	$\log K_J + 6D$
2	1.74	2.24	0.231	3.62
1.5	1.35	2.22	0.219	3.54
1	0.95	1.95	0.204	3.17
0.75	0.72	2.31	0.192	3.46
0.5	0.48	2.16	0.175	3.2
0.1	0.098	2.18	0.109	2.84

Tab. 1: Complex formation constants as a function of ionic strength

The calculated complex formation constants are listed in /1/. We first have to change from the molar to the molal concentration scale. The calculated ionic strengths on the molal scale and the calculated values ( $\log K_J + 6D$ ) are listed in Tab. 1. Using this ex-

trapolation mechanism, the formation constant for the reaction



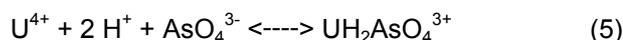
is found to be  $\log K^0 = 3.34 \pm 0.08$ . The slope is calculated to be  $-0.16 \pm 0.04$ .

Introducing the protonation of the arsenic acid /3/



with  $\log \beta_{31}^0 = 20.60$ , the formation constant of the uranium(IV)dihydrogen arsenate complex can be calculated.

For the reaction



the formation constant is  $\log \beta_{121}^0 = 23.94 \pm 0.08$ .

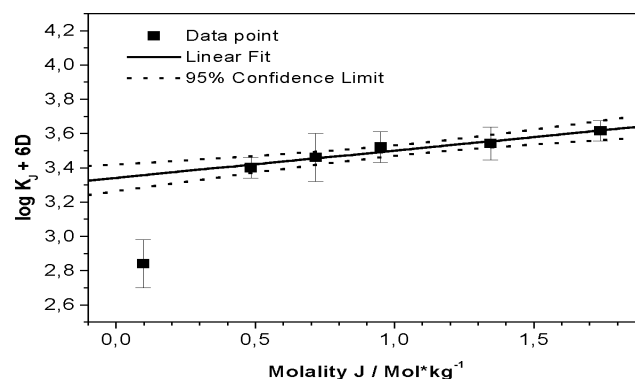


Fig. 2: Extrapolation of the Uranium(IV)-Arsenate Complex Formation Constant to  $I = 0$  M

A speciation diagram comparing the complex formation of uranium(IV) with phosphate and arsenate is shown in Fig. 3. As expected, the complex formation of arsenate is somewhat weaker than that of phosphate.

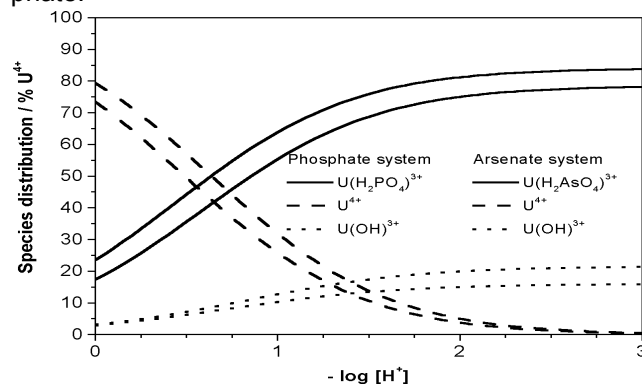


Fig. 3: Speciation of Uranium(IV) in Phosphate and Arsenate Media

## References

- /1/ Geipel, G., Bernhard, G., Report FZR 285 (2000) p. 2-4
- /2/ Geipel, G., Bernhard, G., this report p. 5
- /3/ Grenthe, J., Fuger, R.J., Lemire, A.B., Muller, C., Nguyen-Trung, Wanner, H., *Chemical Thermodynamics of Uranium*, 1st ed., Elsevier Science Publishers, Amsterdam, 1992

# COMPLEX FORMATION OF URANIUM(VI) WITH 2,3 DIHYDROXYBENZOIC ACID STUDIED BY TIME-RESOLVED LASER-INDUCED FLUORESCENCE SPECTROSCOPY WITH ULTRASHORT LASER PULSES (fs-TRLFS)

G. Geipel, G. Bernhard

After testing the fs-laser system /1/ we studied the complex formation of 2,3-dihydroxybenzoic acid with uranium(VI) in the pH range from 3.0 to 4.5. We used uranium in our study so as to control complex formation also by the fluorescence properties of uranium. A 1:1 complex was formed. The formation constant at  $I = 0.1 \text{ M}$  was found to be  $\log K = -3.02 \pm 0.09$ .

Ultrashort laser pulses were used to excite the fluorescence of 2,3-dihydroxybenzoic acid. The excitation wavelength of the laser system was set at 320 nm. This wavelength is in the range of the absorption maximum of 2,3-dihydroxybenzoic acid. The maximum of the emission spectra of the 2,3-dihydroxybenzoic acid is located at 443 nm and the fluorescence lifetime was calculated to be  $375 \pm 36 \text{ ps}$ . The decrease in fluorescence intensity can be described by the Stern-Volmer equation /2/.

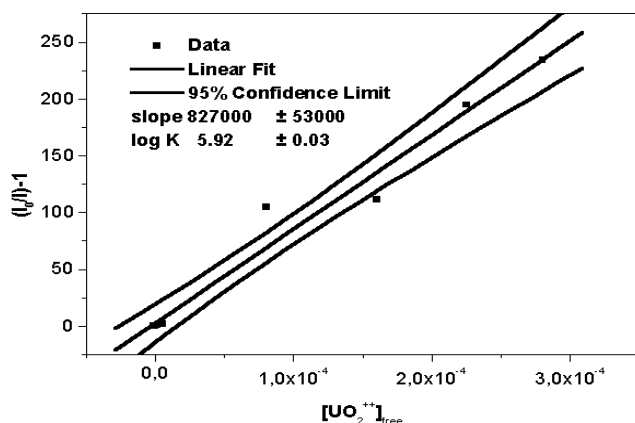


Fig. 1: Stern-Volmer-Plot at pH 4.5

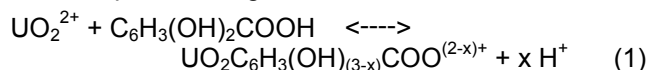
In Fig. 1 this is shown for pH 4.5. We obtain a straight line, whose the slope represents the complex formation constant. It was found to be  $\log K' = 5.92 \pm 0.05$ . The data obtained for all pH values studied are listed in Tab. 1.

pH	Stern-Volmer plot $\log K'$	$\log K'$	slope
3	$3.05 \pm 0.05$	$3.21 \pm 0.16$	$0.77 \pm 0.14$
3.5	$3.76 \pm 0.07$	$3.73 \pm 0.32$	$1.03 \pm 0.08$
4	$5.19 \pm 0.06$	$4.96 \pm 0.25$	$1.09 \pm 0.11$
4.5	$5.92 \pm 0.05$	$5.88 \pm 0.11$	$1.04 \pm 0.14$

Tab. 1: Results of the Stern-Volmer and validation plots

As the ratio  $(I_0/I)$  is linearly dependent on the concentration of the non-complexed uranium, we can assume that a 1:1 complex formation occurs.

The complex-forming reaction can be written as



To validate the formation reaction we performed an additional slope analysis. The law of mass action was rearranged to fit

$$\log\left(\frac{[\text{UO}_2\text{C}_6\text{H}_3(\text{OH})_{(3-x)}\text{COO}^{(2-x)+}]}{[\text{C}_6\text{H}_3(\text{OH})_2\text{COOH}]}\right) = \log K + \log[\text{UO}_2^{2+}] - x \log[\text{H}^+] \quad (2)$$

At constant pH the term for dependence on the hydrogen ion concentration can be included in the formation constant according to

$$\log K' = \log K - x \log[\text{H}^+] \quad (3)$$

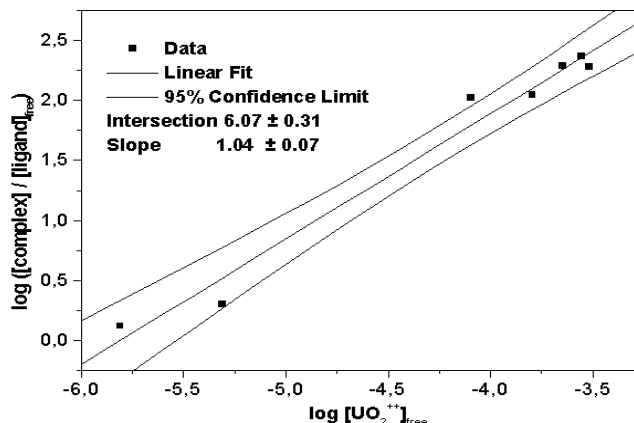


Fig. 2: Validation of the formation constant at pH 4.5

Fig. 2 shows this slope analysis. As expected the slope was found to be  $1.04 \pm 0.14$ . The intersection represents the formation constant and was found to be  $5.88 \pm 0.11$ . This result agrees with the data of the Stern-Volmer plot.

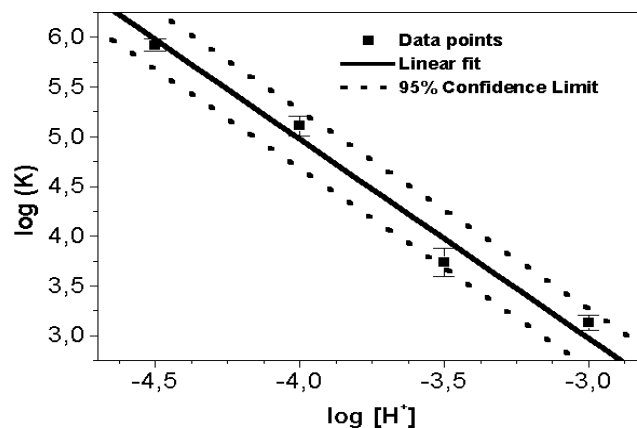
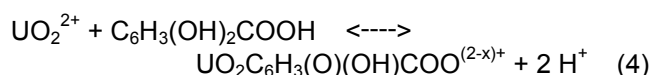


Fig. 3: Formation constant as function of pH

Performing experiments at various pH values, we can determine the value of the number of protons involved in the complex-forming reaction. Fig.3 shows the formation constant  $\log K'$  as function of pH. In the pH range from 3.0 to 4.5 a slope  $x$  of  $-1.95 \pm 0.19$  is obtained from the dependence of  $\log K'$  on the concentration of hydrogen ions. This shows clearly that the phenolic OH group must be involved in the complex formation. The complex formation constant for the reaction



is found to be  $\log K = -3.02 \pm 0.09$ .

## References

- /1/ Geipel, G., Bernhard, G.; Report FZR-318, p.10-11  
 /2/ Klessinger, M., Michl, J.; *Excited States and Photochemistry of Organic Molecules*, VCH Publishers, 1995, p. 297 ff.

# COMPLEX FORMATION OF NEPTUNIUM(V) WITH 2,3-DIHYDROXYBENZOIC ACID STUDIED BY TIME-RESOLVED LASER-INDUCED FLUORESCENCE SPECTROSCOPY WITH ULTRASHORT LASER PULSES (fs-TRLFS)

G. Geipel, G. Bernhard

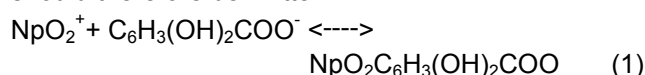
The main goal of fs-TRLFS is the determination of complex formation constants of fluorescent organic ligands with non-fluorescent actinides. As a first example we studied the complex formation of neptunium(V) with 2,3-dihydroxybenzoic acid. In the pH range below 5.0 a 1:1 complex formation was observed. The formation constant was  $\log K = 0.16$ .

As described in [1] we used fs-laser pulses to excite the fluorescence of the 2,3 dihydroxybenzoic acid. The experimental conditions differ in two points:

i) the use of a sealed fluorescence cuvette instead of the flow passing through cell as in the study with uranium, and

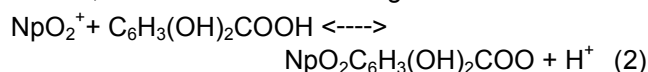
ii) the CCD camera was replaced in this series by a new type with an enhanced CCD chip which has an efficiency of about 60% and is coupled with an imaging telescope to the multichannel plate (MCP). The change in the camera set-up results in a higher spectral resolution and lower detection limits. The spectra do not show the structure caused by light interference with the taper used before. A lower gain of the MCP may also be used for collection of the spectra.

formation constant on the pH as we did in the study of the complex formation with uranium. This can only be interpreted as complex formation of neptunium(V) with the deprotonated carboxylic group of the 2,3-dihydroxybenzoic acid. The complex-forming reaction should therefore be written



The weighted formation constant for reaction (1) is assigned to be  $\log K' = 3.33 \pm 0.07$ .

For comparison with the complex formation of uranium with the 2,3-dihydroxybenzoic acid we have therefore to include the first deprotonation step. The deprotonation constant is found to be  $\log K_1 = -3.17 \pm 0.05$  [2,3]. On this basis we assign for the reaction



the formation constant to be  $\log K = 0.16 \pm 0.09$ .

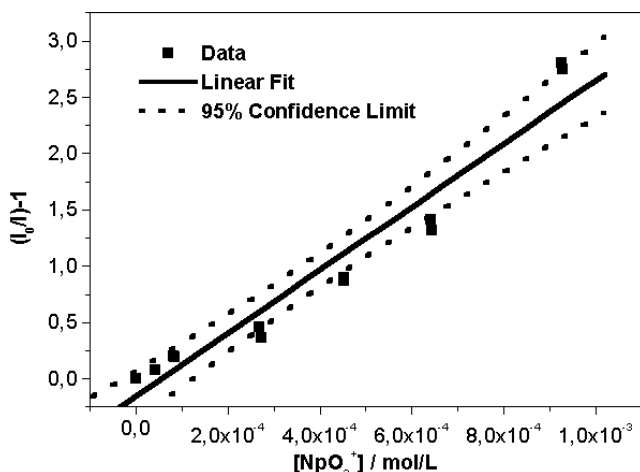


Fig. 1: Stern-Volmer plot at pH 3.0

Fig. 1 shows the Stern-Volmer plot for the  $\text{NpO}_2^+$  - 2,3-dihydroxybenzoic acid system at pH 3.0. The validation of the complex formation at this pH is shown in Fig. 2.

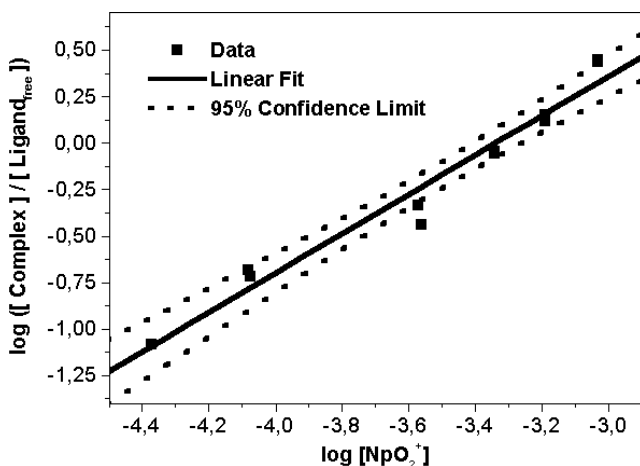


Fig. 2: Validation of the complex formation

We found a 1:1 complex formation. In the pH range from 3.0 to 5.0 we did not find any dependence of the

pH	Stern-Volmer log K'	log K'	Slope
3	$3.49 \pm 0.07$	$3.33 \pm 0.10$	$1.05 \pm 0.07$
4	$3.23 \pm 0.10$	$2.93 \pm 0.29$	$1.50 \pm 0.65$
5	$3.31 \pm 0.14$	$3.28 \pm 0.06$	$1.21 \pm 0.14$
6	$6.89 \pm 0.04$	$6.97 \pm 0.19$	$1.67 \pm 0.10$
7	$7.06 \pm 0.07$	$7.05 \pm 0.23$	$1.94 \pm 0.18$

Tab. 1: Observed formation constants

Some first studies of the pH range above 5.0 show a change in the stoichiometry of the complex formation reaction (Fig.3). Further studies are in progress to determine the complex formation in this pH range.

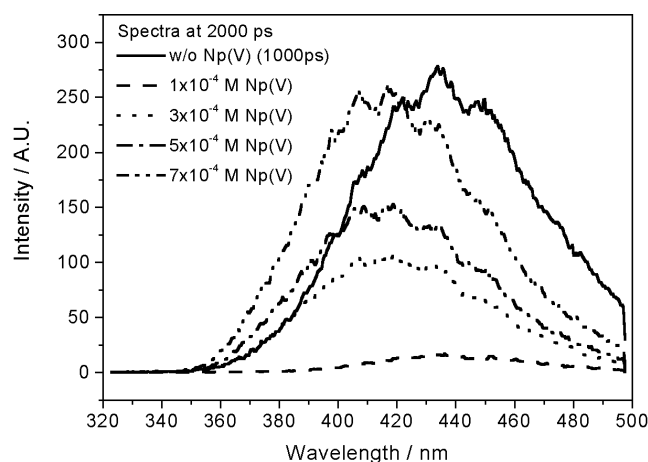


Fig. 3: Spectra of 2,3 Dihydroxybenzoic acid as function of  $\text{Np(V)}$  concentration at pH > 4.0

## References

- [1] Geipel, G., Bernhard, G., this report p. 7
- [2] Geipel, G. et al. publication in preparation
- [3] Harada, H.; Bull.Chem.Soc.Jpn. **44**, 3459 (1971)

# COMPLEX FORMATION OF URANIUM(VI) WITH ORGANIC LIGANDS STUDIED BY FS-TRLFS PART I: BENZOIC ACID

D. Vulpius, G. Geipel, L. Baraniak, G. Bernhard, Th. Fanghänel

The complex formation of uranium(VI) with benzoic acid was studied by time-resolved laser-induced fluorescence spectroscopy with ultrashort laser pulses (fs-TRLFS). The formation constant of the 1:1 uranyl benzoate complex was determined to be  $\log \beta_{11} = 2.99 \pm 0.06$ .

## Introduction

In a previous contribution we reported on the complex formation of uranium(VI) with benzoic acid studied by potentiometric pH titration /1/. This study was preliminary to our main intention of determining formation constants for actinide complexes with organic ligands, using the fluorescence properties of the organic compound. For this purpose time-resolved laser-induced fluorescence spectroscopy with ultrashort laser pulses (fs-TRLFS) was developed at our Institute /2/ and applied for determination of formation constants /3/.

## Experimental

The fluorescence intensity of solutions of  $1.0 \cdot 10^{-4}$  M benzoic acid (Merck, SRM) in CO<sub>2</sub>-free and O<sub>2</sub>-free, deionized water was measured as a function of the uranyl concentration ( $[\text{UO}_2^{2+}] = 1.0 \cdot 10^{-4}$  to  $1.5 \cdot 10^{-3}$  M, Baker, ICP Standard) at an ionic strength of 0.1 M (NaClO<sub>4</sub>) and at  $22 \pm 1$  °C. The pH of these solutions was kept constant at  $4.00 \pm 0.02$ . The pH measurement was carried out with a WTW high performance pH meter (pH 540 GLP) and a Schott combination electrode (BlueLine 16 pH), which was calibrated with NBS buffers at pH 4.006 and 6.865 (WTW). The pH meter reading was converted to  $-\log [\text{H}^+] = 3.96 \pm 0.02$  by recalibration of the electrode with standard solutions of constant ionic strength (0.1 M (NaClO<sub>4</sub>)) and various HCl concentrations ( $1.0 \cdot 10^{-3}$ ,  $2.0 \cdot 10^{-3}$ , and  $5.0 \cdot 10^{-3}$  M). The laser excitation wavelength was 266 nm, and the laser pulse width 130 fs.

## Results

Fig. 1 shows the time-resolved fluorescence spectra of pure benzoic acid at pH 6.0.

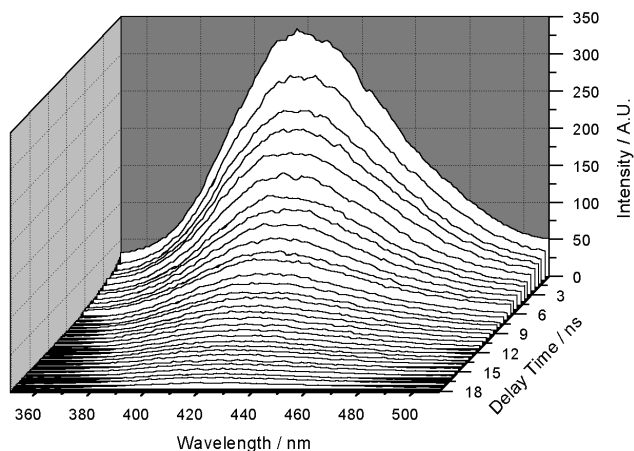


Fig. 1: Fluorescence spectra of benzoic acid at pH 6.0

The fluorescent species is the benzoate ion with an emission maxima at 419 nm. The fluorescence decay is a single exponential decay with a lifetime of  $4.0 \pm 0.1$  ns (Fig. 2).

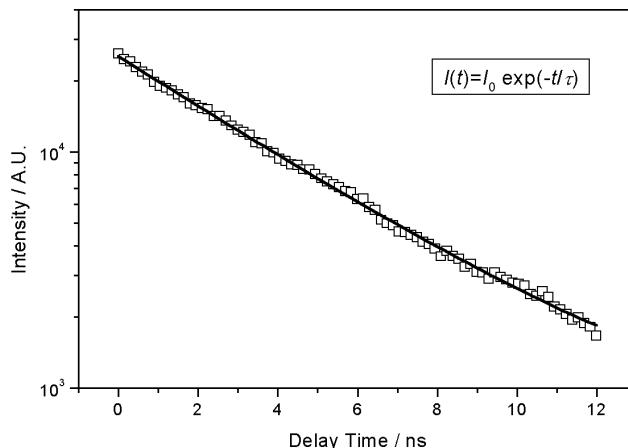


Fig. 2: Fluorescence decay of benzoic acid at pH 6.0

The equilibrium concentrations of all species in the sample solutions were calculated from the ratio of the fluorescence intensities to the initial concentration of benzoic acid. The formation constant was yielded by graphic analysis of the linearized law of mass action of the complex reaction, including the constant pH and the dissociation constant of benzoic acid (Fig. 3). In this way the formation constant of the 1:1 uranyl benzoate complex was determined to be  $\log \beta_{11} = 2.99 \pm 0.06$ . This result is in good agreement with the potentiometrically determined value of  $\log \beta_{11} = 2.91 \pm 0.07$  /1/.

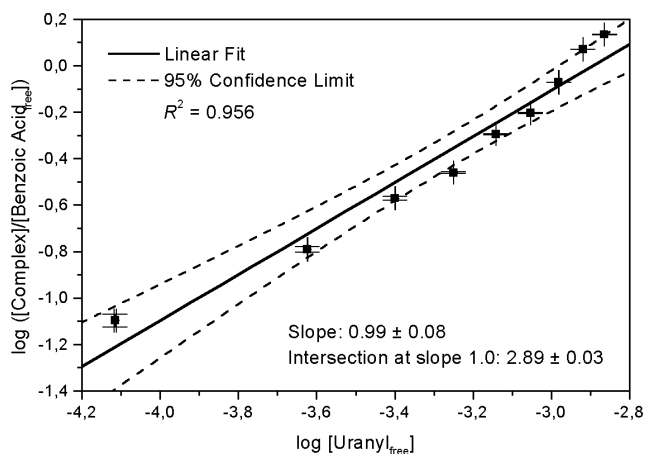


Fig. 3: Graphic determination of the formation constant

## Acknowledgment

This study was supported by the DFG under Contract No. BE 2234/3-1.

## References

- /1/ Vulpius, D. et al., Report FZR-318 (2001) p. 12
- /2/ Rutsch, M. et al., Report FZR-272 (1999) p. 21
- /3/ Geipel, G. et al., Report FZR-318 (2001) p. 10

# COMPLEX FORMATION OF URANIUM(VI) WITH ORGANIC LIGANDS STUDIED BY FS-TRLFS PART II: VANILLIC ACID

D. Vulpius, G. Geipel, L. Baraniak, G. Bernhard, Th. Fanghänel

By application of the time-resolved laser-induced fluorescence spectroscopy with ultrashort laser pulses (fs-TRLFS), the first dissociation constant of vanillic acid was determined to be  $pK_1 = 4.28 \pm 0.05$ . Self-absorption of the vanillic acid fluorescence by the uranium(VI) was observed, which made impossible the determination of the complex formation constant.

## Introduction

We continued our studies on the complexation of uranium(VI) with organic ligands by application of the time-resolved laser-induced fluorescence spectroscopy with ultrashort laser pulses (fs-TRLFS) and investigated the complex formation of uranium(VI) with vanillic acid. Experimental details are described in a previous contribution [1].

## Dissociation Constant of Vanillic Acid

Fig. 1 shows the fluorescence spectra of vanillic acid as a function of pH. The dominating species in the weak acidic region is the single negatively charged vanillate ion with an emission maxima at 328 nm and with a fluorescence lifetime of  $285 \pm 6$  ps. In the strong acidic region, the undissociated molecule of vanillic acid is present, which weakly fluoresces. The emission maxima is at 361 nm, and the fluorescence lifetime is  $74 \pm 5$  ps.

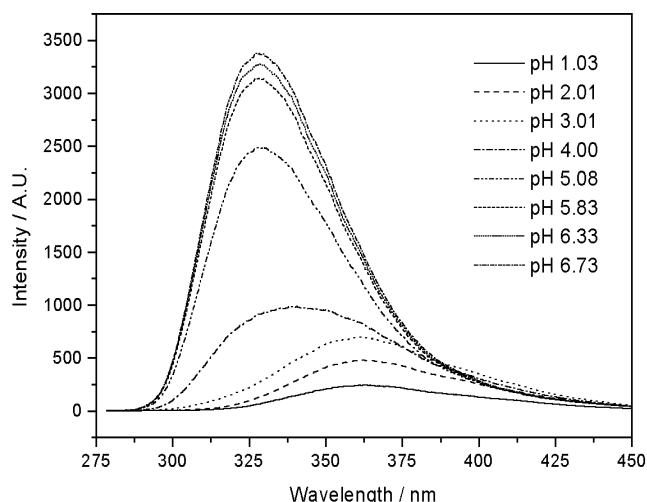


Fig. 1: Fluorescence spectra of vanillic acid as a function of pH

The particular fluorescence intensities of the undissociated molecule and the anion can be calculated from the fluorescence decay curve with the help of the fluorescence lifetimes of each species. The ratio of the concentrations of both species as a function of the hydrogen ion concentration is derived from the ratio of the fluorescence intensities of the anion and the completely dissociated molecule. The intersection of the graphic solution to the linearized law of mass action results in the first dissociation constant of vanillic acid, which was determined to be  $pK_1 = 4.28 \pm 0.05$  at an ionic strength of 0.1 M ( $\text{NaClO}_4$ ) and at  $22 \pm 1$  °C (Fig. 2). This value is in good agreement with results of other methods (Tab. 1).

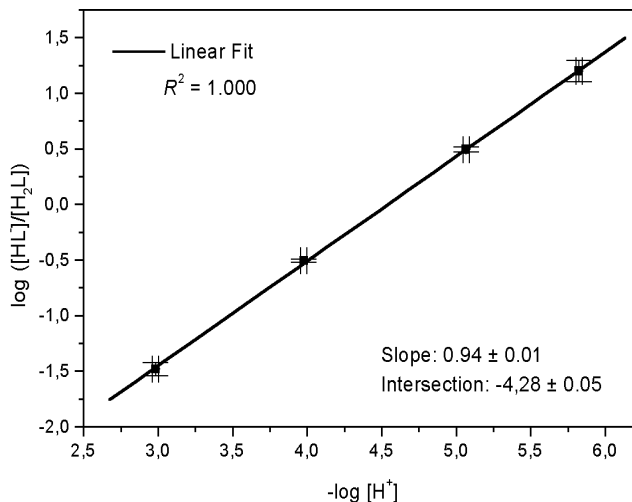


Fig. 2: Graphic determination of the dissociation constant

Reference	Method	$T / ^\circ\text{C}$	$pK_1$
Nor63 [2/]	spectrophotometric	25	$4.30 \pm 0.02^*$
This work	potentiometric	25	$4.35 \pm 0.01$
This work	spectrophotometric	22	$4.28 \pm 0.01$
This work	fs-TRLFS	22	$4.28 \pm 0.05$

\* Calculated from the  $l = 0$  value using the Davies equation

Tab. 1: First dissociation constant of vanillic acid at an ionic strength of 0.1 M

## Complex Formation of Uranium(VI) with Vanillic Acid

The formation constant of the 1:1 uranyl vanillate complex cannot be determined by the method described in [1]. The reason for this is the self-absorption of the vanillic acid fluorescence by the uranium(VI). This effect is stronger at the emission wavelength of the vanillate ion of 328 nm than at that one of the benzoate ion of 419 nm. In consequence, an excessive fluorescence quenching occurs as a function of the uranium(VI) concentration, which pretends a too high complex formation constant.

## Acknowledgment

This study was supported by the DFG under Contract No. BE 2234/3-1.

## References

- [1/ Vulpius, D. et al., this report, p. 9  
[2/ Nordström, C.-G. et al., Suom. Kemistil. **B36**, 105 (1963)

# COMPLEX FORMATION OF URANIUM(VI) WITH GLUCOSE 1-PHOSPHATE

A. Koban, G. Geipel, G. Bernhard

The complex formation of uranium(VI) with glucose 1-phosphate was determined by time-resolved laser-induced fluorescence spectroscopy (TRLFS). The complex shows no fluorescence, and the formation constant of  $UO_2(C_6H_{11}O_6PO_3)$  was calculated to be  $\log \beta_{11}=5.60$  at  $pH=4$ .

The uptake of heavy metals into plants is commonly quantified by the soil-plant transfer factor. Up to now little is known about the chemical speciation of actinides in plants. To compare the spectroscopic data of uranium complexes in plants [1] with model compounds, we investigate the complexation of uranium with relevant bioligands of various functionalities.

We studied the complexation of uranium(VI) with glucose 1-phosphate ( $C_6H_{11}O_6PO_3^{2-}$ , G1P), using TRLFS. The experiments were performed at a fixed uranyl concentration ( $10^{-5}$  M) as a function of the ligand concentrations ( $10^{-5}$  to  $2 \times 10^{-3}$  M) at  $pH=4.0$  and an ionic strength of 0.1 M ( $NaClO_4$ ).

Fig. 1 shows the TRLFS spectra of uranium(VI) as a function of the ligand concentrations.

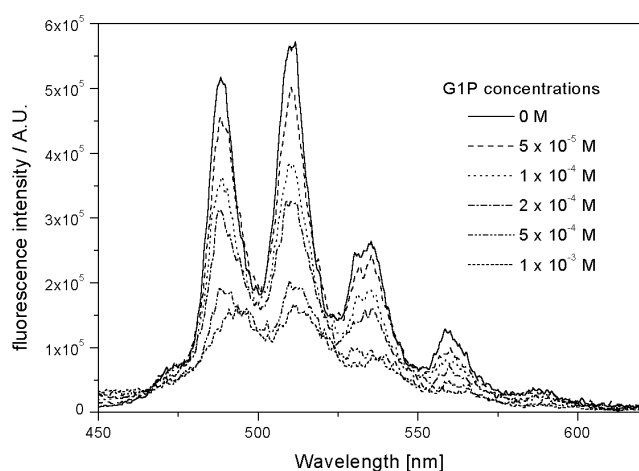


Fig. 1: TRLFS-spectra of uranium(VI) ( $10^{-5}$  M) as a function of the glucose 1-phosphate concentration at  $pH=4$ .

With increasing ligand concentrations we observed a decrease in fluorescence intensities. At higher ligand concentrations only a small red shift of the emission bands caused by the dominant uranyl hydroxide species was detectable (Tab. 1).

c [G1P]	Fluorescence emission bands / nm			
0 M	488.6	510.5	534.5	560.4
$5 \times 10^{-5}$ M	489.1	510.7	534.7	561.0
$1 \times 10^{-4}$ M	488.9	510.7	534.7	560.9
$5 \times 10^{-4}$ M	490.2	511.7	536.5	563.8
$1 \times 10^{-3}$ M	491.9	513.9	538.4	564.5

Tab. 1: Main fluorescence emission bands of uranium(VI) as a function of the glucose 1-phosphate concentration.

The TRLFS spectra indicate the presence of the free uranyl ion with a lifetime of  $1.3 \pm 0.3 \mu s$  and a uranyl hydroxide species with a lifetime of  $15 \pm 3 \mu s$  at higher ligand concentrations. This uranyl hydroxide species was eliminated for further considerations. We

therefore conclude that the complexed uranyl glucose species shows no fluorescence properties.

In view of similar reactions of glucose 1-phosphate with heavy metals and taking into account the values of the dissociation constants of the two protonic ligand  $H_2G1P$  [2] the complex formation reaction at  $pH=4$  can be written as:



To find out the right stoichiometry we performed a slope analysis (Fig. 2). The concentration of the free uranyl ion was determined on the basis of the measured fluorescence spectra. These data were used to calculate the corresponding concentration of the uranyl glucose phosphate complex and the non complexed ligand.

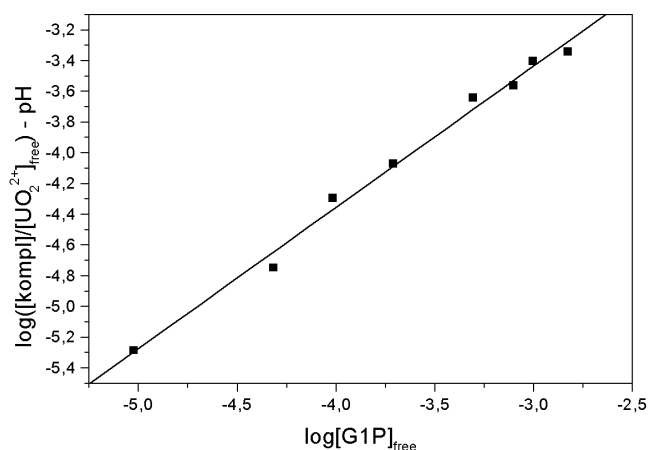


Fig. 2: Slope analysis of the complex reaction of uranium(VI) and glucose 1-phosphate.

The slope of  $0.90 \pm 0.03$  indicates a predominant 1:1 complexation.

Eq. (1) can now be restated as follows:



The equilibration constant of this reaction was calculated to be  $\log k' = -0.38 \pm 0.03$ .

Taking the dissociation of the glucose 1-phosphate



into consideration ( $\log k_2 = -5.98$  [2]) we obtain the complex formation reaction



with a stability constant of  $\log \beta_{11} = 5.60 \pm 0.03$  at  $pH=4$  and ionic strength of 0.1 M.

## References

- /1/ Günther, A. et al., Zwischenbericht DFG-BE 2234/1-1
- /2/ Kramer-Schnabel, U. et al., Inorg. Chem. **30**, 1248 (1991)

# COMPLEX FORMATION OF URANIUM (VI) WITH GLUTATHIONE

A. Günther, G. Geipel, G. Bernhard

We studied the complex formation of uranium (VI) with glutathione by time-resolved laser-induced fluorescence spectroscopy. A 1:1 complex was found with a formation constant of  $\log K = 3.36 \pm 0.09$  at pH 4.

## Introduction

Amino acids, various peptides and proteins are fundamental components of living cells. The amino acids glycine, cysteine and glutamic acid form the tripeptide glutathione by condensation. Glutathione represents the basic element of the phytochelatines. In plant chemistry phytochelatines are well known as heavy metal binding peptides [1]. We studied the complexation of uranium with glutathione as a model compound so as to describe interactions of uranium with plants.

## Experimental and results

The stock solutions of glutathione were freshly prepared from pure chemicals. The concentration of glutathione ranged from  $1 \cdot 10^{-5} \text{M}$  to  $2 \cdot 10^{-4} \text{M}$ . The uranyl concentration was  $1 \cdot 10^{-5} \text{M}$ . All fluorescence measurements were performed at an ionic strength of  $I=0.1 \text{M}$  ( $\text{NaClO}_4$ ). The pH value of the studied solutions was 4. The setup of the time-resolved laser-induced fluorescence spectroscopy was described in [2]. We used the 266nm laser pulse as excitation wavelength.

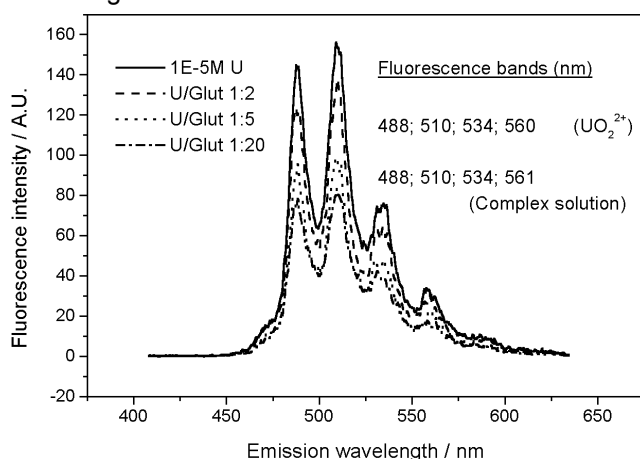
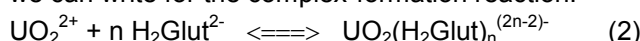


Fig. 1: Fluorescence spectra of uranium (VI) as a function of the glutathione concentration at pH=4

Fig. 1 shows a set of fluorescence spectra of complex solutions. With increasing glutathione concentration we observed a decrease in fluorescence intensity. The position of the emission maxima in the spectra remained unchanged. We derived two fluorescence lifetimes. The shorter one ( $\sim 1.5 \mu\text{s}$ ) was assigned to the free uranyl ion and the larger one ( $\sim 3 \mu\text{s}$ ) to the hydroxide species. The uranyl-glutathione complex does not seem to fluoresce. Considering the protolyse balance at pH 4



we can write for the complex-formation reaction:



By applying the mass action law and transformation on a logarithmic scale, we obtain

$$\log \frac{[\text{UO}_2(\text{H}_2\text{Glut})_n^{(2n-2)-}]}{[\text{UO}_2^{2+}]} = \log K + n \log [\text{H}_2\text{Glut}^{2-}] \quad (3)$$

Equation 3 is a linear function of  $\log[\text{H}_2\text{Glut}^{2-}]$ . The concentrations of species involved are determined via the free uranyl concentration, which is obtained from the fluorescence intensity of the uranyl ion in the spectra.

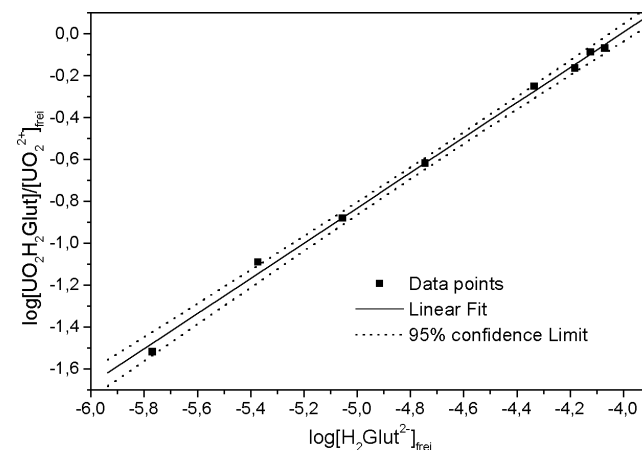


Fig. 2: Logarithm of the concentration ratio  $[\text{UO}_2\text{H}_2\text{Glut}]/[\text{UO}_2^{2+}]$  as function of the free glutathione concentration

The slope  $n$  of the linear fit, illustrated in Fig.2, was determined to be  $0.84 \pm 0.02$ , which indicates the formation of a 1:1 complex. A formation constant was calculated to be  $\log K_{(I=0.1\text{M})} = 3.36 \pm 0.09$ .

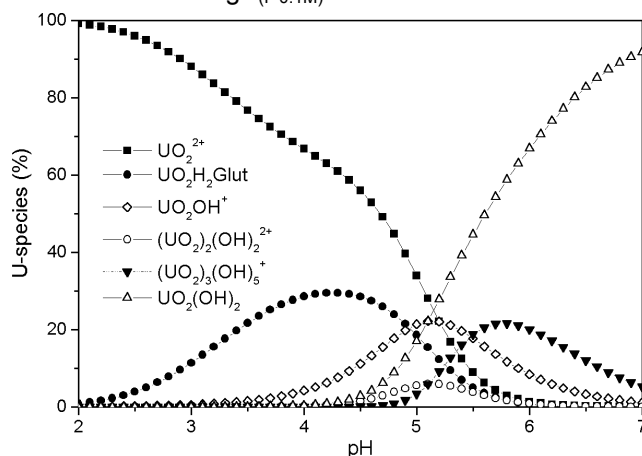


Fig. 3: Speciation of uranium (VI) in the presence of glutathione as a function of pH  $[\text{U}_0]=1\text{E-}5\text{M}$ ;  $[\text{Glut}_0]=1\text{E-}4\text{M}$

The speciation in Fig. 3 shows that only 30% of glutathione is fixed in the complex by 10% excess of glutathione at pH4.

## Acknowledgment

This study was supported by DFG (BE 2234/1-1, 1-2).

## References

- [1] Hock, B., Elstner, E.F.; *Lehrbuch der Pflanzentoxikologie*, Schadwirkungen auf Pflanzen, Spektrum Akad. Verlag GmbH, Heidelberg 53 (1995)
- [2] Geipel, G. et al.; *Radiochim. Acta* **75**, 199-204 (1996)

# SYNTHESIS AND CHARACTERIZATION OF HUMIC ACIDS WITH DISTINCT REDOX CAPACITIES

S. Sachs, K.H. Heise, G. Bernhard

Various humic acids with distinct redox capacities were synthesized, based on the oxidation of hydroquinone in alkaline solution in the presence or absence of amino acids. The synthesized humic acids show Fe(III) redox capacities which are up to 10 times higher than that of natural humic acid from Aldrich.

## Introduction

Humic acids (HA) can affect the oxidation state of actinide ions in natural systems, thus influencing the migration behavior of these pollutants. In order to study the redox properties of HA and the redox stability of actinide humate complexes in more detail as well as stabilizing the lower oxidation states of actinide ions in migration experiments with HA, we developed HA with distinct redox functionalities. The redox activity of HA can be ascribed to the hydroquinone-quinone system and to the oxidation of phenols. In order to obtain HA with a distinct redox behavior, our aim was to synthesize HA with large amounts of phenolic OH groups.

## Experimental

The syntheses performed are based on the oxidation of hydroquinone in alkaline solution in the presence or absence of amino acids (glycine and glutamic acid). Potassium peroxodisulfate was used as the oxidizing agent [1,2]. The humic acid-like fractions of the oxidation products were separated from the reaction mixture by precipitation with HCl, dialyzed, and lyophilized. All synthesized HA were characterized in terms of their elemental composition, functional group content and their structure. The Fe(III) redox capacities (RC) of these HA were additionally determined as explained in [3] ([Fe(III)]<sub>0</sub>: 8.6±0.1 mmol/L, [HA]: 0.12 g/L, pH 3, I: 0.1 M KCl) and compared with the synthetic HA type M42 [4] and natural HA from Aldrich (AHA).

By way of examples we will discuss the following HA: *type R9* - oxidation product of hydroquinone, *type R17* - oxidation product of hydroquinone and glycine and *type R18* - oxidation product of hydroquinone and glutamic acid.

## Results and discussion

Tab. 1 summarizes some characteristics of HA types R9, R17 and R18 compared with HA type M42 and AHA. All humic acid-like oxidation products of hydroquinone show larger amounts of phenolic and other acidic OH groups than HA type M42 and AHA. HA type R9 has the highest phenolic OH group content but a lower amount of COOH groups. By contrast HA types R17 and R18 synthesized in the presence of amino acids show COOH group contents that are comparable to AHA.

Humic acid	COOH (meq/g)	PEC <sup>a</sup> (meq/g)	phenol. OH <sup>b</sup> (meq/g)
R9	1.92 ± 0.05	2.68 ± 0.01	7.2 ± 0.1
R17	4.33 ± 0.17	4.57 ± 0.12	5.5 ± 0.4
R18	4.09 ± 0.05	4.61 ± 0.07	5.8 ± 1.5
M42 (M145)	3.76 ± 0.09	3.51 ± 0.07	2.0 ± 0.2
AHA (A2/98)	4.49 ± 0.14	4.64 ± 0.36	3.1 ± 0.1

<sup>a</sup> PEC: Proton exchange capacity, <sup>b</sup> phenolic and other acidic OH groups.

Tab. 1: Functional group contents of HA

Fig. 1 shows the RC of HA types R9, R17 and R18 as a function of time compared with HA type M42 and AHA. The RC of the HA after about 7 weeks equilibration are summarized in Tab. 2.

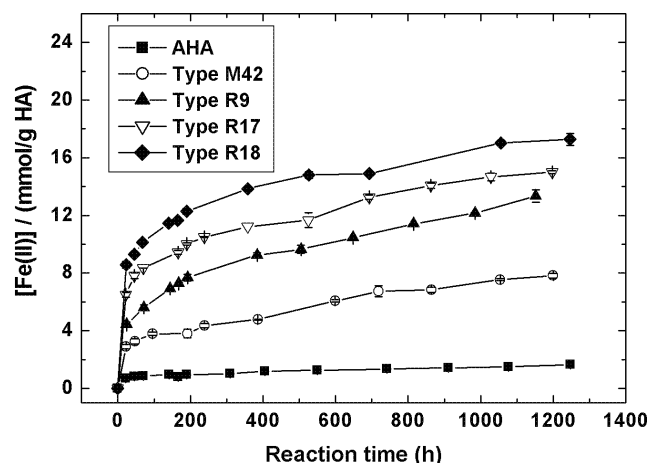


Fig. 1: Reduction of Fe(III) by different humic acids

Humic acid	Fe(III) RC (meq/g HA)	Fe(III) RC/phenolic OH
R9	13.4	1.9
R17	15.0	2.7
R18	17.3	3.0
M42 (M145)	7.8	3.9
AHA (A2/98)	1.6	0.5

Tab. 2: Redox capacities of HA after 7 weeks

All synthetic HA based on hydroquinone show a significantly higher Fe(III) RC than HA type M42 and AHA. It can therefore be concluded that it is possible to synthesize humic acid-like substances with distinct RC based on the oxidation of hydroquinone. The RC of these substances can be changed by varying the synthesis conditions. Referring the RC of the HA to their phenolic/acidic OH group content (Tab. 2), it becomes possible to draw conclusions concerning the kind of redox active, i.e. electron-transferring, functional groups. For all synthetic HA this ratio is higher than 1. That means that there are still other functional groups than phenolic/acidic OH groups and/or other processes which contribute to the reduction of Fe(III) ions.

## Acknowledgment

This work was supported by the BMWi (No.02E9299).

## References

- Eller, W., Koch, K., Ber. Dt. Chem. Ges. **53**, 1469 (1920)
- Adhikari, M. et al., Proc. Indian Natn. Sci. Acad. **51A**, 876 (1985)
- Mack, B. et al., Report FZR-285 (2000) p.40
- Pompe (Sachs), S. et al., Report FZR-290 (2000)

# NIR SPECTROSCOPIC STUDY OF THE NEPTUNIUM(V) COMPLEXATION BY HUMIC ACIDS WITH DIFFERENT FUNCTIONALITIES

S. Sachs, K.H. Heise, G. Bernhard

The influence of phenolic OH groups on the neptunium(V) complexation by humic acids was studied at pH 7 and pH 8 applying chemically modified humic acids with blocked phenolic OH groups.

## Introduction

In order to answer the question about the influence of different functional groups on the metal ion complexation by humic acids (HA) we continued our studies on the Np(V)-HA-complexation using HA with different functionalities /1/. We studied the Np(V)-HA-complexation by unmodified and chemically modified HA with blocked phenolic and other blocked acidic OH groups /2/ by near-infrared (NIR) spectroscopy.

## Experimental

Np(V) humate solutions were prepared under N<sub>2</sub> atmosphere from commercially available natural HA Aldrich (AHA), synthetic HA type M42, as well as modified HA AHA and M42 with blocked phenolic and other blocked acidic OH groups (AHA-PB, M42-PB) /2/. The phenolic/acidic OH group content of AHA, AHA-PB, M42 and M42-PB amounts to 3.1 meq/g, 0.5 meq/g, 2.0 meq/g and 0.5 meq/g, respectively. In our experiments the HA concentration ([HA(I)] /3/) was held constant at 1·10<sup>-3</sup> mol/L. The Np(V) concentration was varied between 5·10<sup>-5</sup> and 1.3·10<sup>-3</sup> mol/L. The studies were performed in 0.1 M NaClO<sub>4</sub> solutions at pH 7 for all HA and at pH 8 for AHA and AHA-PB.

## Results and discussion

The NIR absorption spectra were deconvoluted into single peaks for the free NpO<sub>2</sub><sup>+</sup> ion and the Np(V) humate complex (NpO<sub>2</sub>HA(I)) to determine the species concentration in solution (Fig. 1).

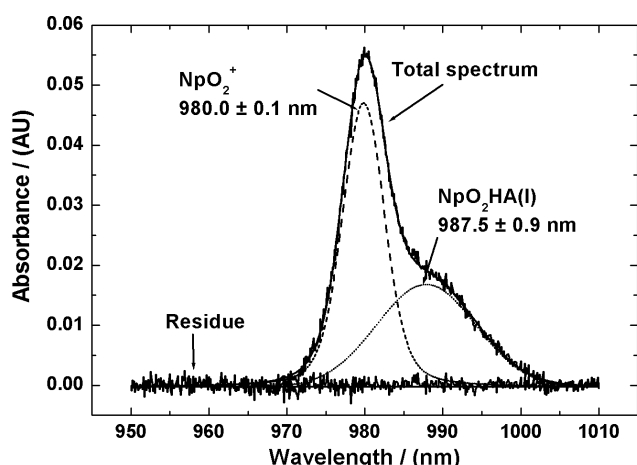


Fig. 1: NIR absorption spectrum of Np(V) in HA solution and its deconvoluted absorption bands (AHA, [HA(I)]: 1·10<sup>-3</sup> mol/L, [NpO<sub>2</sub><sup>+</sup>]: 1.7·10<sup>-4</sup> mol/L, pH 7, I: 0.1 M NaClO<sub>4</sub>)

The experimental data were evaluated applying the metal ion charge neutralization model /3/. According to this model HA should have comparable Np(V) complexation constants (log β). Differences in the complexation behavior of HA under the given experimental conditions should be reflected in different

loading capacities (LC, /3/), which represent the mole fraction of maximal available metal ion complexing sites of HA under the applied conditions. Tab. 1 summarizes the spectroscopically determined complexation data (LC, log β) for the investigated HA at pH 7 and pH 8.

Humic acid	pH	LC <sup>a</sup> / (%)	log β <sup>a</sup>
AHA	7.0	10.0 ± 1.5	3.87 ± 0.19
	8.0	35.3 ± 3.7	3.59 ± 0.17
AHA-PB	7.0	6.5 ± 2.4	3.39 ± 0.15
	8.0	12.3 ± 2.6	3.46 ± 0.22
M42	7.0	11.2 ± 1.1	3.50 ± 0.15
M42-PB	7.0	5.3 ± 1.0	3.48 ± 0.11

<sup>a</sup> ± 3σ

Tab. 1: Complexation data for the complexation of Np(V) by modified and unmodified HA.

Within the experimental errors, the HA show similar Np(V) complexation constants that are comparable to literature data, e.g., for HA GoHy-537 /4/. However, comparing the LC of the corresponding modified and unmodified HA at pH 7 and pH 8 it becomes obvious that modified HA AHA-PB and M42-PB have significant lower LC than the original HA AHA and M42, respectively. This result points to a decrease of the mole fraction of HA binding sites for the Np(V) complexation due to the blocking of phenolic/acidic OH groups. Thus, it can be concluded that phenolic OH groups can be involved into the interaction between HA and Np(V) in the neutral pH range. Comparable results were already found for the uranium(VI) complexation by HA at pH 4 /2/. Although the blocking of phenolic OH groups decreases the number of HA complexing sites, the structural parameters of Np(V) humate complexes are not significantly changed due to this chemical modification. This was found by EXAFS measurements /1/.

Varying the pH of the Np(V) humate solutions from pH 7 to pH 8, the LC of HA AHA as well as of HA AHA-PB increases as expected. However, the reduction of the LC due to the modification (LC<sub>AHA</sub>→LC<sub>AHA-PB</sub>) is higher at pH 8 (65 %) than at pH 7 (35 %). That points to the fact that the influence of phenolic and other acidic OH groups on the Np(V) complexation by HA increases with increasing pH.

## Acknowledgment

This work was supported by the BMWi (No. 02E9299).

## References

- /1/ Pompe (Sachs), S. et al., Report FZR-318, p.15 (2001)
- /2/ Pompe (Sachs), S. et al., Radiochim. Acta **88**, 553 (2000)
- /3/ Kim, J.I. et al., Radiochim. Acta **65**, 111 (1994)
- /4/ Marquardt, C. et al., Radiochim. Acta **80**, 129 (1998)

# PLUTONIUM(III) HUMATE COMPLEXATION STUDIED BY XAFS SPECTROSCOPY

K. Schmeide, S. Sachs, T. Reich, C. Hennig, H. Funke, A. Roßberg, G. Geipel, K.H. Heise, G. Bernhard

Structural parameters of the near-neighbor surrounding of Pu(III) sorbed onto humic substances were determined at pH 1 by extended X-ray absorption fine structure (EXAFS) spectroscopy. The structural parameters of the Pu(III) humates are compared with literature data of Pu(III) and Pu(IV) hydrates.

## Introduction

The objective was to investigate the structure of Pu(III) in complexes with humic substances. Our previous XAFS study /1/ had shown that part of the Pu(III) humate was oxidized to Pu(IV). Therefore, we repeated this experiment under improved conditions. For the sample preparation, the pH value was lowered from 2 to 1. The samples were sealed in polyethylene cuvettes and transported to Grenoble under N<sub>2</sub> atmosphere.

## Experimental

<sup>242</sup>Pu was purified by anion exchange chromatography using TEVA resin™. Purified Pu(IV) was electrochemically reduced to Pu(III). Pu(III) samples were prepared from Kranichsee fulvic acid (KFA) and from synthetic humic acid type M42 at pH 1 (0.1 M HClO<sub>4</sub>) under inert gas conditions. The Pu loading of the resulting wet pastes of KFA and M42 was 11.6 and 10.7 mg Pu per g sorbent, respectively. Pu L<sub>III</sub>-edge XAFS spectra were collected in fluorescence mode at the Rossendorf Beamline at the ESRF in Grenoble.

## Results and discussion

The trivalent oxidation state of Pu and its stability in the complexes with humic substances within the time of the experiment is verified by XANES spectroscopy. In Fig. 1, the XANES spectra of Pu(III)-KFA and Pu(III)-M42 are shown in comparison to that of Pu(III) hydrate. The energy scale of the spectra was calibrated with a Zr metal foil (Zr K edge at 17998 eV). The edge energy of the three spectra is identical (Pu(III) hydrate: 18059.0 eV, Pu(III) humates: 18059.2 eV). This confirms that the humate complexes contain exclusively Pu(III).

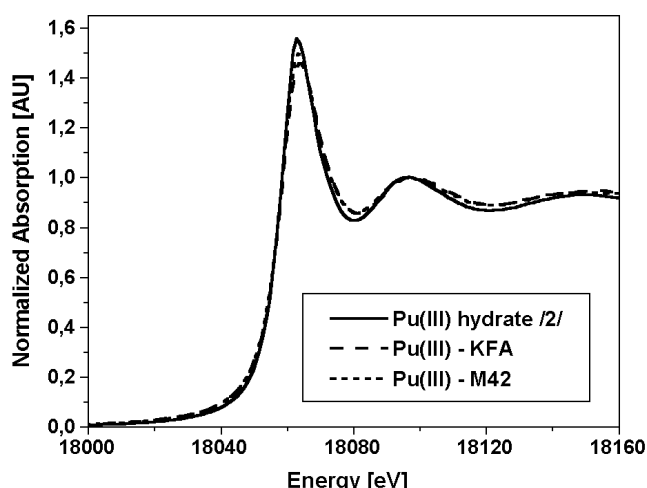


Fig. 1: Normalized Pu L<sub>III</sub>-edge XANES spectra

The Pu L<sub>III</sub>-edge k<sup>3</sup>-weighted EXAFS spectra of the Pu(III) humates and corresponding Fourier transforms (FTs) are shown in Fig. 2. Both the EXAFS oscillations and the FTs of the samples are similar. The FTs indicate a single coordination shell (Pu-O) arising from the ligands.

The structural parameters given in Tab. 1 agree with the conclusion drawn from the XANES spectra. The Pu-O bond length in the Pu(III) humate complexes is significantly longer than that of Pu(IV) hydrate. Furthermore, no evidence for the formation of polynuclear Pu(IV) species was found in the EXAFS spectra.

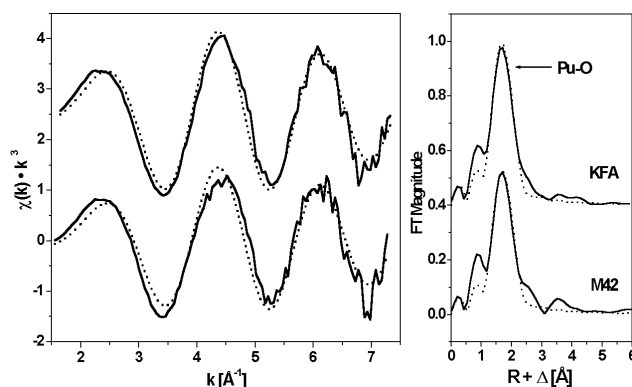


Fig. 2: Raw Pu L<sub>III</sub>-edge k<sup>3</sup>-weighted EXAFS spectra and corresponding Fourier transforms of Pu(III) samples (without phase corrections). Solid lines: experiment, dashed lines: fit

Sample	Shell	N	R [Å]	σ <sup>2</sup> [Å <sup>2</sup> ]	E <sub>0</sub> [eV]
Pu(III)-KFA	Pu-O	7.3±1.2	2.45±0.02	0.0150	-17.3
Pu(III)-M42	Pu-O	6.1±1.4	2.45±0.02	0.0137	-17.0
Pu(III)·nH <sub>2</sub> O /2/	Pu-O	7.6±0.6	2.48±0.01	0.0102	-16.8
Pu(IV)·nH <sub>2</sub> O /3/	Pu-O	8	2.39	0.0118	

The 95 % confidence limits are given for N and R as estimated by EXAFSPAK.

Tab. 1: Structural parameters of Pu samples

Within the experimental error, the coordination numbers determined for the Pu-O shell of the humate complexes agree well with the value reported for the hydrated Pu(III) aquo ion in 1 M HClO<sub>4</sub> /2/. The bond lengths determined for the Pu(III) humate complexes are 0.03 Å shorter than for the Pu(III) hydrate. A similar shortening of the bond length has been observed for U(VI) and Np(IV) humates /4, 5/ upon complexation of these actinides with the functional groups (predominantly -COOH) of the humic substances.

## Acknowledgment

This work was supported by the BMWi (no. 02E9299).

## References

- /1/ Schmeide, K. et al., Report FZR-318, p.16 (2001)
- /2/ Reich, T. et al., Report FZR-285, p.72 (2000)
- /3/ Ankudinov, A.L. et al., Phys. Rev. B **57**, 7518 (1998)
- /4/ Denecke, M. et al., Radiochim. Acta **82**, 103 (1998)
- /5/ Schmeide, K. et al., Report FZR-318, p.14 (2001)

# COMPLEX FORMATION OF URANIUM(VI) WITH LIGNIN DEGRADATION PRODUCTS

D. Vulpius, L. Baraniak, G. Bernhard, Th. Fanghänel

The complex formation of uranium(VI) with benzoic acid, phenol, 4-hydroxybenzoic acid, and vanillic acid was studied by potentiometric pH titration. Only carboxylic 1:1 complexes were found in the log K range from 2.90 to 2.97.

## Introduction

Monomeric intermediate products of the lignin degradation such as 4-hydroxybenzoic acid and vanillic acid (4-hydroxy-3-methoxybenzoic acid) may play an important role in the migration of uranium(VI) in flooded mines. It is, therefore, necessary to study the complexation behavior of uranium(VI) with these organic compounds and to determine the formation constants of the possible complexes. Experimental details of the determination of complex formation constants by potentiometric pH titration are described in a previous contribution /1/.

## Dissociation Constants of the Ligands

In order to calculate complex formation constants from titration curves as shown in Fig. 1, the dissociation constants of the ligands have to be known. It is, furthermore, reasonable to study the complexation behavior of those compounds which are basic components of the more complicated ligands in order to obtain an indication of possible complexes of these ligands. The dissociation constants of the above-mentioned lignin degradation products as well as their carboxylic and phenolic basic compound are listed in Tab. 1.

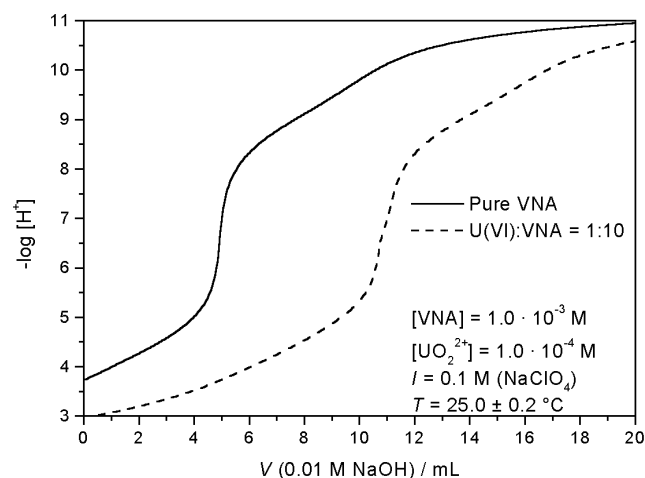


Fig. 1: Titration curves of pure vanillic acid (VNA) and vanillic acid with addition of uranium(VI)

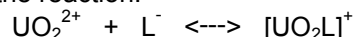
Ligand	Reference	pK <sub>1</sub> (carboxylic)	pK <sub>2</sub> (phenolic)
Benzoic ac.	NIST /2/ this work	4.01 ± 0.02 4.06 ± 0.01	
Phenol	NIST /2/ this work		9.77 ± 0.07 9.92 ± 0.01
4-Hydroxybenzoic ac.	NIST /2/ this work	4.37 ± 0.01 4.41 ± 0.01	8.99 ± 0.04 9.06 ± 0.01
Vanillic ac.	Nor63 /3/ this work	4.30 ± 0.02* 4.35 ± 0.01	9.18 ± 0.02* 8.94 ± 0.01

\* Calculated from the  $I = 0$  value using the Davies equation

Tab. 1: Dissociation constants at  $I = 0.1$  M and 25 °C

## Complex Formation Constants

The formation constants of the various uranyl complexes are reported in Tab. 2. Log K values are calculated for the reaction:



where  $\text{L}^-$  is the single negatively charged anion of the ligand.

Ligand	Reference	T / °C	log K
Benzoic ac.	Ram71 /4/ this work	31	2.57
		25	2.91 ± 0.07
Phenol	NIST /2/ this work	20 25	5.8 no complex
4-Hydroxybenzoic ac.	Ram71 /4/ this work	31	2.38
		25	2.90 ± 0.03
Vanillic ac.	this work	25	2.97 ± 0.06

Tab. 2: Formation constants of the 1:1 uranyl complexes at  $I = 0.1$  M

Only carboxylic 1:1 complexes were found. Speciation diagrams as shown in Fig. 2 demonstrate that the carboxylic complexes occur in the weak acidic region. The existence of the uranyl phenolate complex could not be confirmed.

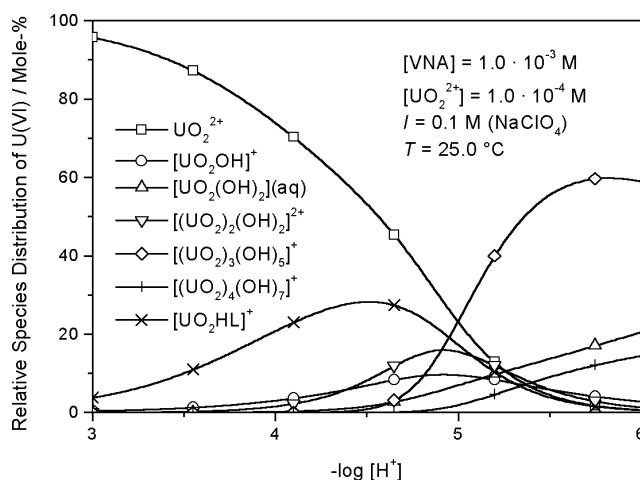


Fig. 2: Relative species distribution of uranium(VI) in vanillic acid as a function of the hydrogen ion concentration

## Acknowledgment

This study was supported by the DFG under Contract No. BE 2234/3-1.

## References

- /1/ Vulpius, D. et al., Report FZR-318 (2001) p. 12
- /2/ Martell, A.E. et al., *NIST Critically Selected Stability Constants of Metal Complexes Database*, Version 5.0, 1998
- /3/ Nordström, C.-G. et al., *Suom. Kemistil.* **B36**, 105 (1963)
- /4/ Ramamoorthy, S. et al., *J. Inorg. Nucl. Chem.* **33**, 2713 (1971)

# REDOX REACTIONS IN FLOODED URANIUM MINES CAUSED BY NATURAL WOOD DEGRADATION

A. Abraham, L. Baraniak, G. Bernhard

Answering the question whether U(VI) and As(V) will be reduced and precipitated as U(OH)<sub>4</sub> and As<sub>2</sub>S<sub>3</sub> in mine water as a result of natural wood degradation. Redox equilibria were calculated, depending on the decreasing redox potential.

## Introduction

Natural wood degradation under anaerobic conditions generates a strong reducing environment characterized by the release of hydrogen sulfide and methane. Under such conditions some important mine water constituents will be successively reduced, often with the result of a drastic change in mobility. Using the data provided by Sigg et al. /1/ and Brookins /2/, the redox reactions following each other with decreasing potential were calculated (Fig.1).

## Results and Discussion

When the redox potential decreases, the dissolved oxygen is first consumed. Then the manganese oxides, such as *pyrolusite*, *manganite*, *hausmannite*, are reduced in the range from 530 to 550 mV at pH 7, resulting in an Mn<sup>2+</sup> concentration from 3,6·10<sup>-5</sup> to 1,5·10<sup>-4</sup> mol/L (2 - 8 ppm Mn<sup>2+</sup>), i.e. solid oxides are dissolved into manganese(II).

Stronger reducing conditions lead to the reduction of uranium(VI) and iron(III). A decrease in Eh to a level of 240 mV in acidic solution (pH < 4.8) causes the reduction of uranium(VI) to insoluble uranium(IV)-hydroxide. If carbonate is present in a concentration of 2·10<sup>-2</sup> mol/L, the redox potential has to fall to 70 mV to precipitate uranium in that way. If the redox potential falls below zero, iron oxides such as *goethite*, *haematite* and *magnetite* are dissolved. Eh values between 5 and -30 mV relate to Fe<sup>2+</sup> concentrations in the range from 3,6·10<sup>-5</sup> to 1,4·10<sup>-4</sup> mol/L (2 - 8 ppm Fe<sup>2+</sup>). In competition with iron(III) reduction, arsenic(V) is reduced to arsenic(III) in the Eh range from +92 to -86 mV. At the beginning of HS<sup>-</sup> formation arsenic(III) is precipitated as As<sub>2</sub>S<sub>3</sub> (*auripigment*). In the presence of 5·10<sup>-5</sup> M H<sub>3</sub>AsO<sub>3</sub> this reaction starts at a HS<sup>-</sup> concentration of 4,2·10<sup>-11</sup> mol/L corresponding to a redox potential of -155 mV. Arsenic(III) is precipitated by a HS<sup>-</sup> concentration of 4,2·10<sup>-9</sup> mol/L which is reached at a potential of -170 mV, i.e. the immobilization of arsenic as an *auripigment* takes place in an Eh interval of 15 mV.

With a further small decrease the sulfate reduction increases. A redox potential of -182 mV is adjusted by a sulfide-to-sulfate-ratio of 10<sup>-5</sup>. Starting with a sulfate concentration of 2·10<sup>-2</sup> mol/L the formation of sulfide also leads to the precipitation of FeS<sub>2</sub>. A potential of -150 mV is required for that. Which means that the reversal of *pyrite* oxidation takes place parallel with the *auripigment* formation.

A further decrease in Eh is not possible because the sulfate concentration is relatively high and the processes involving sulfate reduction take place in the range from -150 to -180 mV. The reduction of dissolved organic matter to methane at a level of 10 ppm requires a redox potential of -294 mV. There is therefore no danger of methane generation in flooded

mines. In that respect sulfate is a naturally barrier that cannot be overcome in the mine water.

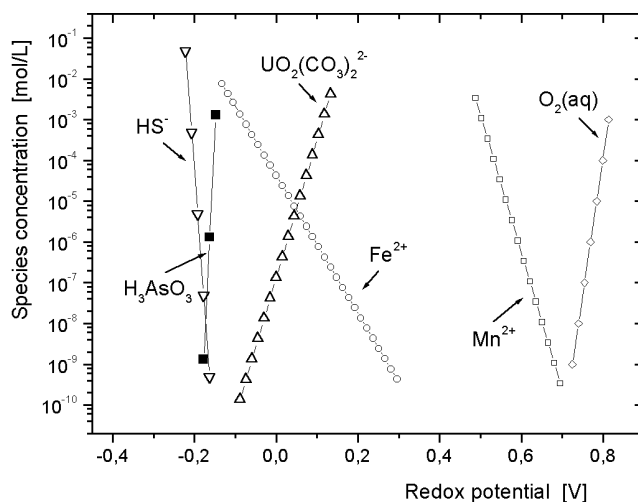


Fig. 1: Reduction of oxygen, Mn(IV), Fe(III), U(VI) As(V) and sulfate under mine water conditions

## Conclusion

The reductive immobilization of uranium and arsenic in the water of flooded mines is highly desirable as they would be stored as insoluble solids on the mine ground and would be excluded from being transported with the flowing water through the underground passages. The uranium content of the outflowing water from the flooded mine near the village of Pöhla (Erzgebirge) dropped by more than one order of magnitude (from 6 to 0.3 ppm) over a period of 5 years corresponding to a decrease of redox potential from 67 to 29 mV. That means that large amounts of uranium were immobilized as solid U(OH)<sub>4</sub>. In that way a natural purification process is given ever new impetus by the permanent microbial wood degradation. The risk of contaminating adjoining ground water tables decreases as the reductive immobilization proceeds. The main question is whether a comparable reducing environment develops in the mine water as it does in a bog ground where an intensive wood degradation takes place. The influence of the degradation of structural wood reinforcements in flooded mines on the mine water chemistry should be examined in environmental risk assessments and in modelling the long-term behaviour of flooded underground mines.

## References

- /1/ Sigg, L. et al.: *Aquatische Chemie*, Teubner, Stuttgart, 1994, S. 200
- /2/ Brookins, D.G.: *Eh-pH Diagrams for Geochemistry*, Springer, Berlin, 1988, p. 34

## COMPLEXATION OF CURIUM(III) BY GLYCOLIC ACID: TRFLS STUDIES

Th. Stumpf, Th. Fanghänel, I. Farkas<sup>1</sup>, I. Grenthe<sup>1</sup>

<sup>1</sup>Royal Institute of Technology (KTH), Department of Chemistry, Stockholm, Sweden

The complexation processes of Cm(III) by glycolic acid was investigated by time-resolved laser fluorescence spectroscopy. The fluorescence emission spectra of Cm(III) show three species: Cm/glycolate complex 1, 2 and 3 which were characterized by their peak maximum and their fluorescence emission lifetime /1/.

It is well-known that the acidity of the OH-group(s) in hydroxy-carboxylates increases strongly when they are coordinated to metal ions and that the resulting complexes are so stable that precipitation of hydrous oxides does not take place even at very high pH. These findings indicate that it is possible to investigate the solution chemistry of actinides at high pH, a region largely unexplored. Information of this type might be used to separate trivalent lanthanides and actinides, processes where  $\alpha$ -hydroxycarboxylates are commonly used. We utilized Cm(III) as a model for actinide(III) elements because its chemistry can be studied using time-resolved laser fluorescence spectroscopy (TRLFS) even at trace metal concentrations. This reduces the radiation level and has the additional advantage of avoiding precipitation of solid phases and the formation of polynuclear complexes.

The fluorescence spectra of  $9 \times 10^{-8}$  mol/L Cm(III) in 1.0 M sodium glycolate as a function of pH are shown in Fig. 1.

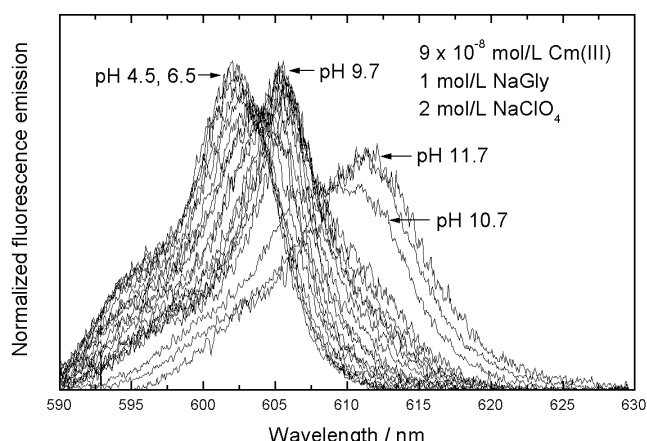


Fig. 1: Fluorescence emission spectra of Cm(III) in 1.0 mol/L sodium glycolate solution at various pH; spectra are scaled to the same peak area.

In the pH range between 4.5 and 6.5 only one Cm(III) peak with a maximum at 602.3 nm is observed. Its intensity decreases at pH > 6.5. In the same range a second peak at 605.6 nm appears simultaneously. The latter grows to a maximum at pH = 9.7 and then decreases as a third peak with a maximum at 611.3 nm appears. The extraordinary red-shift to 611.3 nm indicates a very strong binding between the curium and the glycolic acid.

From the measured composite spectra we calculated the contributions of the pure components using an eigenvector analysis. The measured Cm(III) spectra were resolved into three components with maxima at 602.3 (Cm complex 1), 605.6 (Cm complex 2) and 611.3 nm (Cm complex 3). Cm complex 1 and 2 are

characterized by the same fluorescence emission lifetime of  $206 \pm 3 \mu\text{s}$  implying that the number of quenching ligands in the first Cm(III) coordination sphere remains unchanged. An explanation for this observation is the formation of ternary hydrolyzed glycolate species at higher pH values. OH<sup>-</sup> ions act as quencher similar to H<sub>2</sub>O. The slope analysis for the reaction Cm complex 1  $\leftrightarrow$  Cm complex 2 + nH<sup>+</sup> indicates the exchange of one proton and supports the assumption that a ternary hydroxo/glycolate/Cm complex is formed. The larger red-shift from 605.6 nm (Cm complex 2) to 611.3 nm (Cm complex 3) in the Cm/glycolate system at high pH (> 9.7) is the result of a stronger change in the ligand field of the Cm(III) ion during the reaction Cm complex 2  $\leftrightarrow$  Cm complex 3. Similar large red-shifts have been observed with ligands like EDTA /2/ and we interpret the changes observed in our experiment due to the formation of strong complexes with oxyacetate, obtained by deprotonation of the coordinated  $\alpha$ -OH group in glycolate. The experimental lifetime of  $295 \pm 15 \mu\text{s}$  gives strong support to this view. Further evidence for the formation of complexes containing coordinated oxyacetate is provided by the slow ligand exchange reaction. We conclude that Cm(III) forms nine coordinated complexes with the stoichiometry:

Cm complex 1 [Cm(HOCH<sub>2</sub>COO)<sub>4</sub>(H<sub>2</sub>O)]<sub>9</sub>,

Cm complex 2 [Cm(HOCH<sub>2</sub>COO)<sub>4</sub>(OH)]<sub>9</sub><sup>2-</sup> and

Cm complex 3 [Cm(OCH<sub>2</sub>COO)(HOCH<sub>2</sub>COO)<sub>3</sub>(OH)]<sub>9</sub><sup>3-</sup>.

As a conclusion the Cm(III)/glycolate complexes are illustrated schematically in Fig. 2

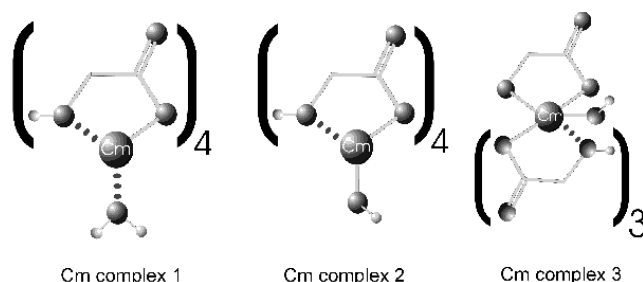


Fig. 2: Cm(III)/glycolate complexes found at  $9 \times 10^{-8}$  mol/L Cm(III) in 1.0 mol/L sodium glycolate solution are illustrated schematically.

### References

- /1/ Stumpf, T. et al., J. Chem. Soc., Dalton Trans., submitted  
 /2/ Kim, J.I. et al., Eur. J. Solid State Inorg. Chem. **28**, 347-350 (1991)

# THERMOCHROMATOGRAPHIC VOLATILITY STUDIES OF PLUTONIUM OXIDES

S. Hübener, S. Taut, A. Vahle, Th. Fanghänel

The volatility of plutonium oxides in the  $O_2$ - $H_2O_{(g)}/SiO_{2(s)}$  system has been studied by thermochromatography. The experimental results indicate the oxidation of Pu(IV) to Pu(VI) by moist oxygen.

## Introduction

For more than 50 years  $PuO_2$  has been recognized to be the highest plutonium oxide until Haschke et al. /1/ reported the oxidation of  $PuO_2$  to  $PuO_{2+x}$  by water and moist oxygen. The report by Haschke et al. stimulated numerous studies dealing with the oxide chemistry of plutonium, e.g. mass spectrometric measurements by Ronchi et al. /2/ and thermochromatography experiments by Domanov et al. /3/.

In continuation of volatility studies of oxidic uranium species /4/ we studied the volatility of plutonium oxides in the  $O_2$ - $H_2O_{(g)}/SiO_{2(s)}$  system by thermochromatography. Uranium was processed simultaneously as a reference element.

## Experimental

The experimental setup was nearly the same as used in the uranium studies /4/. The commercial gradient oven HTM LORA 36, moveable on a sledge, was used. Open tubular quartz glass columns with an inner diameter of 3.5 mm were applied. The thermochromatographic samples were prepared from solutions of  $^{233}U$  and  $^{242}Pu$  in diluted  $HNO_3$ . A quartz wool plug was soaked with aliquots of the solutions containing  $10^{15}$  to  $10^{16}$  actinide atoms. Silica boats were used alternatively to quartz wool as sample carriers. The actinide solution was evaporated to dryness. Fuming with nitric acid was three times repeated to remove residual chloride ions. The actinide nitrate samples were inserted into the column in the starting position of thermochromatography. A mixture of helium and oxygen in the ratio of 1:1 was used as the carrier gas at a total flow rate of  $100\text{ cm}^3\text{ min}^{-1}$ . The carrier gas was moistened by bubbling through water at defined temperatures. Prior to thermochromatography the actinide nitrates were converted into  $UO_3$  and  $PuO_2$ , respectively, by heating at 700 K for 10 min. To start thermochromatography the hot oven was shifted into the working position. The duration of chromatography was varied between 30 and 120 min. To end a thermochromatography experiment the carrier gas flow was interrupted and the column removed from the oven within 10 seconds. Then, the column was cut into 2 cm sections which were leached with hot nitric acid. Thin-layer samples were prepared from the acidic solution by evaporation on glass disks. The actinide concentration of these samples was determined by alpha spectrometry.

## Results and Discussion

Fig. 1 shows a chromatogram at a water vapor pressure of 2 kPa after 30 min chromatography time as an example. Plutonium proved to be volatile in moist oxygen as reported earlier for uranium /4/. However, the plutonium volatility is considerably lower than that of uranium. The volatilization of uranium starts at

about 1175 K but plutonium becomes volatile only above 1300 K, presumably as  $PuO_2(OH)_2$  formed according to reaction (1).

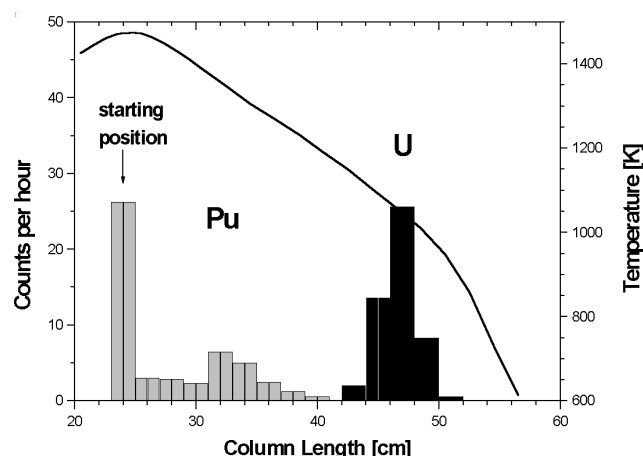
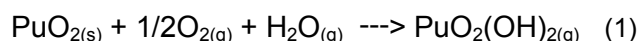


Fig. 1: Thermochromatogram of  $^{233}U$  and  $^{242}Pu$  at a vapor pressure of 2 kPa.

As can be seen from the chromatogram in Fig. 1 plutonium is deposited at considerable higher temperatures than uranium. Both actinides, plutonium and uranium, react preferably with silica to nonvolatile compounds or solid solutions. For this reason the volatilization yields are lower than 1 %. However, even such a low volatilization yield indicates the oxidation of Pu(IV) to Pu(VI) by moist oxygen. Further evidence for this interpretation comes from the experimental finding that thorium and protactinium oxides are quantitatively retained at the starting position of thermochromatography under conditions favorable for the volatilization of plutonium.

## References

- /1/ Haschke, J.M., Allen, T.H., Morales, L.A.; Science **287**, 285 (2000)
- /2/ Ronchi, C., Capone, F., Colle, J.Y., Hiernaut, J.P.; J. Nucl. Material **280**, 111 (2000)
- /3/ Domanov, V.P., Buklanov, G.V., Lobanov, Yu.V.; Int. Conf. „Actinides-2001“, abstract 7I02, Hayama, Japan, November 4-9, 2001
- /4/ Hübener, S., Taut, S., Vahle, A.; Report FZR-318 (2001) p.60

## CHEMICAL INVESTIGATION OF HASSIUM (Hs, Z = 108)

A. Vahle for a Univ. Bern - PSI - GSI - JINR - LBNL - Univ. Mainz - FZR - IMP - collaboration

For the first time, a Hs containing compound has been investigated chemically. With the formation of a very volatile tetroxide, Hs behaves as expected and is a typical member of group 8 of the periodic table.

### Introduction

The heaviest element, whose chemical behavior has been studied so far is bohrium (Bh) with  $Z=107$  /1/ behaving like a typical member of group 7 of the periodic table. The longest-lived  $\alpha$ -decaying isotope of the next heavier element hassium (Hs,  $Z=108$ ) is  $^{269}\text{Hs}$  ( $T_{1/2}=11.3$  s) which has been identified in the decay chain of  $^{277}112$  /2, 3/. Hs is supposed to be a member of group 8 of the periodic table of the elements and should thus form a very volatile tetroxide. Relativistic density functional calculations predicted the electronic structure of  $\text{HsO}_4$  to be similar to the one of  $\text{OsO}_4$  /4/. Application of different semiempirical models of the interaction of a  $\text{MeO}_4$  molecule with quartz surface predicted the adsorption behavior of  $\text{OsO}_4$  and  $\text{HsO}_4$  to be very similar /4/. Extrapolations of trends within group 8 of the periodic table also predicted  $\text{HsO}_4$  and  $\text{OsO}_4$  to behave similar in a gas adsorption chromatography experiment /5/. Hs isotopes were produced directly in the reaction  $^{248}\text{Cm}(^{26}\text{Mg};5,4n)^{269,270}\text{Hs}$  with cross-sections of 6 pb and 4 pb (within a factor of 3), respectively /6/.

### Experimental

A detailed description of the experimental techniques used for the production and detection of Hs isotopes is given in a contribution to the PSI-annual report /6/.

### Results

Seven decay chains were detected in the course of the experiment which were attributed to  $^{269}\text{Hs}$  or the so far unknown isotope  $^{270}\text{Hs}$  /6/. Using the newly built Cryo Qn-Line Detector COLD (an improved version of the Cryo-Thermochromatography Separator CTS developed at Berkeley /7/) the deposition temperature of the Hs containing molecules was determined to  $(-44\pm 5)$  °C giving strong evidence of the formation of  $\text{HsO}_4$ . In an irradiation of a  $^{152}\text{Gd}$  target,  $^{172}\text{Os}$  ( $T_{1/2}=19.2$  s) was produced in the reaction  $^{152}\text{Gd}(^{26}\text{Mg};6n)$  and a deposition temperature of  $(-82\pm 5)$  °C was measured for  $^{172}\text{OsO}_4$ . The deposition distribution in the COLD array along the detector pairs is shown in Fig.1. The white area indicates decays originating from either  $^{269}\text{Hs}$  or  $^{270}\text{Hs}$  where a definite assignment to either isotope was not possible. From these temperatures the adsorption enthalpy was deduced by applying a Monte-Carlo simulation based on a microscopic description of the transport process in the chromatography column /8/, i.e. in the COLD system.

Since the half-life of the nuclide is a crucial parameter in this simulation and this value has not yet been measured for  $^{270}\text{Hs}$ , only the three events assigned to  $^{269}\text{Hs}$  were used for the simulation.  $\Delta H_{\text{ads}}(\text{HsO}_4) = (-46\pm 3)$   $\text{kJ}\cdot\text{mol}^{-1}$  (95 % c.i.) was evaluated, compared to  $\Delta H_{\text{ads}}(\text{OsO}_4) = (-39.5\pm 1.0)$   $\text{kJ}\cdot\text{mol}^{-1}$ . The latter value is

in good agreement with  $\Delta H_{\text{ads}}(\text{OsO}_4) = (-38.0\pm 1.5)$   $\text{kJ}\cdot\text{mol}^{-1}$  evaluated in earlier experiments.

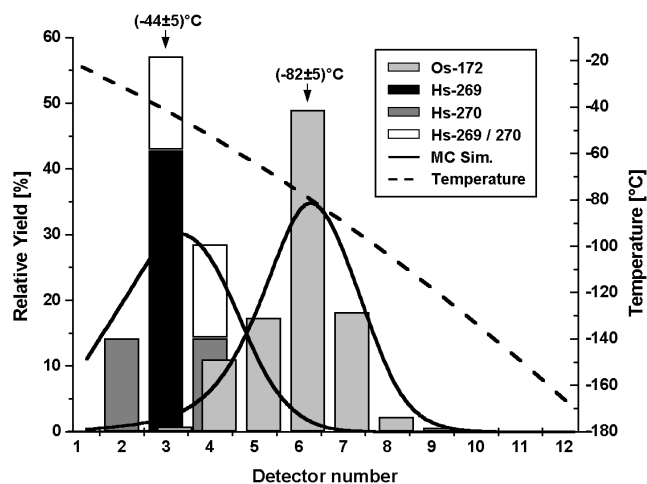


Fig. 1: Merged thermochromatograms of  $\text{OsO}_4$  and  $\text{HsO}_4$ . The solid lines represent results of a Monte-Carlo Simulation with  $\Delta H_{\text{ads}}$  values of  $-39.5$   $\text{kJ}\cdot\text{mol}^{-1}$  ( $\text{OsO}_4$ ) and  $-46$   $\text{kJ}\cdot\text{mol}^{-1}$  ( $\text{HsO}_4$ ), respectively. The dashed line indicates the temperature gradient.

### Discussion

Hs was shown to form a very volatile oxide, presumably  $\text{HsO}_4$ . Therefore it behaves like a typical member of group 8 of the periodic table.

### References

- /1/ Eichler, R. et al., Nature **407**, 63 (2000)
- /2/ Hofmann, S. et al., Z. Phys. **A354**, 229 (1996)
- /3/ Hofmann, S. et al., Rev. Mod. Phys. **72**, 733 (2000)
- /4/ Pershina, V. et al., J. Chem. Phys. **115**, 792 (2001)
- /5/ Düllmann, Ch.E. et al., J. Phys. Chem. A (submitted)
- /6/ Türlér, A. et al., PSI Annual Report 2001, 3 (2002)
- /7/ Kirbach, U. et al., Nucl. Instrum. Meth. A (in press)
- /8/ Zvara, I., Radiochim. Acta **38**, 95 (1985)

**Interaction of Actinides/Radionuclides with  
Surfaces of Rocks, Minerals and Colloids**

# SORPTION OF U(VI) ON GRANITE: COMPARISON OF EXPERIMENTAL AND PREDICTED U(VI) SORPTION DATA

T. Arnold, E. Krawczyk-Bärsch, G. Bernhard

*The sorption of uranyl(VI) on granite is predicted by the superpositioning of simultaneously occurring, with each other competing, surface reactions of the mineralogical rock constituents and the aqueous metal species. The predictions were compared with experimental sorption data and it was found that the predictions were in good agreement with the experimental results.*

## Introduction

The sorption of uranyl(VI) on granite was predicted over a pH range from 3.5 to 9.5 and then compared with experimental uranyl(VI) sorption data on granite. The predictions were obtained by the following approach.

## Approach

A mineralogical characterization of the granite was conducted. It was found that the studied granite from Eibenstock/Germany was composed of 45 Vol.% quartz, 35 Vol.% orthoclase, 7.5 Vol.% albite, 7.5 Vol.% biotite, 4.0 Vol.% muscovite and 1.9 Vol.% opaque minerals.

Then the necessary Surface Complexation Model (SCM) parameters, e.g. surface site density, surface acidity constants, specific surface area were determined by conducting the appropriate experiments or measurements, e.g. constant pH adsorption isotherms, acid base titrations, and BET measurements. That followed sorption experiments with pure mineral phases, which were beforehand identified in the granite. For these sorption experiments as well as the sorption experiments with granite the 63 to 200  $\mu\text{m}$  fraction and  $1 \times 10^{-6}$  M initially added uranium were used. The Diffuse Double Layer Model (DDLDM) was then used together with the experimental sorption data and the computer code FITEQL /1/ to calculate surface complex formation constants of uranyl(VI) sorbing on the mineralogical granite constituents. The sorption of uranyl(VI) on granite was then predicted. The prediction was obtained completely independent from any experimental uranyl(VI) sorption data on granite. It was exclusively based on its mineralogical constituents and previously determined surface complex formations constants.

## Predictions

One modification to the above outlined approach had to be undertaken to obtain a good prediction. This modification arose from the fact that the softer minerals biotite and muscovite in the granite 63 to 200  $\mu\text{m}$  fraction were, as a result of the grinding process, distinctively smaller than the harder grains quartz and albite. Conclusively, the smaller grain size had to be taken into consideration and an appropriate specific surface area for these minerals had to be used in the modeling. The grain size of muscovite and biotite was determined by SEM investigations of the granite 63 to 200  $\mu\text{m}$  powder fraction. The specific surface areas for biotite and muscovite were taken from the < 20  $\mu\text{m}$  grain size fraction, as determined by SEM investigations. The predicted uranyl(VI) sorption on granite over a pH range from 3.5 to 9.5 is shown in Fig. 1 together with experimental uranyl(VI) sorption data on granite.

As shown in Fig. 1 the predicted and the experimental uranyl(VI) sorption data are in very good agreement, clearly showing the great potential of this approach /2/ to model heavy metal sorption on rocks.

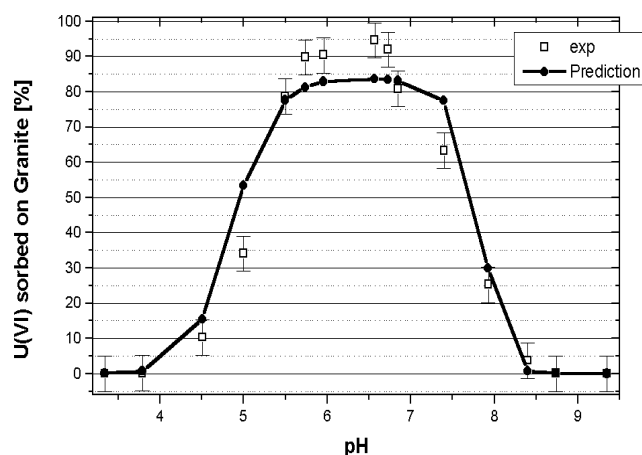


Fig. 1: Predicted uranyl(VI) sorption data compared with experimental uranyl(VI) sorption data on granite.

Mineral	grain size fraction [ $\mu\text{m}$ ]	specific surface area [ $\text{m}^2/\text{g}$ ]
Quartz	63-200	0.2
Albite	63-200	0.2
Orthoclase	63-200	0.9
Muscovite	63-200	1.4
Biotite	63-200	1.8
Muscovite	< 20	3.0
Biotite	< 20	4.5

Tab. 1: Relationship between grain size fraction and specific surface area for the mineralogical granite constituents.

## Acknowledgements

The studies were funded by the Deutsche Forschungsgemeinschaft (DFG) under the project number Ni 210/6-2

## References

- /1/ Herbelin, A., Westall, J.: *FITEQL Version 3.2*. Report 96-01, Dep. of Chem., Oregon State University (1996)
- /2/ Arnold, T. et al.: *Journal of Contaminant Hydrology* **47**, 219-231 (2001)

## NEPTUNIUM(V) SORPTION ONTO GRANITE AND ITS MINERAL CONSTITUENTS IN THE ABSENCE AND PRESENCE OF HUMIC ACID

K. Schmeide, K.H. Heise, G. Bernhard

We studied the sorption of neptunium(V) onto granite and its mineral constituents (quartz, orthoclase, albite, biotite and muscovite) in the absence and presence of humic acid (HA) in batch experiments as a function of pH.

### Introduction

Knowledge on the sorption behavior of actinides on geologic materials is essential for the safety assessment of radioactive waste disposal sites. It is influenced, amongst others, by the presence of HA.

### Experimental

Experimental conditions of batch experiments:  $[\text{NpO}_2^+] = 1.3 \times 10^{-6}$  M,  $[\text{HA}] = 27$  mg/L (synthetic HA type  $^{14}\text{C-M42}$  /1/),  $I = 0.1$  M  $\text{NaClO}_4$ , solid solution ratio: 50 mg/10 mL, pH 4-11,  $\text{N}_2$  atmosphere.  $^{233}\text{Pa}$  was separated from  $^{237}\text{Np}$  using Dowex-50 prior to each sorption step. Np and HA were added simultaneously to the preconditioned minerals (63-200  $\mu\text{m}$  grain size fractions). Contact time: 160 h. Determination of  $[\text{Np}]$  and  $[\text{HA}]$  by means of LSC ( $\alpha/\beta$ -discrimination).

### Results and discussion

The Np and HA sorption in experiments without and with HA is shown for granite in Fig. 1 and, exemplary for the mineral constituents of granite, for muscovite in Fig. 2.

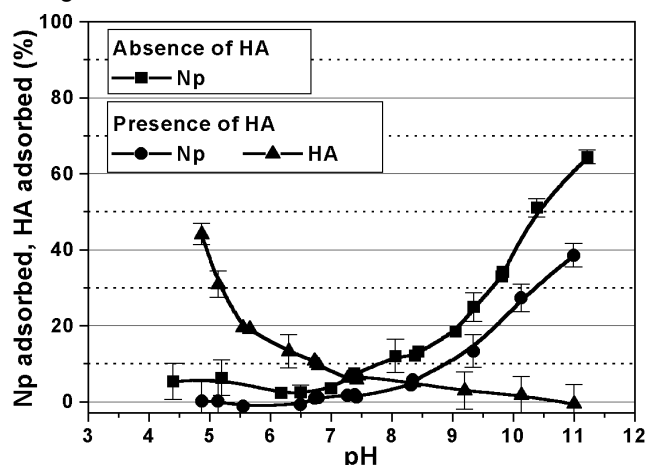


Fig. 1: Np and HA uptake by granite

The results of Np and HA sorption onto granite and its mineral constituents can be summarized as follows.

#### Sorption experiments in the absence of HA:

The Np sorption generally starts between pH 7 and pH 8 and increases with increasing pH value. This trend correlates with the formation of Np(V) hydrolysis species in solution ( $\text{NpO}_2\text{OH}_{(\text{aq})}$ ).

#### Sorption experiments in the presence of HA:

As expected, the HA sorption decreases with increasing pH value. Compared to the Np sorption in the absence of HA, the Np sorption onto granite and biotite is decreased by HA between pH 6.5 and 11. The Np sorption onto muscovite and orthoclase is somewhat increased by HA between pH 6 and 9.5 and above pH 9.5 relatively strongly decreased. The Np sorption onto albite and quartz is not changed by HA up to pH 10 and 9, respectively, and at higher pH values, it is relatively strongly decreased.

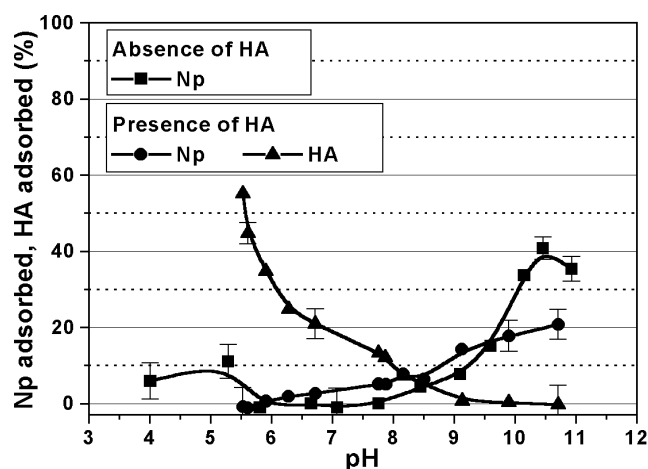


Fig. 2: Np and HA uptake by muscovite

Np speciation calculations show that relatively little  $\text{NpO}_2\text{HA}(\text{l})$  is formed between pH 6 and 10 with a maximum of 10 % at pH 8.5. For the pH region higher than 9, the formation of the mixed complex  $[\text{NpO}_2(\text{OH})\text{HA}]_{\text{coll.}}$  is suggested /2/. Presently, this complex cannot be quantified thermodynamically, however, this complex would explain the strong reduction of the Np sorption by HA at pH values higher than 9 and 10, respectively.

Since, besides granite, only biotite shows a similar reduction of Np sorption in experiments with HA between pH 7 and 11, it is concluded that biotite is the dominating mineral phase in the rock material granite for the Np sorption. Mössbauer spectroscopic measurements have shown that in un-weathered biotite 84.5 % of  $\text{Fe}_{\text{Total}}$  occur as Fe(II) /3/. This Fe(II) occurring in biotite and thus, also in granite could lead to a reduction of Np(V) to Np(IV). Especially in Np sorption experiments in the presence of HA, the combination of Fe(II) and HA could lead to a reduction of Np(V) to Np(IV). Since Np(IV) is generally stronger complexed by HA due to its higher charge, the Np sorption onto granite and biotite would be reduced compared to experiments without HA.

The redox stability of Np humate complexes, the kinetics of the redox processes and the formation of humic colloids will be studied in more detail applying NIR spectroscopy, liquid-liquid extraction using TTA and ultrafiltration. Thereby, the Np/HA equilibration time prior to addition to the rock material will be varied.

#### Acknowledgment

This work was supported by the BMWi (no. 02E9299).

#### References

- /1/ Pompe, S. et al., Report FZR-318, p.31 (2001)
- /2/ Marquardt, C. et al., Radiochim. Acta **80**, 129 (1998)
- /3/ Arnold, T., personal communication

# FERRIHYDRITE FORMATION DURING THE DISSOLUTION OF CHLORITE AND ITS EFFECT ON THE SORPTION BEHAVIOR OF U(VI)

E. Krawczyk-Bärsch, T. Arnold, F. Brandt<sup>1</sup>, D. Bosbach<sup>1</sup>, G. Bernhard

<sup>1</sup> Institute of Nuclear Waste Management, Forschungszentrum Karlsruhe, Karlsruhe, Germany

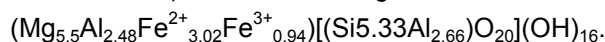
*During the dissolution of a Fe-rich chlorite spherical ferrihydrite particles are formed in neutral and alkaline solutions. The ferrihydrite particles are predominantly covering the {hk0} faces due to the reactivity of the edge surfaces of sheet silicates. Their huge specific surface area is significantly influencing the natural attenuation processes of contaminants, i.e. uranium.*

## Introduction

The abandoned uranium mines in the Western Erzgebirge in Germany are mostly related to the rock phyllite. In the present time many of these mines are being flooded. The flood water which contains uranium is penetrating through cracks and fissures of the phyllite leading to dissolution processes. One of the major components in the phyllite is a Fe-rich chlorite. During the dissolution of the chlorite the major cations  $\text{Al}^{3+}$ ,  $\text{Fe}^{2+}$ , Mg and Si are released into the aqueous solution leaving a dissolved chlorite mineral which is degenerating to vermiculite. Depending on the pH of the solution newly Fe-minerals are forming by precipitation due to the low solubility of Fe in a pH-range above 5. These secondarily formed minerals often represent the most reactive fractions of soils and are dominating its chemical behavior.

## Experimental

The chlorite used for the experiment, was a ripidolite chlorite (CCa-2) from Flagstaff Hill (El Dorado County, California, USA) with the following chemical formula:



In a batch experiment a solid concentration of 0.5 g chlorite (63–200  $\mu\text{m}$  grain size) was mixed with 40 mL  $\text{NaClO}_4$  solution in a polypropylene centrifuge tube and rotated end-over-end for two months without adjusting the pH. The experiment was carried out at room temperature, under oxic condition and with an ionic strength of 0.1 M to approximate natural weathering conditions. At the end of the experiment a pH value of 7.04 was measured. The bulk of the chlorite particles was separated by centrifugation at 2500 g for one hour. The chlorite residue of the centrifugated suspension was dried at 40 °C and part of it was prepared for Scanning Electron Microscopy (SEM) by carbon-coating for the microscopically characterization in Secondary Electron detection mode (SE).

## Results and discussion

In SE mode a large number of small particles was detected on the chlorite surfaces as individual particles. Based on their spherical character and small particles sizes (Fig. 1), they were identified as ferrihydrite ( $5\text{Fe}_2\text{O}_3 \cdot 9\text{H}_2\text{O}$ ), which were formed during the dissolution of chlorite by oxidation and precipitation of the released  $\text{Fe}^{2+}$  cations in neutral or alkaline solutions /1/. The sorbed ferrihydrite particles are preferentially located on the edge surface, i.e. the {hk0} faces of the chlorite platelet. The average particle coverage was determined with the software from SCION Corporation /2/ on numerous different areas. On the {hk0} faces the particle coverage was determined as  $0,276 \mu\text{m}^2 / 1 \mu\text{m}^2$ , i.e. 27,6 % of the {hk0} faces were covered with ferrihydrite particles. The

average particle coverage on the basal planes {001} was found to be only  $0,030 \mu\text{m}^2 / 1 \mu\text{m}^2$ . This is equivalent to 3,0 % coverage. This predominantly coverage of the {hk0} faces with ferrihydrite particles as coatings can be explained due to the reactivity of the edge surfaces of sheet silicates /3/. In contrast, the {001} surfaces were found to be almost non-reactive.

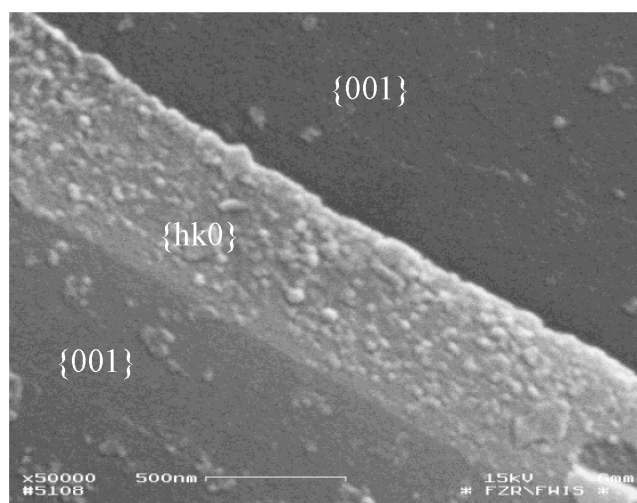


Fig. 1: Spherical ferrihydrite particles on the edge surface of the chlorite crystals. - SEM, SE-detection;

The formation of secondarily formed ferrihydrite coatings has significant consequences for risk management. Ferrihydrite is known to have a huge specific surface area which significantly influence the natural attenuation processes of contaminants, i.e. uranium in the near surface environment. Fractions of uranium are fixed to both ferrihydrite and chlorite during the dissolution of the mineral, but as a secondarily formed phase ferrihydrite is dominating the sorption behavior of uranium on chlorite /4/.

## Acknowledgment

This work was supported by DFG (BE 2234/4-1). The authors wish to thank E. Christalle for SEM investigations.

## References

- /1/ Krawczyk-Bärsch et al.: Chemical Geology (submitted)
- /2/ Rasband, W.: *Scion Image Beta 4.02 for Windows 95, 98 ME, NT 2000 and XP* (2000)
- /3/ Bosbach, D. et al.: *Amer. Mineral.* **85**, 1209-1216 (2000)
- /4/ Arnold, T. et al.: *Chemical Geology* **151**, 129-141 (1998).

# SORPTION OF URANIUM(VI) ONTO SCHWERTMANNITE - EXAFS INVESTIGATIONS

M. Walter, T. Arnold, H. Funke, T. Reich, G. Bernhard

*In acid mine drainage conditions uranium(VI) adsorbs on goethite and schwertmannite, forming surface complexes with the ferric iron polyhedra and sulfate, respectively. The structure of these surface species was identified by EXAFS.*

The ferric oxide schwertmannite ( $\text{Fe}_{16}\text{O}_{16}(\text{OH})_{12-9}(\text{SO}_4)_{2-3.5} \cdot n\text{H}_2\text{O}$ ,  $n \sim 10$ ) is commonly formed in acid mine drainage waters. It is formed in the presence of high sulfate concentrations in the pH-range from 2.8 to 4.5 /1/. Because of its large specific surface area, it may influence the migration of uranium(VI) by sorption processes. The aim of this study was to obtain structural information about uranium(VI) surface complexes by Extended X-ray Absorption Fine Structure (EXAFS) spectroscopy. Goethite was included in our investigations as a reference material to compare and interpret the schwertmannite data.

## Experimental

Samples for EXAFS analysis were prepared under  $\text{N}_2$ -atmosphere using 200 mg of schwertmannite or goethite. We used initial uranium(VI) concentrations of  $1 \times 10^{-5}$  M for pH 6.5, and  $5 \times 10^{-5}$  M for the pH 4.2 sorption samples. The ionic strength was adjusted using 0.01 M  $\text{Na}_2\text{SO}_4$  or  $\text{NaClO}_4$ , respectively. EXAFS spectra were recorded at room temperature in fluorescence mode at the ESRF in Grenoble. The measured EXAFS oscillations were fitted, using the EXAFSPAK program and are shown in Fig. 1. The theoretical phase shifts and backscattering amplitudes were calculated with FEFF8.

## Results

All distances of the equatorial oxygens are about 2.37 Å (Table 1). They are significantly shorter than the typical values for the aquatic  $\text{UO}_2^{2+}$  ion of 2.41 Å /2/, which indicates strong interactions.

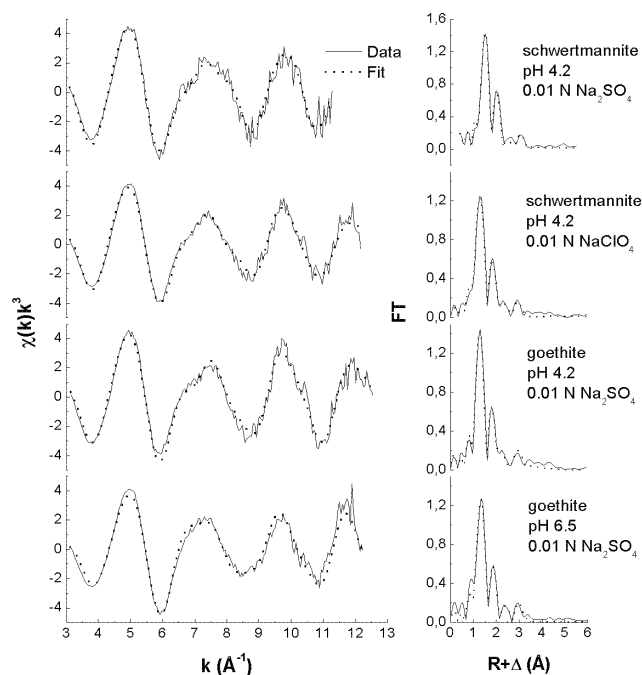


Fig. 1: EXAFS and Fourier Transforms of the uranium(VI) sorption samples

U(VI) - sample	Shell	N	R (Å)	$\sigma^2$ (Å <sup>2</sup> )	$\Delta E_0$
schwertmannite pH 4.2	Oax.	2.3	1.76	0.0029	-14
	Oeq.	5.6	2.38	0.011	
	S	1.3 <sup>f</sup>	3.66	0.005	
schwertmannite pH 4.2 0.01 N $\text{NaClO}_4$	Oax.	2.1	1.77	0.0029	-15
	Oeq.	4.7	2.37	0.012	
	C	1.4 <sup>f</sup>	2.93	0.004	
	Fe	0.7 <sup>f</sup>	3.46	0.008	
goethite pH 4.2 0.01 N $\text{Na}_2\text{SO}_4$	Oax.	1.9	1.76	0.0012	-16
	Oeq.	6.8	2.36	0.016	
	C	1.7 <sup>f</sup>	2.92	0.0056 <sup>f</sup>	
	Fe	0.6 <sup>f</sup>	3.44	0.0045	
goethite pH 6.5 0.01 N $\text{Na}_2\text{SO}_4$	Oax.	2 <sup>f</sup>	1.79	0.0022	-12
	Oeq.	3.8	2.36	0.010	
	C	1.1 <sup>f</sup>	2.93	0.0005	
	Fe	0.4	3.43	0.004 <sup>f</sup>	

<sup>f</sup> parameter was fixed during the final fit,  $\Delta E_0$  is given in eV,  $\Delta N = \pm 25\%$ ,  $\Delta R = \pm 0.01$  Å

Tab. 1: Structural parameters of sorbed uranium(VI) surface species on schwertmannite and goethite

An iron backscatterer was clearly found for uranium(VI) sorbed onto goethite at pH 4.2 and 6.5 in a sulfate-rich solution as well as for schwertmannite at pH 4.2 in perchlorate solution. Such a uranium - iron distance is indicative of a bidentate inner sphere complexation /3/. In contrast, the EXAFS of uranium(VI) sorbed onto schwertmannite at pH 4.2 in sulfate-rich solutions shows only a sulfur backscatterer at a distance of 3.66 Å, indicating a monodentate uranium(VI) - sulfate coordination. This could be interpreted either as uranium(VI) surface complexes with the structural sulfate of the schwertmannite lattice ( $\equiv\text{SO}-\text{UO}_2$ ,  $\equiv(\text{SO})_2=\text{UO}_2$ ) or as a ternary surface complex ( $\equiv\text{FeO}-\text{SO}_4-\text{UO}_2$ ). A light backscatterer, like carbon, at a distance of 2.9 Å improves the fit. Although this uranium(VI) - carbon interaction is typical of a bidentate complexation /4/, ternary uranium(VI) - carbonate complexes are ruled out by the sorption conditions (pH, high sulfate concentration).

## Acknowledgment

EXAFS measurements were made at Rossendorf Beamline (BM20) at ESRF under experiment numbers 20-01-41 and 20-01-52.

## References

- 1/ Cornell, R.M., Schwertmann, U.: *The iron oxides*, VCH Verlag, Weinheim (1996)
- 2/ Dent, A.J., et al., *J. Colloid Interface Sci.* **150**, 45-60 (1992)
- 3/ Reich, T., et al., *J. Elec. Spec. Rel. Phe.* **96**, 237-234 (1998)
- 4/ Bargar, J.R., et al., *Geochim. Cosmochim. Acta* **64**, 2737-2749 (2000)

# USING SPECTROSCOPIC EVIDENCE BY EXAFS TO MODEL THE SORPTION OF URANYL(VI) ON SCHWERTMANNITE

T. Arnold, M. Walter, G. Bernhard

Spectroscopic evidence obtained by EXAFS investigations together with experimental results from batch sorption experiments were used to calculate the surface complex formation constant of uranyl(VI) sorbing on the schwertmannite surface. It was found that the dominating sorbed uranyl(VI) surface species is a bidentate mononuclear surface species,  $[(XO)_2(UO_2^{2+})]^0$ . Its formation constant  $\log K$  was calculated with the computer code FITEQL and a value of  $\log K = -4.77$  was obtained.

## Introduction

Schwertmannite is an oxidation product of pyrite and forms only in the pH range of 2.5 to 4.5. It is generated in nature by bacterial oxidation of Fe(II) in acid mine effluents or acid sulfate soils. In these environments ferrous iron is oxidized by acidophilic bacteria, such as *T. ferrooxidans*, and precipitates as schwertmannite, instead of ferrihydrite. In addition, the occurrence of schwertmannite is not only restricted to sulfidic ore bodies, but is also precipitating out of acid coal mine drainage. It is also found in drainage waters of uranium mines, e.g. Königstein/Saxony Germany, where uranium was mined by acid leaching with sulfuric acid.

## Results

EXAFS investigations were conducted to identify the structure of the sorbed uranyl(VI) on the schwertmannite surface. The sample preparation and the interpretation of the obtained EXAFS data is described in detail in /1/. It was found that the EXAFS data were best described with a bidentate mononuclear surface complex. Such a surface complex is depicted in Fig. 1.

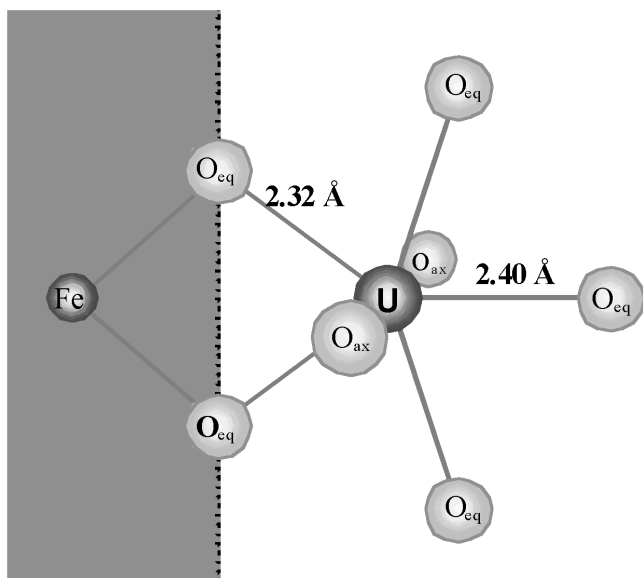


Fig. 1: Uranyl(VI) surface complex on the schwertmannite surface identified by EXAFS.

As indicated in Fig.1 the two equatorial oxygen atoms, involved in the surface complex formation, show a smaller distance of 2.32 Å to the uranyl(VI) atom as the remaining three equatorial oxygen atoms which show a distance of 2.40 Å to the uranyl(VI) atom. The resulting chemical reaction for this surface complex is:



The results of the batch experiments have shown that no sorption of uranyl onto schwertmannite was de-

tected below pH 3. However, with increasing pH the uranyl sorption increased. At pH 4.4, 80 % of the initially added uranium was sorbed onto schwertmannite, indicating that this mineral acts as strong sorbent for uranium(VI). The experimental data of the sorption experiments conducted at two different ionic strengths (0.1 M and 0.01 M  $NaClO_4$ ) and initially added uranyl(VI) concentrations of  $1 \times 10^{-6}$  M, shown in Fig. 2, indicate that the sorption of uranyl(VI) onto schwertmannite seems to occur by chemisorption rather than by physisorption, because variations in ionic strength have no influence on the uranium sorption behavior. This is in accordance with the interpretation of the EXAFS data.

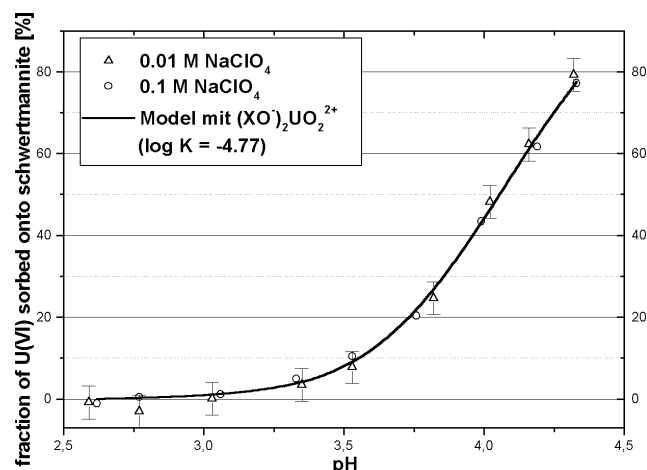


Fig. 2: Experimental and modeled uranyl(VI) sorption data on schwertmannite.

The DDLM (Diffuse Double Layer Model) was used together with the computer code FITEQL Version 3.2 /2/ to model the sorption results and to calculate formation constants for uranium surface complexes on the schwertmannite surface. The formation constants for known aqueous uranium (VI) complexes /3/, the surface acidity constants determined in acid base titration experiments and the above given chemical reaction were included in the calculation. Based on the experimental results, the surface complex formation constant  $\log k$  was optimized with FITEQL and a value of -4.77 was obtained.

## Acknowledgments

The studies were funded by the DFG under the project number Ni 210/6-2.

## References

- /1/ Walter, M. et al., this report p.24
- /2/ Herbelin, A., Westall, J., FITEQL Report 96-01, Dep. of Chem., Oregon State University (1996)
- /3/ Grenthe, I. et al., *Chemical Thermodynamics of Uranium*, Elsevier Science, Amsterdam (1992)

# EXAFS INVESTIGATION ON URANYL SORBED ONTO MONTMORILLONITE

C. Hennig, T. Reich, H. Funke, A. Rossberg, R. Dähn<sup>1</sup>, A. Scheidegger<sup>1</sup>  
<sup>1</sup> Paul Scherrer Institut, Waste Management Laboratory, CH – 5232 Villigen

Uranium  $L_{III}$ -edge EXAFS measurements on uranyl sorbed onto montmorillonite reveals that uranyl uptake at pH 5-7 and an initial uranyl concentration of  $5 \cdot 10^{-5}$  M takes place preferred as bidentate inner-sphere complexation on aluminol groups of the montmorillonite edge sites.

Depending on the reaction conditions (see Tab. 1), the distances between the  $U-O_{eq}$  pair vary slightly between 2.34 Å and 2.37 Å and the coordination numbers  $N(U-O_{eq})$  are in the range of 5.7 to 6.2. These distances are far from values for mononuclear outer-sphere uranyl aquo-complexes with  $U-O_{eq}$  distances between 2.41 Å–2.43 Å obtained at lower pH values by Dent et al. /1/, Chrisholm-Brause et al. /2/, and Sylwester et al. /3/. The short  $U-O_{eq}$  distances indicate that an inner-sphere complexation process dominates the sorption under the used experimental conditions.

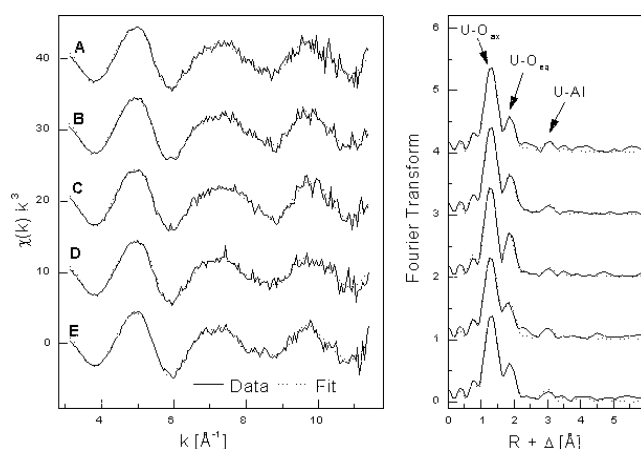


Fig. 1: Uranium  $L_{III}$ -edge  $k^3$ -weighted EXAFS spectra (left) and the corresponding Fourier transforms (right)

A comparison of the samples **A**, **D**, and **E** with identical background electrolyte concentration shows that with increasing pH the  $U-O_{eq}$  distance decreases only slightly from 2.36 Å to 2.34 Å within the error limit of distance determination. At the high concentration of the background electrolyte, cation exchange processes are suppressed and sorption onto edge sites is favored. For comparison, the electrolyte concentration in sample **C** was reduced to 0.01 M  $NaClO_4$ . For this sample, the best fit for the distance  $U-O_{eq}$  is 2.37 Å, indicating no significant increase of the uranyl fraction bound by outer-sphere complexation in the interlayers. The obtained structural parameters indicate that also for a low ionic strength the inner-sphere coordination is predominant at pH 5. In comparison Sylwester et al. /3/ observed at low ionic strength (0.01M NaCl) and pH 4 that outer-sphere complexation is the predominant uranyl uptake mechanism on montmorillonite. However, it seems that at pH 5 the inner-sphere complexation mechanisms are favored. A difference in uranium loading was created for samples **A** and **B**. The observed change in the relation between inner-sphere and outer-sphere uranyl species as a function of surface coverage, as described by Chrisholm-Brause et al. /2/, was not observed for these samples.

The FT of all samples shows a peak at  $R+\Delta \approx 3.0$  Å indicating the interaction between the uranyl moiety and the substrate. A fit of this shell with Si or Al including fixed Debye-Waller factors together with the constrained parameters of the  $U-O_{ax}$  MS contribution gives distances of approximately 3.40-3.44 Å and a coordination number between 0.5 and 0.8.

	Sample	Shell	R [Å]	N	$\sigma^2$ [Å <sup>2</sup> ]
<b>A</b>	5.04·10 <sup>-5</sup> M U, pH 5.02, 0.1 M NaClO <sub>4</sub> 1751 ppm	U-O <sub>ax</sub>	1.78	2.0(2)	0.0026
		U-O <sub>eq</sub>	2.36	6.2(15)	0.017
		U-Al	3.43	0.6(2)	0.003*
<b>B</b>	8.40·10 <sup>-5</sup> M U pH 5.14, 0.1 M NaClO <sub>4</sub> 2473 ppm	U-O <sub>ax</sub>	1.78	2.0(2)	0.0022
		U-O <sub>eq</sub>	2.36	6.1(8)	0.015
		U-Al	3.43	0.5(2)	0.003*
<b>C</b>	5.04·10 <sup>-5</sup> M U pH 5.17, 0.01 M NaClO <sub>4</sub> 2613 ppm	U-O <sub>ax</sub>	1.77	1.9(2)	0.0016
		U-O <sub>eq</sub>	2.37	5.7(8)	0.014
		U-Al	3.44	0.5(2)	0.003*
<b>D</b>	5.04·10 <sup>-5</sup> M U pH 5.98 0.1 M NaClO <sub>4</sub> 2241 ppm	U-O <sub>ax</sub>	1.77	2.0(2)	0.0033
		U-O <sub>eq</sub>	2.35	5.9(7)	0.015
		U-Al	3.41	0.8(2)	0.003*
<b>E</b>	5.04·10 <sup>-5</sup> M U pH 7.08 0.1 M NaClO <sub>4</sub> 2961 ppm	U-O <sub>ax</sub>	1.78	1.9(2)	0.0021
		U-O <sub>eq</sub>	2.34	5.8(9)	0.013
		U-Al	3.40	0.6(2)	0.003*

Tab. 1: EXAFS structural parameters

The coordination of the sorbed uranyl ion was analyzed using geometrical differences of  $[SiO_4]$  tetrahedra and  $[AlO_6]$  octahedra in the montmorillonite structure. Typical bond U-Si distances in edge-sharing fashion are 3.16 Å and in corner-sharing fashion 3.81 Å /4/. Using a model of  $[AlO_6]$  octahedra with typical Al-O distances between 1.85-1.97 Å connected with an U(VI) polyhedron with  $U-O_{eq}$  distances of 2.35 Å in an edge-sharing fashion gives U-Al distances of 3.3-3.5 Å. Hypothetical U-Al bond distances assuming a monodentate bonding between the uranyl unit and the  $[AlO_6]$  octahedra exceed the experimentally observed bond distances. Therefore, we conclude that the substrate peak at  $R+\Delta \approx 3.0$  Å originates from a preferred sorption to the hydroxylated aluminol edge sites by an inner-sphere, mononuclear complexation mechanism in bidentate fashion /5/.

## References

- /1/ Dent, A.J. et al., J. Colloid Interface Sci. **150**, 45-60 (1992)
- /2/ Chrisholm-Brause, C. et al., Geochim. Cosmochim. Acta **52**, 3625-3631 (1994)
- /3/ Sylwester, E.R. et al., Geochim. Cosmochim. Acta **64**, 2431-2438 (2000)
- /4/ Demartin, F. et al., Acta Cryst. **C48**, 1-4 (1992)
- /5/ Hennig, C. et al., Radiochim. Acta, in press

# TIME-RESOLVED LASER FLUORESCENCE SPECTROSCOPY (TRLFS): INVESTIGATIONS OF THE INTERACTION OF Cm(III) WITH FERRIHYDRITE

S. Stumpf<sup>1</sup>, Th. Stumpf, Th. Fanghänel, J.I. Kim<sup>1</sup>

<sup>1</sup>Forschungszentrum Karlsruhe, Institut für Nukleare Entsorgung, Karlsruhe, Germany

The sorption of actinides onto Ferrihydrite is proved by EXAFS. Investigations of the sorption process of Cm(III) onto the iron mineral by TRLFS led to the conclusion that in case of sorption the Cm(III) fluorescence emission is totally deleted (quenching processes). This fact applies as well for the sorption onto colloidal Ferrihydrite as onto thin films out of Ferrihydrite.

For the long-term performance assessment of nuclear waste repositories, knowledge concerning the interactions of actinide ions with mineral surfaces is imperative. The mobility of released radionuclides is strongly dependent on the sorption/desorption processes at mineral surfaces. Therefore, it is necessary to characterize the surface species formed and to elucidate the reaction mechanisms involved. Insight into the sorption mechanisms and identification of surface species is of cardinal importance for a reliable predictive modeling of sorption reactions. Hydrated iron oxides (Ferrihydrite) are globally of great importance in the environment. In addition to clay minerals and humic acids, Ferrihydrite represents another important class of sorption interfaces in the geosphere /1/. Ferrihydrite is present either as discrete mineral phase or as sediment coating and product of corrosion respectively. It is able to dominate the retardation of radionuclides in particular the actinides in the near-field as well as in the far-field of a nuclear waste repository. Time-resolved laser fluorescence spectroscopy (TRLFS) allows due to its high fluorescence yield speciation studies of Cm(III) in the nanomolar concentration range.

Fig. 1 shows the emission spectra of  $2 \times 10^{-7}$  mol/L Cm(III) in the presence of 0.12 g/L Ferrihydrite colloids 6 nm in size ( $=1.19 \times 10^{-3}$  mol/L Fe) at different pH values. With increasing pH the intensity of the Cm(III) emission is decreasing. Furthermore there is no peak shift detectable that could indicate a sorption process occurring in this pH range as it was found in the comparable alumina system /2/.

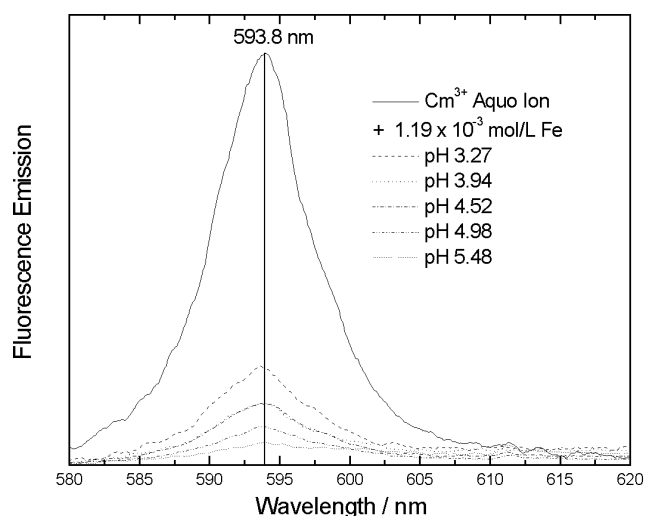


Fig. 1: Fluorescence Emission spectra of Cm(III) in the presence of Ferrihydrite colloids at various pH.

Further experiments verified that this behavior cannot be attributed to light absorption by Fe but to a

radiationless energy transfer from the sorbed Cm(III) to Fe (quenching processes). In the whole pH range a monoexponential decay behavior with a lifetime of  $68 \pm 3 \mu\text{s}$  is observed which is identical with the lifetime of the Cm(III) aqueous ion. To reduce the quenching effect and to observe the Cm(III) sorption onto Ferrihydrite silica and latex particles were coated with Ferrihydrite ("coated colloids"). EXAFS measurements with coated latex particles in the presence of Am(III) validate the sorption of the actinide onto Ferrihydrite.

Fig. 2 shows the emission spectra of  $2 \times 10^{-7}$  mol/L Cm(III) in the presence of Ferrihydrite coated Latex colloids 0.2  $\mu\text{m}$  in size at different pH values.

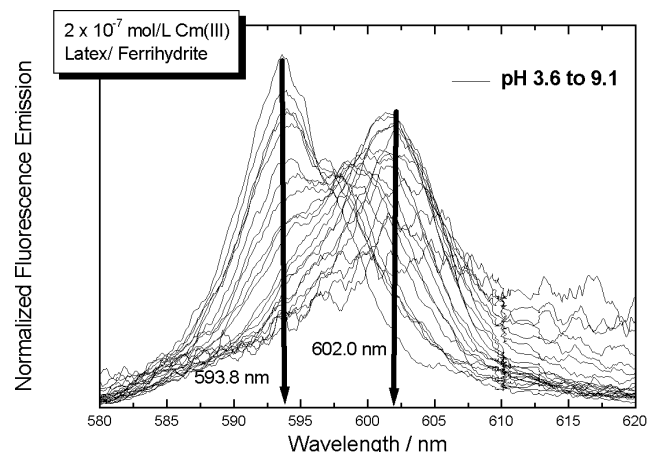


Fig. 2: Fluorescence Emission spectra of Cm(III) in the presence of Ferrihydrite coated Latex particles at various pH; spectra are scaled to the same peak area.

With increasing pH a decrease of the signal belonging to  $\text{Cm}^{3+}_{\text{aq}}$  at 593.8 nm and a significant shift towards 602.0 nm is observed. Furthermore there is an obvious loss of fluorescence emission intensity. The same experiment was carried out with uncoated latex colloids. The emission spectra are identical in both systems except for the fluorescence emission intensity, which does not decrease in the case of uncoated latex colloids. Obviously Cm(III) is sorbed as well onto latex as onto Ferrihydrite. In case of sorption onto the iron mineral again quenching processes take place. The study prove the fact that the fluorescence emission of Cm(III) is totally deleted in the case of sorption onto iron mineral phases.

## References

- /1/ Jambor, J.L. et al., Chem. Rev. **98**, 2549-2585 (1998)
- /2/ Stumpf, Th. et al., J. Colloid Interface Sci. **238**, 219-224 (2001)

# A TIME-RESOLVED LASER FLUORESCENCE SPECTROSCOPY (TRLFS) STUDY OF THE INTERACTION OF TRIVALENT ACTINIDES (CURIUM(III)) WITH CALCITE

Th. Stumpf, Th. Fanghänel

*Cm(III) interaction with calcite was investigated in the trace concentration range. Two different Cm(III)/calcite sorption species were found. The first Cm(III) sorption species consists of a curium ion that is bonded onto the calcite surface. The second Cm(III) sorption species has lost its complete hydration sphere and is incorporated into the calcite bulk structure /1/.*

Carbonates are among the most important secondary alteration products that are formed during the degradation of cement in radioactive waste repositories. More over calcite is a constituent of bentonite backfill materials and it is an omnipresent solid phase in the geosphere. It is the aim of the present work to study by time-resolved laser fluorescence spectroscopy (TRLFS) the mechanism of the Cm(III) uptake by calcite. Cm(III) was chosen as a representative for trivalent actinides. Its high fluorescence spectroscopy sensitivity enable speciation studies in the nanomol concentration range. In previous spectroscopic studies of the Cm(III) sorption onto  $\gamma$ -alumina /2/, smectite, kaolinite /3/ and silica /4/ different surface-sorbed curium species have been identified.

Selected fluorescence emission spectra of Cm(III) ( $8.9 \times 10^{-8}$  mol/L) in calcite suspension (1.0 g/L) measured at different contact times are presented in Fig. 1.

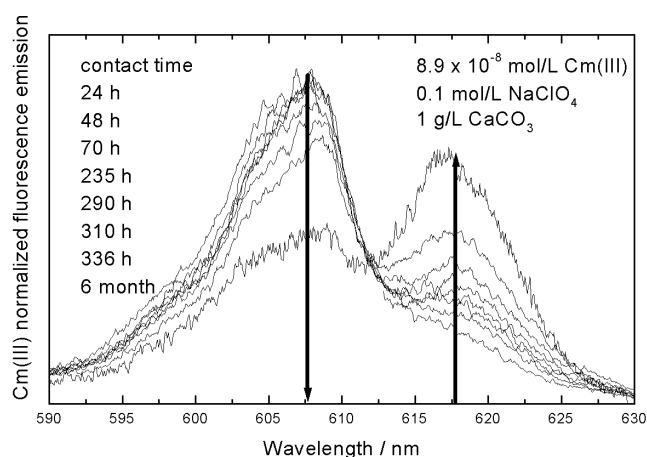


Fig. 1: Fluorescence emission spectra of Cm(III) in aqueous calcite suspension at various contact times; spectra are scaled to the same peak area.

All spectra show two peak maxima at 607.5 nm and 618.0 nm. This two emission bands can be assigned to two different Cm(III) species sorbed onto calcite. With increasing contact time the fluorescence intensity of the first species decreases and the intensity of the second species increases. The spectrum of this first sorption complex in the calcite system is very similar to the spectrum of the Cm(III) tetracarboxylate complex in solution. However the formation of  $\text{Cm}(\text{CO}_3)_4^{5-}$  can be ruled out under the present conditions. The formation of detectable amounts of the tetracarboxylate complex in solution requires orders of magnitude higher carbonate concentration ( $\log[\text{CO}_3^{2-}] > -2$ ) as present in the calcite suspension. As both species, the first Cm(III)/calcite sorption species and the Cm(III) tetracarboxylate complex in solution, show almost identical emission bands we conclude that the ligand field and hence the first coordination sphere

should be very similar in both species. The unusual extraordinary red shift of the fluorescence emission of the second Cm/calcite complex with a peak maximum at 618.0 nm indicates a considerable large change of the ligand field of the actinide ion which could be caused by a change in the coordination number of Cm(III).

In Fig. 2 the fluorescence intensity (in logarithmic scale) are plotted as a function of the delay time. The relaxation follows a bi-exponential decay law.

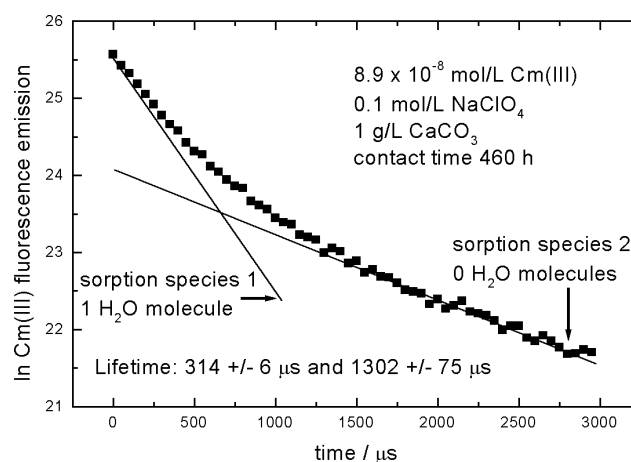


Fig. 2: Time dependency of the fluorescence emission decay of Cm(III) in aqueous calcite suspension.

For the first Cm(III) sorption species a lifetime of  $\tau = 314 \pm 6 \mu\text{s}$  and for the second species  $\tau = 1302 \pm 75 \mu\text{s}$  have been determined. The second value is very close to the calculated radiative lifetime for Cm(III). Hence, the excited state is not quenched by OH vibrations. Applying the linear correlation between the decay rate  $k_{\text{obs}} [\text{ms}^{-1}]$  (reciprocal lifetime of the excited state) and the number of water molecules in the first coordination sphere of the Cm(III) species

$$n(\text{H}_2\text{O}) = 0.65k_{\text{obs}} - 0.88$$

it follows, that the first species contains one water molecule in the first coordination sphere, while the second species has lost its complete hydration sphere. This is a clear indication for the incorporation of the Cm(III) into the bulk structure of the calcite lattice.

## References

- /1/ Stumpf, Th. et al., J. Colloid Interface Sci., accepted
- /2/ Stumpf, Th. et al., J. Colloid Interface Sci. **238**, 219-224 (2001)
- /3/ Stumpf, Th. et al., Environ. Sci. Technol. **35**, 3691-3694 (2001)
- /4/ Chung, K.H. et al., Radiochim. Acta **82**, 215-219 (1998)

# INNER-SPHERE, OUTER-SPHERE AND TERNARY SURFACE COMPLEXES: A TRLFS STUDY OF THE SORPTION PROCESS OF EUROPIUM(III) ONTO SMECTITE

Th. Stumpf, Th. Fanghänel, A. Bauer<sup>1</sup>, F. Coppin<sup>2</sup>, J.I. Kim<sup>1</sup>

<sup>1</sup>Forschungszentrum Karlsruhe, Institut für Nukleare Entsorgung, Karlsruhe, Germany

<sup>2</sup>Univ. Paul Sabatier, Toulouse, France

The surface sorption process of Eu(III) onto smectite was investigated by TRLFS in the trace concentration range. With increasing pH the formation of an inner-sphere Eu(III) surface complex was observed. The differences in the spectra and the fluorescence emission lifetimes of the surface sorbed Eu(III) in presence and absence of carbonate indicate the formation of ternary clay/Eu(III)/carbonate complexes /1/.

Clay minerals are known to be highly efficient in radionuclide retention in natural water systems. They are proposed as backfill in future nuclear waste repositories. Prediction of the retention mechanisms of radionuclides is a fundamental concern in evaluating the suitability of proposed sites for the geologic disposal of nuclear waste. In our study Eu(III) was used as a chemical homologue for trivalent actinides (e.g., Am(III) and Cm(III)). The aim of the time-resolved laser fluorescence spectroscopy (TRLFS) study was to investigate the sorption mechanism of Eu(III) onto smectite and to study the influence of CO<sub>2</sub> on the sorption mechanism.

The evolution of the fluorescence emission spectra of 3.3x10<sup>-6</sup> mol/L Eu(III) with 0.25 g/L smectite in aqueous suspension at various pH is shown in Fig. 1.

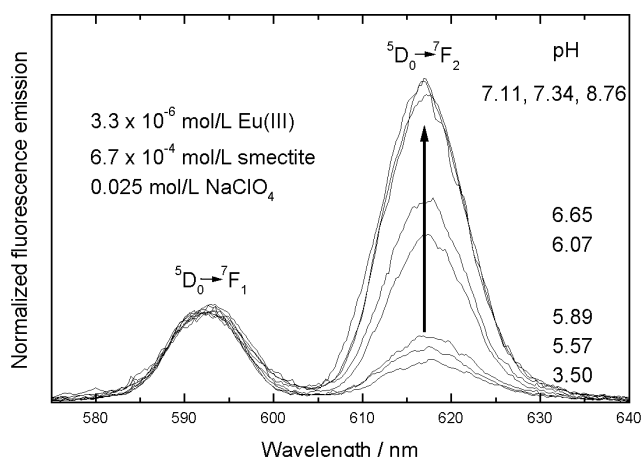


Fig. 1: Fluorescence emission spectra of Eu(III) in aqueous smectite suspension at various pH; spectra are scaled to the same peak area.

With increasing pH the intensity of the peak corresponding to the  $^5D_0 \rightarrow ^7F_2$  transition increases. The  $^7F_1/^7F_2$  ratio changes from  $2.00 \pm 0.03$  at pH 3.50 to  $0.24 \pm 0.03$  at pH  $\geq 7.11$ . It is remarkable that the spectra of the Eu(III) species at pH 3.5 show no difference to spectra of the Eu<sup>3+</sup> aquo ion although at this pH considerable amounts of the Eu(III) is sorbed according to  $K_D$  values. This observation indicates that at low pH the sorbed Eu(III) ion is bonded by outer-sphere complex formation. The change of the transition ratio of the fluorescence emission of Eu(III) at pH  $> 3.5$  in the smectite suspension is caused by a change in the ligand field of the europium ion and indicates inner-sphere complex formation.

Fluorescence emission spectra of 3.3 x 10<sup>-6</sup> mol/L Eu(III) in carbonate free smectite suspension at an ionic strength of 0.025 mol/L NaClO<sub>4</sub> were measured. The peak evolution with pH looks nearly similar to the

spectra observed under natural conditions. But at pH  $\geq 6.65$  the  $^7F_1/^7F_2$  ratios of the two systems differ. The increase in intensity of the  $^7F_2$  transition is stronger pronounced in presence of carbonate than in absence, indicating a bigger change in the ligand field of the europium during the sorption process in the presence of CO<sub>2</sub>. From this we suggest that under natural conditions ternary surface/Eu(III)/carbonate complexes are formed. To validate the suggestion we compared the fluorescence emission lifetimes of sorbed europium species at pH 7.1 prepared under atmospheric conditions and prepared in a carbonate free surrounding. The result is illustrated in Fig. 2.

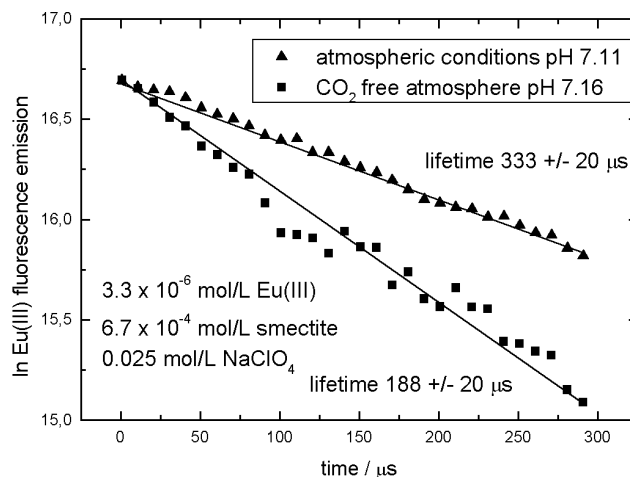


Fig. 2: Fluorescence emission lifetimes of Eu(III) in smectite suspension under atmospheric conditions and in carbonate free atmosphere.

The fluorescence emission lifetime of sorbed Eu(III) under atmospheric conditions is  $333 \pm 20 \mu\text{s}$  corresponding to  $2.6 \pm 0.3$  H<sub>2</sub>O molecules /2/ in the first coordination shell of the metal ion. For the lifetime of the surface sorbed Eu(III) in a CO<sub>2</sub> free atmosphere  $188 \pm 20 \mu\text{s}$  are measured and  $5.1 \pm 0.6$  H<sub>2</sub>O are calculated. This result is in good agreement with values found for Cm(III) surface complexes with clays /3/. The explanation for a difference of 2-3 water molecules in the first coordination sphere of the sorbed europium in absence and presence of carbonate is the suggested formation of ternary surface complexes.

## References

- 1/ Stumpf, Th. et al., Radiochim. Acta., accepted
- 2/ Horrocks, W. DeW et al., J. Am. Chem. Soc. **101**, 334-340 (1979)
- 3/ Stumpf, Th. et al., Environ. Sci. Technol., **35**, 3691-3694 (2001)

# THE IMPACT OF WATER CHEMISTRY ON U(VI) SCAVENGING BY FLOODING WATER COLLOIDS (KÖNIGSTEIN URANIUM MINE)

H. Zänker, W. Richter

*The scavenging by colloids can immobilize U(VI). However, the interdependence of the water chemical processes and the sensitivity of sorption to pH complicates the quantitative description of scavenging.*

The flooding water investigated had a pH of 5.6 and an Eh of 450 mV, the concentrations of important constituents were  $C_{Ca}$  0.9 mM,  $C_{Fe}$  0.3 mM,  $C_U$  0.05 mM,  $C_{SO_4}$  1.2 mM,  $C_{CO_3}$  1.0 mM and  $C_{O_2}$  0.11 mM. Almost 90% of the iron was divalent. Because of the Eh value we assume that the uranium was hexavalent. Colloid concentrations in the range of 2 to 3 mg/L were found. The colloid size was 100 to 200 nm, the major constituents of the colloids were oxyhydroxides and/or hydroxy sulfates of iron. More details on the chemical parameters of the water and the colloid inventories are given in /1/. As has already been shown in /1/, a significant fraction of the uranium of the flooding water was colloid-borne. In waters of pH 4 to 6, the adsorption of U(VI) onto mine water colloids is neither prevented by high acidity nor by the formation of dissolved uranyl carbonate complexes /2/. However, the scavenging of U by colloids shows a sensitive response to changes in water chemistry. This will be demonstrated by the simulation of a mine-related phenomenon, the oxidation of iron(II) by diffusing air.

The generation of  $Fe^{3+}$  due to air results in the immediate formation of Fe(III) particles by hydrolysis. The colloid concentration of our samples showed an increase by a factor of about 10 when the access of air was allowed. On the other hand, the hydrolysis of  $Fe^{3+}$  lead to a decrease in pH. After about 10 days the pH started increasing again due to the destruction of carbonate by the acid produced and the degassing of  $CO_2$ . Thus the course of the pH shows a minimum.

The stages the samples underwent are:

- Stage 1:** High fraction of  $Fe^{2+}$ , pH relatively high (5.5).
- Stage 2:** Fe completely oxidized, pH rather low (4.5).
- Stage 3:**  $CO_2$  degassed, pH relatively high again (4.8).

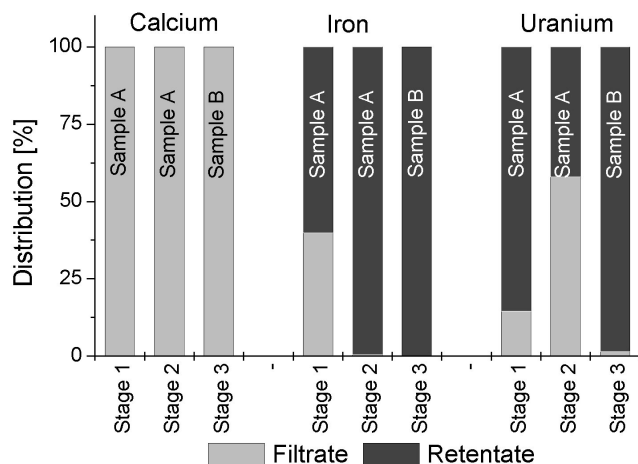


Fig. 1: Percentage distribution of Ca, Fe and U in the sample fractions obtained from ultrafiltration with 30-kD (about 2-nm) membranes on samples at stages 1, 2 and 3.

Fig. 1 shows the colloid-borne fractions of Ca, Fe and U at the three stages. The case of Ca is trivial: At all three stages the Ca passed through the 30-kD ultrafilter. Ca shows no tendency to occur in colloid-borne forms. At stage 1 part of the iron is filterable, part is not. The latter represents the iron that is still divalent. At stages 2 and 3 all the iron is oxidized and thus filterable. The uranium is mostly colloid-borne at stage 1. At stage 2 the amount of colloidal carrier material (Fe(III) particles) has increased. Nevertheless, most of the U(VI) is filter-passing at this stage. This is due to the decreased pH at stage 2. At stage 3 the pH is higher again and the concentration of carbonate is near 0. Both facts make almost 100% of the uranium filterable (colloid-borne).

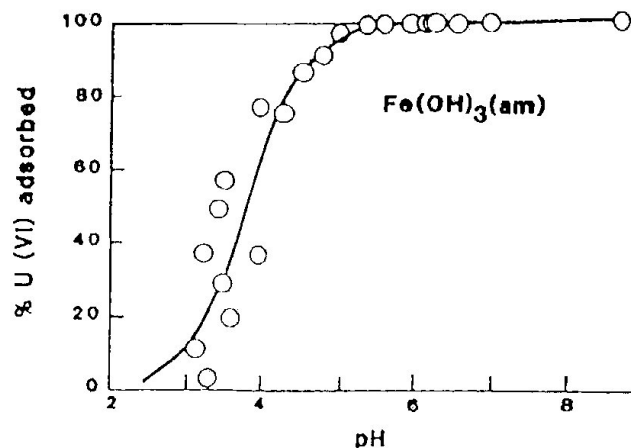


Fig. 2: Adsorption of uranyl vs. pH at  $\Sigma U = 10^{-5} M$  onto a 1 g/L suspension of amorphous ferric hydroxide in 0.1 M  $NaNO_3$ . According to /3/.

Fig. 2 shows an “adsorption edge” of U(VI) on synthetic Fe(III) hydroxide /3/. Similar “adsorption edges” are to be expected for real mine water colloids. Obviously, the pH values of our flooding water samples were in the vicinity of the point of inflection of the underlying “adsorption edge”. This explains the sensitive reaction of the amount of sorbed uranyl to pH changes of only tenths of pH units. The scavenging of uranyl by aggregating and sedimenting flooding water colloids can significantly contribute to the immobilization of U(VI) in the pH range 4 to 6 (“natural attenuation”). However, the interdependence of the chemical processes in the flooding water and the sensitivity of uranyl adsorption to smallest pH changes makes the quantitative description of the effect a non-trivial problem that needs further study.

## References

- /1/ Richter, W., Zänker, H., Report FZR-318 (2001) p.21
- /2/ Zänker, H. et al., Radiochim. Acta **88**, 619 (2000)
- /3/ Hsi, C.-K. D., Langmuir, D., Geochim. Cosmochim. Acta **49**, 1931 (1985)

# COLLOID INVESTIGATIONS OF ACID ROCK DRAINAGE SOLUTION FROM AN ABANDONED Zn-Pb-Ag MINE BY ULTRAFILTRATION AND PCS MEASUREMENTS

W. Richter, H. Zänker

Acid rock drainage (ARD) solution from an abandoned ore mine was investigated by photon correlation spectroscopy, ultrafiltration and ICP-MS. A colloid concentration of about 1 g/L was found. The prevailing particle size was  $< 5$  nm.

Acid rock drainage (ARD) consists of highly mineralized, red-coloured solutions which are formed by the sulphide oxidation process in the pores of ore mines. We took samples of ARD from the abandoned Zn-Pb-Ag mine at Freiberg for colloid-chemical investigations. The particle size of this water having a pH of 2.72 and a sulphate concentration of 411 mMol/L was determined by photon correlation spectroscopy (BI-90, Brookhaven Instruments Corp., Holtsville, USA) at a laser wavelength of 514.5 nm and a laser power of 400 mW. For deriving the particle size distribution we used the CONTIN deconvolution. Microfiltration was carried out with Nuclepore filters (Costar, Cambridge, USA) and ultrafiltration with YM membranes (Amicon, Beverly, USA). The filtrates and retentates were analysed by inductively coupled plasma mass spectroscopy and/or atomic absorption spectroscopy (ICP-MS, Elan 5000 and AAS 4100, Perkin Elmer, Überlingen, Germany). PCS was possible on all filtrates. The scattered light intensity (count rate of the photomultiplier) of the filtrates decreased with decreasing filter pore size: 153, 22, 8.5 and 5.3 kcps for the raw sample and 400 nm, 50 nm and 30 kD filtrates.

Fig. 1 shows the autocorrelation functions of several sample fractions. These contain information on the time-dependent relaxation of concentration fluctuations in a solution. Monodisperse spherical particles of 10 nm, for instance, reach practically full relaxation after 100  $\mu$ s. As one can see, the autocorrelation functions of the raw sample and the 400 nm filtrate consist primarily of components of relaxation times larger than 100  $\mu$ s. But the autocorrelation functions of the 50 nm and 30 kD filtrates differ from them. They show their major decay before 100  $\mu$ s. These features of the scattered light fluctuations are also reflected in the CONTIN deconvolutions of the autocorrelation functions shown in Fig. 2. They show that most of the larger submicron particles have been removed by 50 nm filtration and 30 kD ultrafiltration so that also the ultrafine particles  $< 5$  nm are detectable by PCS. In the presence of larger submicron particles the detection of extremely small colloid particles by PCS can be prevented by optical masking, since the  $r^6$  of the scattered light intensity is dependent on the particle radius  $r$  in the range of Rayleigh scattering.

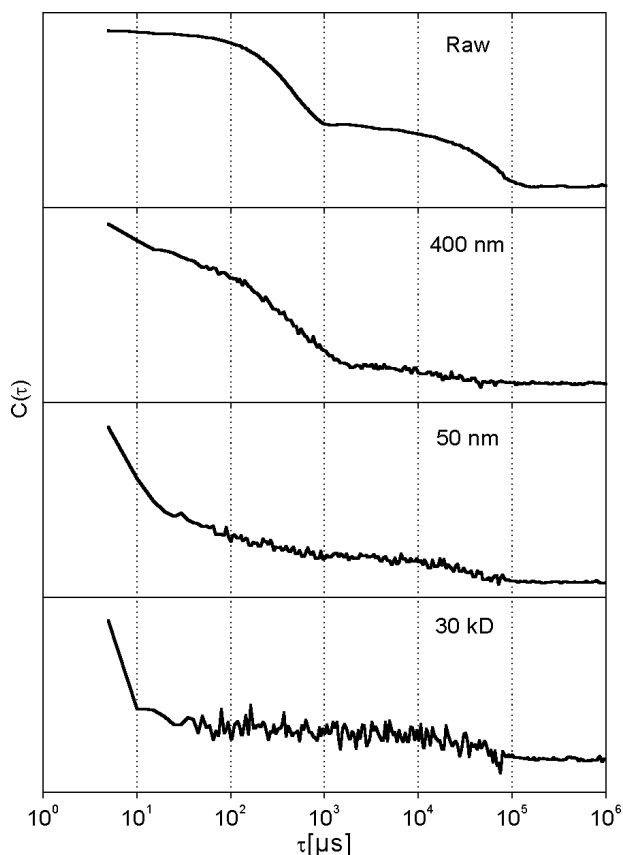


Fig. 1: Autocorrelation functions of the light scattered from the filtrates of ARD samples.

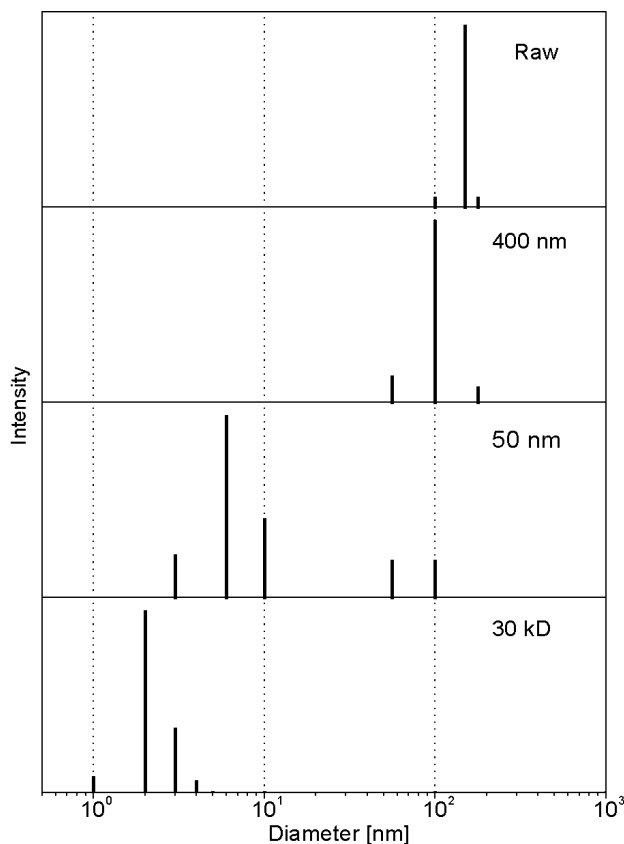


Fig. 2: Light-intensity weighted particle size distribution in the ARD sample filtrates derived by CONTIN deconvolution of the autocorrelation functions.

# CORRECTION OF SORPTION DATA OF $^{234}\text{U}$ CONTAMINATED WITH $^{232}\text{U}$

C. Nebelung

In sorption experiments with  $^{234}\text{U}$  onto various solid materials we measured not only a decrease in the  $\alpha$  activity caused by sorption. The  $\alpha$  spectra measured by liquid scintillation (LS) after sorption also differ from the spectra before sorption. By peakfitting the spectra we measured both  $^{234}\text{U}$  and also  $^{232}\text{U}$  accompanied by its daughter products. Only 81.9% of the  $\alpha$  activity is caused by  $^{234}\text{U}$ , 2.6% by  $^{232}\text{U}$  and 15.5% by its daughter products. For determination of uranium sorption data it is necessary to distinguish between the uranium activity and the activity of the other nuclides.

## Experimental

The  $^{234}\text{U}$  tracer solution used for sorption experiments was analyzed by  $\alpha$  spectrometry, using semiconductor detectors. The  $\alpha$  activity of all  $\alpha$ -emitting nuclides in the solution was determined. In the sorption experiments the  $\alpha$  activity remaining in the liquid phase was measured by LS (Wallac system 1414) and compared with the  $\alpha$  activity of the following solutions: a solution free of added activity (zero effect) and a solution free of solids but possessing the same initial activity as the original solution (reference solution). The LS  $\alpha$  spectra were deconvoluted by peakfitting.

## Results

Fig. 1 shows the  $\alpha$  spectrum (measured with a semiconductor) of an aliquot of the  $^{234}\text{U}$  tracer solution. The comparison between the activity contents of the  $\alpha$ -emitting nuclides and the mass contents determined by the specific activities of each nuclide is given in Tab. 1. Very small masses of  $^{232}\text{U}$  and its daughter products cause measurable activities.

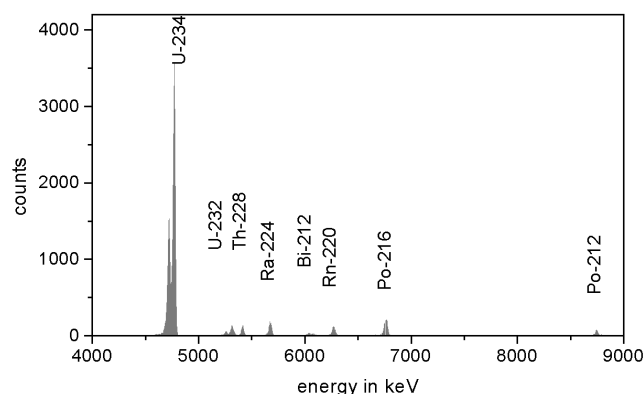


Fig. 1: Alpha spectrum of the  $^{234}\text{U}$  standard

Nuclide	half-live /1/	$\alpha$ activity /%	mass /%
$^{234}\text{U}$	$2.455 \cdot 10^5$ a	81,90	99.9991
$^{232}\text{U}$	68.9 a	2.65	0.0009
$^{228}\text{Th}$	1.9116 a	3.09	$3 \cdot 10^{-5}$
$^{224}\text{Ra}$	3.66 d	3.50	$< 10^{-6}$
$^{220}\text{Rn}$	55.6 s	2.42	$< 10^{-6}$
$^{216}\text{Po}$	0,216 s	4.22	$< 10^{-6}$
$^{212}\text{Bi}$	60.55 m	1.37	$< 10^{-6}$
$^{212}\text{Po}$	0.299 $\mu\text{s}$	0.85	$< 10^{-6}$

Tab. 1: Alpha activities and masses of the nuclides in the  $^{234}\text{U}$  tracer solution

The LS  $\alpha$  spectra after sorption of uranium show higher  $\alpha$  activities of the  $^{232}\text{U}$  daughter products. Spectrum (a) in Fig. 2 is the LS spectrum of a reference sample with a total activity of 1120 Bq, including a  $^{234}\text{U}$  activity of 957 Bq (85%). In sorption sample (b) with the same initial activity after sorption (170 days)

a total  $\alpha$  activity of 26.7 Bq was found. It contained only 7.4 Bq  $^{234}\text{U}$  (28%). After four weeks the same sample was measured again (c). Now a total  $\alpha$  activity of 8,5 Bq with 7.4 Bq  $^{234}\text{U}$  (87%) was analyzed. Immediately after sampling not only the remaining uranium with the daughter products but also daughter products of the sorbed uranium were measured in the solution. After four weeks the short-lived daughter products of the sorbed uranium were decayed.

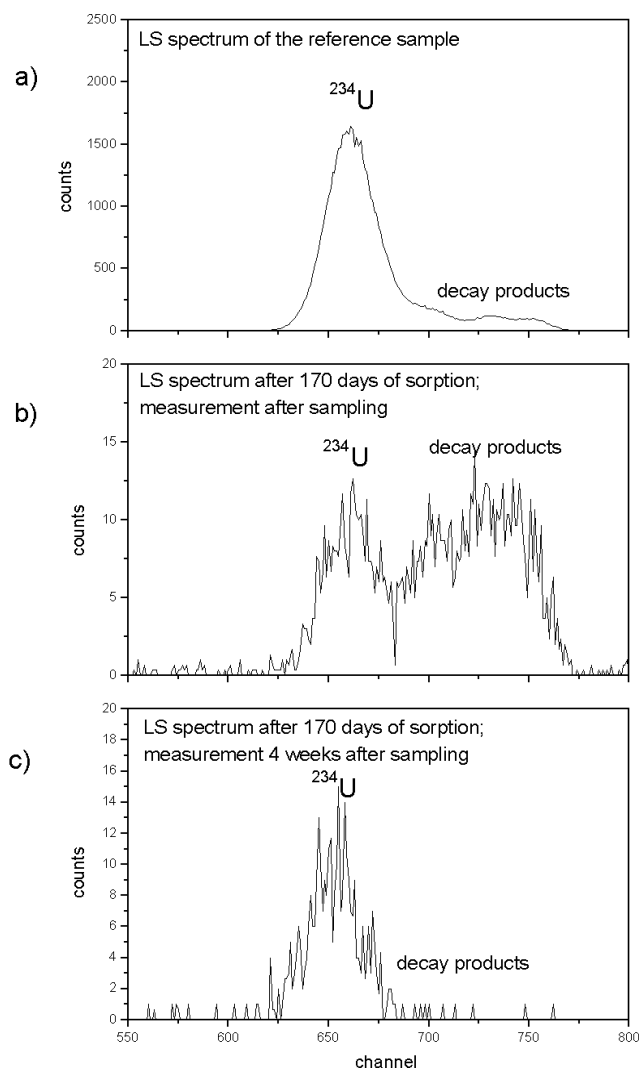


Fig. 2: Alpha spectra measured by liquid scintillation

In extreme cases all uranium was sorbed. Then only the decay products of the sorbed  $^{232}\text{U}$  but no uranium itself were measured after sampling. It is therefore necessary to fit the spectra or to wait four weeks before starting measurements.

## References

/1/ Chu, S.Y.F., Ekström, L.P., Firestone, R.B. *The Lund/LBNL Nuclear Data Search Version 2.0*, February 1999

# SEPARATION OF URANIUM(VI) FROM AQUEOUS SOLUTION BY TEXTILE BOUND CALIX[6]ARENES

K. Schmeide, K. Jansen<sup>1</sup>, D. Keil<sup>2</sup>, K.H. Heise, G. Bernhard

<sup>1</sup>Deutsches Textilforschungszentrum Nord-West e.V. Krefeld, <sup>2</sup>SynTec GmbH Wolfen

The separation of uranium(VI) from aqueous solution by textile bound calix[6]arenes was studied as a function of pH value and of uranium concentration in solution by means of batch experiments. Furthermore, the kinetics of the uranium binding was studied as well as the possibility for remobilization of the bound uranium.

## Introduction

The separation of uranium(VI) from aqueous solution by calix[6]arenes, functionalized with carboxylic or hydroxamic groups at the lower rim, by means of solvent extraction has been described in the literature (e.g., /1-3/). To develop a new procedure applicable for purification of uranium contaminated seepage and mine waters we fixed uranophile calix[6]arenes onto textile substrate. For this, the calix[6]arenes were statistically functionalized by spacer groups (n-alkyl groups) that allow their fixation onto polyester fabric. In this study, we determined the binding properties of mono-p-nonyl-penta-p-tert-butyl-calix[6]arene hexacarboxylic acid fixed onto polyester fabric towards uranium(VI) by means of batch experiments. The results are compared with those obtained for reference material (polyester fabric, not modified with calixarenes).

## Experimental

In separation experiments, 0.5 g calixarene modified polyester fabric were shaken with 20 mL aqueous uranium solution for 6 hours. The pH of the aqueous solution was initially adjusted and measured after reaching equilibrium. The uranium content in the aqueous phase was determined by ICP-MS (results are corrected for uranium sorption onto vial walls). In remobilization experiments, 0.2 g uranium loaded calixarene modified polyester fabric from separation experiments were washed 3 times with 7 mL Milli-Q water, 2 times with 7 mL 0.01 M HCl and 3 times with 7 mL 0.1 M HCl for 2 hours each time.

## Results and discussion

According to the separation experiments (Fig. 1), 97.2% to 98.4% of the uranium present in the initial solution ( $1 \times 10^{-6}$  M) is separated by the calixarene modified polyester fabric in the pH range 7.07 to 7.51.

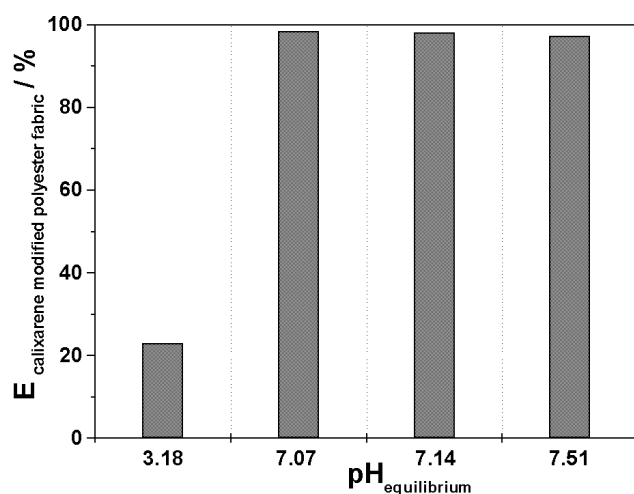


Fig. 1: Separation of uranium from aqueous solution by calixarene modified polyester fabric as a function of pH ( $[UO_2^{2+}]_{initial} = 1 \times 10^{-6}$  M).

Only 27% of the uranium is bound by the reference material under the same experimental conditions. This means, the uranium separation is enhanced by about 70% due to the fixed calixarene. Kinetic experiments at pH 7.5 have shown that the uranium binding by calixarene modified polyester fabric reaches equilibrium within 150 min.

As shown for pH 3.18 in Fig. 1, the uranium separation in the acidic pH range is very low. This indicates a limited applicability of textile bound calixarenes in the acidic pH range.

A loading test with increasing uranium concentration in aqueous solution ( $5.2 \times 10^{-8}$  M to  $2.2 \times 10^{-4}$  M) at pH 5 shows that up to an initial uranium concentration of  $9.8 \times 10^{-6}$  M 92% to 99% of the uranium is separated by the calixarene modified polyester fabric. Maximal  $7.6 \times 10^{-7}$  mol uranium is bound per 1 g of the calixarene modified polyester fabric.

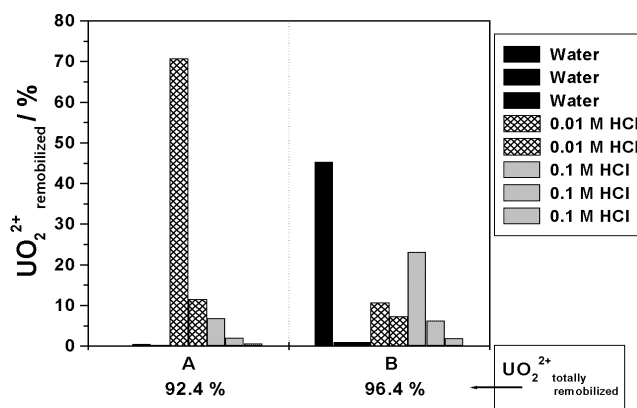


Fig. 2: Remobilization of uranium from calixarene modified polyester fabric (A) and reference material (B) by water, 0.01 M HCl and 0.1 M HCl.

The remobilization experiments (Fig. 2) have shown that from the reference material 47.2% of the bound uranium is remobilized already by rinsing of the material with water. In contrast to this, only 1% of the bound uranium can be remobilized from calixarene modified polyester fabric by rinsing with water. However, the remobilization of the uranium is possible with 0.01 M HCl (82.1%) and 0.1 M HCl (9%). This verifies that the uranium is strongly bound by the calixarene fixed onto the polyester fabric. The textile filter material can be regenerated under acidic conditions.

## Acknowledgment

This work was supported by the BMBF (No. 0339917).

## References

- /1/ Shinkai, S. et al., J. Chem. Soc., Chem. Commun., 233 (1986)
- /2/ Nagasaki, T. et al., J. Chem. Soc., Perkin Trans. 2, 1063 (1991)
- /3/ Schmeide K. et al., Report FZR-318, p.17 (2001)

**Interaction of Actinides/Radionuclides  
with Biological Systems**

## COMPARATIVE ANALYSIS OF BACTERIA IN URANIUM MINING WASTES

T. Tzvetkova, K. Flemming, S. Selenska-Pobell

*Compositional analysis of predominant bacterial groups in three different kinds of uranium wastes gives indications for different biogeological processes running at the studied sites which seems to be influenced by the anthropological activities involved in the production of uranium.*

Predominant bacterial populations were analyzed in two uranium mill-tailings (MT), in one uranium mining waste pile (UMW), and in one uranium mining depository site (DS). One of the mill-tailings, namely the Gittersee/Coschütz (Gitt-MT), is located near the city of Dresden (Germany). The second one (Sh-MT) is located near Shiprock, New Mexico (USA). The JG-UMW is situated near the town of Johannegeor-

genstadt (Germany) and represents reminders of uranium mining. In the case of the depository site Gu-DS, located in Gunnison, Colorado (USA), rests of uranium ores after mining were transported and stored at a site with appropriate geologic characteristics and with low human density in order to reduce any hazardous consequences due to the migration of radionuclides.

Geogr. origin	$\alpha$ -Proteo-bacteria	$\beta$ -Proteo-bacteria	$\gamma$ -Proteo-bacteria	$\delta$ -Proteo-bacteria	HA group	CFB group	Gram <sup>+</sup> Low G+C	GNSB	<i>Nitrospira/ L. ferrooxidans</i>	ANAMMOX	Novel divisions
Gitt-MT	7%	15%	54%	-	-	20%	4%	-	-	-	-
Sh-MT	9%	4%	17%	8%	-	-	35%	13%	10%	4%	-
JG-UMW	29%	8%	21%	12%	25%	-	-	2%	3%	-	-
Gu-DS	16%	7%	52%	5%	9%	-	-	-	-	-	11%

Tab. 1: Size of the bacterial populations at the studied sites.

As evident from the results presented in Tab. 1, populations of  $\alpha$ -,  $\beta$ -,  $\gamma$ -Proteobacteria were found in all kinds of the uranium wastes. The  $\gamma$ -Proteobacteria were most predominant in the Gitt-MT and in the Gu-DS. In agreement to our previous observations /1/ the main representatives of this bacterial group in all samples were affiliated to *Pseudomonas*. Relatively high was the part of  $\alpha$ -Proteobacteria, in particular of those acting as plant symbionts, in the samples of JG-UMW and Gu-DS. This observation indicates that at that sites a bioremediation in advanced stages occurs.  $\delta$ -Proteobacteria were identified in the soil samples from the Sh-MT, JG-UMW and the Gu-MT. Interestingly, this bacterial group, consisting mainly of sulfate and metal reducing bacteria, was demonstrated to be predominant in the water samples of these environments /2, 3/. The latter is an indirect indication for metal reduction, especially for U-reduction and precipitation from the liquid wastes at that sites /3/. Surprisingly, no  $\delta$ -Proteobacteria were found in Gitt-MT, instead, a population of the  $\beta$ -Proteobacteria was identified in a higher density than in the other three sites.

Significant differences were found in the distribution of bacteria from the phyllums Holophaga / Acidobacterium (HA), Cytophaga / Flavobacterium / Bacteroides (CFB) and of the Gram<sup>+</sup> bacteria with low G+C content between the two uranium mill-tailings on one hand and the UMW and the DS on the other hand. Members of the HA phylum seems to be characteristic for the UMW and DS. For the MT Gram<sup>+</sup>-bacteria and CFB are more specific. This observation is not surprising, bearing in mind the high levels of toxic As-compounds in the mill-tailings and the ability of these two groups of bacteria to biotransform them. Members of CFB are also indicative for changes from oligotrophic to organotrophic conditions in the environment as these bacteria are known as most rapidly adaptive to higher nutrient levels /4/. Hence, the significant amount of CFB in the Gitt-MT is an indication for actively running biological processes there. In the

Sh-MT, in contrast, CFB were not found, instead relatively large populations of green non-sulfur bacteria (GNSB) and *Nitrospira/Leptospirillum ferrooxidans* were identified. The latter are typical for natural and commercial metal-leaching environments /2/. On the basis of the above mentioned observations one may consider the Gitt-MT much more remediated than the Sh-MT.

Interesting is the presence of Planctomycetales (ANAMMOX) in the soil samples of the Sh-MT, which are possibly involved in anaerobic oxidation of ammonium to molecular nitrogen. In our previous work representatives of the same bacterial group were found in drain waters of the Gitt-MT /2/. These bacteria are possibly responsible for the observed strong ammonium fluctuations in the deep waters of the two mentioned mill-tailings (Phill Long and Claudia Helling, personal communications).

The presence of relative large number of representatives from novel not yet characterized bacterial divisions in the samples of the Gu-DS is interesting but not surprising. Such representatives are possibly also present within the not yet analyzed individual clones of the 16S rDNA libraries of the all site studied. The latter represent about 50% of the constructed clones and are under investigation in our laboratory.

### Acknowledgements

This work was supported by grant SMWK 7531.50-03-607 from the Sächsisches Staatsministerium für Wissenschaft und Kunst, Dresden, Germany.

### References

- /1/ Selenska-Pobell, S., et al., Antonie van Leeuwenhoek, **79**, 149-161 (2001)
- /2/ Selenska-Pobell, S. In: *Interactions of Microorganisms with Radionuclides*, Elsevier Sciences, Oxford, UK, pp. 225-253, (2002)
- /3/ Chang, et al., Appl Environ Microbiol **67**, 3149-3160 (2001)
- /4/ Lebaron, P., et al., FEMS Microbiol Ecol **34**, 255-266, (2001)

## PARTIAL ANALYSIS OF THE CENTRAL DOMAIN OF THE *Bacillus sphaericus* JG-A12 S-LAYER PROTEIN

M. Schnorpfel, J. Raff, K. Flemming, S. Selenska-Pobell

310 amino acids from the central domain of the *B. sphaericus* JG-A12 S-layer were analyzed. In contrast to the N-terminal domain of this protein, which possesses a unique structure, the part studied in this work shares a significant identity with the corresponding parts of several other *B. sphaericus* S-layers.

Recently we demonstrated that the N-terminal domain (NTD) of the crystalline S-layer protein of the uranium mining waste pile isolate *B. sphaericus* JG-A12 differs significantly from those of the other *B. sphaericus* S-layers studied up to date [1], see also Fig. 1.

In this work a part of the S-layer gene corresponding to the 3' end of the N-terminal domain and to the beginning of the central domain (CD) of the matured S-layer protein of this strain was studied. The amino acid sequences derived from the primary structure of the sequenced part of the gene were compared with the corresponding amino acid stretches of the known *B. sphaericus* S-layers (see Fig. 1). From the scheme presented in Fig. 1 it is evident that the NTD of the JG-A12 S-layer possesses a low identity of 24% with the NTD of the other S-layer proteins. In contrast, the part of the CD of the S-layer of *B. sphaericus* JG-A12 studied in this work shares high identity with the CDs of the S-layers of *B. sphaericus* P1 and *B. sphaericus* ATCC4525. Very high is the identity found in the first 125 amino acids of the CDs. It represents 74% for the S-layer of *B. sphaericus* P1 and 67% (not shown in the figure) for that of *B. sphaericus* ATCC4525. The same S-layer regions of the latter two strains also possess a high identity of 59% with each other (see Fig. 1). The identity of these three proteins decreases slowly in the further region of about 200 amino acids studied (see Fig. 1).

Interestingly, the high identity shared between the NTD of the S-layer of *B. sphaericus* 2362 and the NTDs of the S-layers of *B. sphaericus* P1 and *B. sphaericus* ATCC4525 ceases suddenly at the beginning of the central domain and drops rapidly to the extremely low value of 11% (see Fig 1).

The abrupt changes in the identity between the NTDs and the CDs in the cases of the S-layers of JG-A12 and 2362 in comparison with the S-layers of the strains 4525 and P1 may be explained by a horizontal transfer and exchange of parts of the S-layer genes with those of some other, phylogenetically unrelated bacterial strain.

The S-layer proteins of the strains 4525 and P1 seems to be products of genes which were subjected to a continuous "vertical" evolution, while those of JG-A12 and 2362 are most probably products of two genes that were naturally recombined via lateral DNA transfer. Interestingly, in the case of the JG-A12 S-layer the NTD is unique, while in the case of the 2362 the CD is unique. In both cases, the remaining parts of the proteins share significant homology with the above mentioned two proteins of the strains 4525 and P1, which on the basis of our analysis, may be considered standard for the species *B. sphaericus*. It is noticeable that the S-layers sharing high homology at

the beginning of their CDs, namely those of JG-A12, P1, and 4525, build protein lattices with a square symmetry (2). The analysis of the whole molecules of the S-layers of P1 and 4525 demonstrates also that the homology of the remaining parts of these two proteins in the direction of the C terminus drops by up to 24%.

On the basis of these observations one may conclude that the first 125 amino acids of the CDs of these three proteins are possibly responsible for the symmetry of the matured protein crystals. Indeed, the S-layer of 2362, which differs significantly in this part of the CD from the above mentioned ones, has an oblique symmetry (3, 4). Further analyses of the JG-A12 S-layer will possibly allow to find characteristics explaining the high capability of this protein to interact with uranium and other metals as well as its relatively high instability in comparison with the S-layers of the other *B. sphaericus* strains studied up to date.

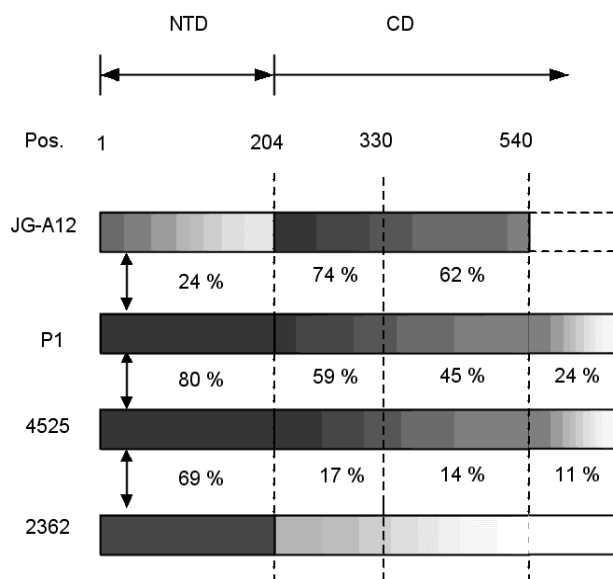


Fig. 1: Schematic comparison of the S-layers of *B. sphaericus* JG-A12, *B. sphaericus* P-1, *B. sphaericus* 4525, and *B. sphaericus* 2362

### Acknowledgement

This work was supported by grants SE 671/7-1 from the Deutsche Forschungsgemeinschaft (DFG) and SMWK.7531.50-03.0370-01/5 from the Sächsisches Staatsministerium für Wissenschaft und Kunst, Dresden, Germany.

### References

- [1] Raff, J. et al., Report FZR-318 (2001) p. 38
- [2] Wahl, et al., Biotechnol. Letters **23**, 1485 (2001)
- [3] Sidhu, M.S., Olsen, I. Microbiology **143**, 1039-1052 (1997)
- [4] Raff, J. et al., PhD Thesis (2002)

# BIOSORPTION OF URANIUM AND COPPER BY *BACILLUS SPHAERICUS* JG-A12 CELLS, SPORES AND S-LAYER PROTEINS EMBEDDED IN SOL-GEL CERAMICS

J. Raff, U. Soltmann<sup>1</sup>, S. Matys<sup>2</sup>, H. Boettcher<sup>1</sup>, W. Pompe<sup>2</sup>, S. Selenska-Pobell

<sup>1</sup> Arbeitsgruppe Funktionelle Schichten, GMBU e.V., Dresden, Germany

<sup>2</sup> Institut für Materialwissenschaft, Technische Universität Dresden, Dresden, Germany

Vegetative cells, spores and stabilized S-layer sheets of *B. sphaericus* JG-A12 were embedded in SiO<sub>2</sub> bulk particles using sol-gel techniques. In sorption experiments the metal binding capacity of the free biocomponents and the corresponding biological ceramics were compared.

Bacteria living in environments highly polluted with radionuclides and heavy metals are well adapted to the complex and toxic conditions there. This adaptation includes resistance to the toxic compounds present and also the development of detoxification strategies. Such bacteria are therefore suitable for the construction of biological ceramics, which are used for cleaning waste waters polluted with various radionuclides and heavy metals. In former experiments we showed the selective binding of U, Cu, Pb, Al and Cd from drain waters of a uranium mining waste pile by cells and spores of *Bacillus sphaericus* JG-A12. This *Bacillus* strain was recovered from the uranium mining waste pile called "Haberland" situated near the town of Johannegeorgenstadt [1]. This bacterium possesses a surface layer (S-layer) as the outermost component of its cell wall, which differs at its N-terminal domain significantly from all other S-layers studied up to date [2]. Vegetative cells, spores and stabilized S-layer sheets of this strain were used to construct biological sol-gel ceramics (biocers) [3]. In this study the metal-binding capacity of the biocers and of the single components was investigated. Various kinds of biological ceramics were prepared by dispersing vegetative cells, spores and 1-ethyl-3-(N,N'-dimethylaminopropyl)-carbodiimide cross-linked S-layer sheets of *B. sphaericus* JG-A12 in aqueous silica nanosols, gelling and drying [3]. Sorption experiments with uranium and copper were carried out with 200 mg dry weight of sieved silica gel particles (xerogel or biocers) of a size of 355-500 µm containing 36.4 mg equal to  $2.6 \times 10^{10}$  cells, 17.23 mg equal to  $2.8 \times 10^{10}$  spores, or 36.4 mg S-layer sheets. The composite materials and the single components were shaken in 35 ml 0.9 % NaClO<sub>4</sub> pH 4.5 with  $9 \times 10^{-4}$  M uranium or copper at 30 °C for 48 h. The amount of sorbed metals was calculated by measuring the metal concentration in the supernatant, using ICP-MS.

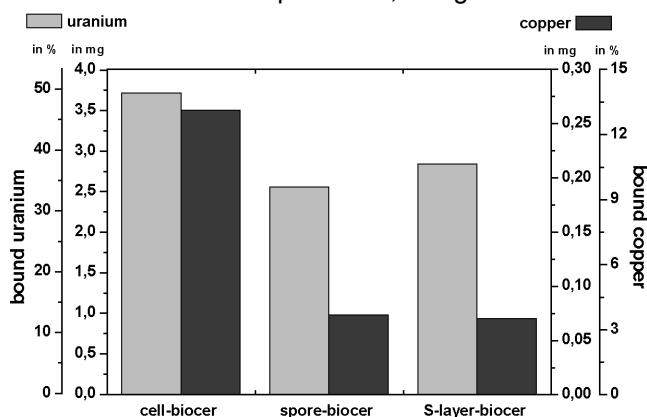


Fig. 1: Uranium and copper sorption by 200 mg dry weight of various biocers (absolute amounts in mg and relative amounts in % off all).

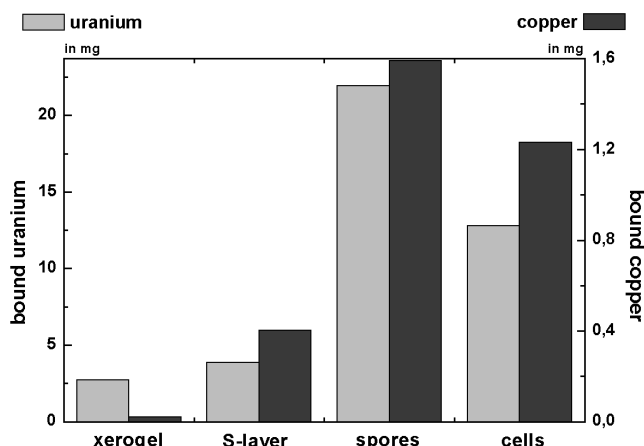


Fig. 2: Uranium and copper sorption by 200 mg dry weight of the single components.

As evident from the results presented in Fig. 1, the metal-binding capacity of biocers depends on the embedded biocomponent. Immobilized cells showed the highest capacity, followed by immobilized S-layer fractions and spores. The latter is not in good agreement with the binding characteristics of the single components (see Fig. 2). Spore biocers have only 50 % of the theoretical binding capacity calculated from the capacity of the single components. In contrast, biocers with cells or S-layer bind 75 % or more of this theoretical value. The low metal-binding capacity of biocers with spores may be connected with the formation of a more compact bioceramic of lower porosity due to the small size and rather high density of the spores, which are nearly water free. The pure silica particles also bind uranium. In all cases the binding capacity for uranium is much higher than that for copper, but copper binding is more specific for the biocomponent. The metal-binding capacity is increased by using various drying methods or by adding water-soluble additives such as sorbitol during the production of the sol-gel ceramics. Uranium and copper were completely removed from the biocer by washing with 0.5 M citric acid, pH 4.5. In contrast, by washing twice with 0.9 % NaClO<sub>4</sub>, pH 4.5 only 19 % of the sorbed uranium and 50 % of the sorbed copper were removed.

## Acknowledgement

This work was supported by grant SE 671/7-1 from the Deutsche Forschungsgemeinschaft (DFG).

## References

- [1] Selenska-Pobell, S. et al., FEMS Microbiology Ecology **29**, 59 (1999)
- [2] Raff, J. et al., Report FZR-318, p. 38 (2001)
- [3] Soltmann, U. et al., 2002 (in press)

# CHARACTERIZATION OF THE URANIUM (VI) COMPLEXES FORMED BY THE CELLS OF THREE *A. ferrooxidans* ECO-TYPES USING TIME-RESOLVED LASER-INDUCED FLUORESCENCE SPECTROSCOPY (TRLFS)

M. Merroun, G. Geipel, S. Selenska-Pobell

TRLFS was used to study the properties of the uranium complexes formed by the cells of the three recently described eco-types of *A. ferrooxidans* /1/. The results demonstrate that the lifetimes of the complexes are type-specific and are increasing in the same order as the capability of the bacterial strains to accumulate uranium.

Microorganisms, possess abundant functional groups, such as carboxyl, hydroxyl and phosphate on their surface that bind metal ions. In order to clear the role of these groups in the biosorption process, it is useful to characterize the metal-microbial complexes using physical methods such as time-resolved laser-induced fluorescence spectroscopy (TRLFS).

Sample	Emission maxima (nm) (Halfwidth (nm))			
UO <sub>2</sub> <sup>2+</sup> , 0.5 mM, pH 2	491.1 (13.1)	512.2 (14.7)	536 (17.8)	561.2 (15.8)
<i>A. ferrooxidans</i> type I	496.1 (12.6)	517.2 (13.0)	540.9 (13.5)	566.4 (18.4)
<i>A. ferrooxidans</i> type II	495.4 (18.4)	516.8 (13.6)	540.8 (13.8)	566.4 (17.8)
<i>A. ferrooxidans</i> type III	496.3 (14.8)	517.5 (12.8)	541.6 (13.7)	566.3 (11.4)
U-ATP	495.3 -	516.5 -	540.2 -	564.6 -

Tab. 1: Spectroscopic parameters of the bacterial UO<sub>2</sub><sup>2+</sup>-complexes

In this study we used TRLFS to characterize the uranium complexes built by three eco-types of *A. ferrooxidans*. In Figure 1 the lifetimes are shown of the *A. ferrooxidans* uranium complexes. The lifetime  $\tau_1$  for uranyl ion (aq) was determined as 1.4-1.5  $\mu$ s, while the lifetime  $\tau_2$  attributed to the uranyl species bound to the biomass of the *A. ferrooxidans* eco-type I was estimated as 23.6  $\mu$ s. The lifetimes of the uranium complexes bound to type II and III ( $\tau_2$ ) were determined as 44.6 and 25.8  $\mu$ s, respectively.

The emission fluorescence bands of the *A. ferrooxidans* uranium complexes studied using TRLFS (Tab. 1) indicate that organic phosphate residues are coordinated to the uranyl ions. These results are in agreement with those found using other physical methods such as EXAFS and EDX /1/. In addition, TRLFS can distinguish the uranium complexes formed by the three bacterial eco-types. The results of this work demonstrate that the uranium complexes built by the three eco-types of *A. ferrooxidans* have different lifetimes. In addition, the amount of the uranium bound increases with increasing the formation constant values (mass action law). Therefore the amount of uranium accumulated by the three bacterial eco-types increases with the increase of lifetime of the corresponding uranium complexes.

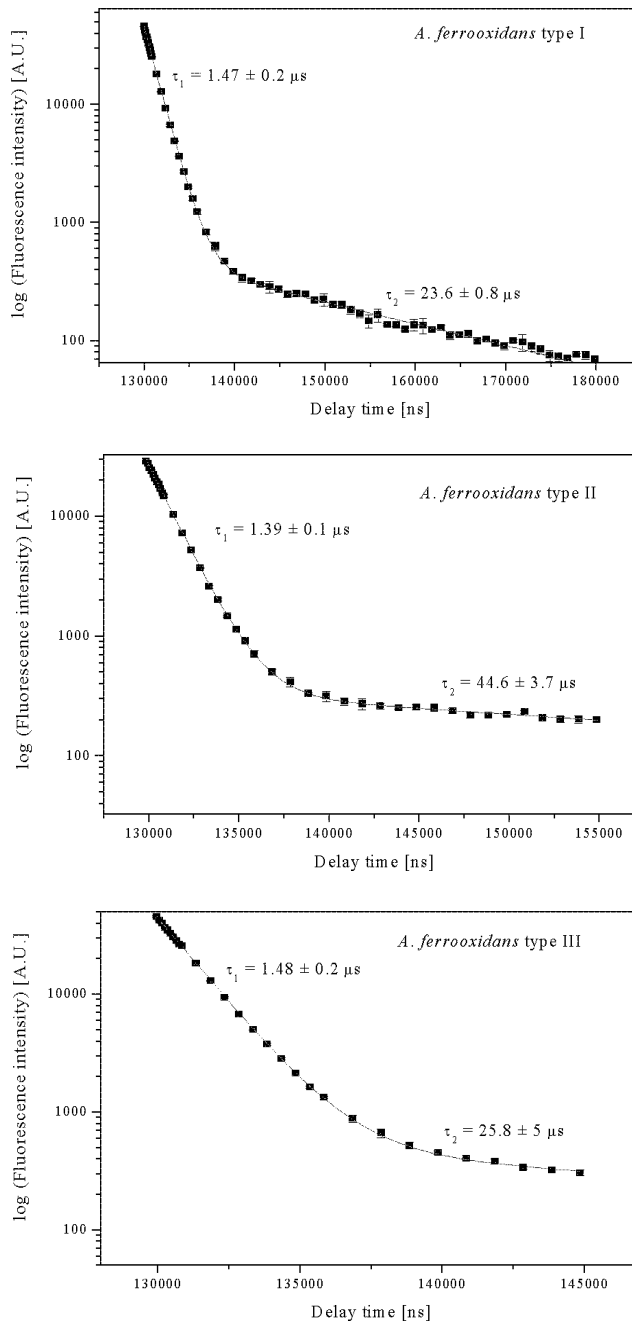


Fig. 1: Time-dependency of emission decay of U(VI)-*A. ferrooxidans* complexes

## Acknowledgment

This study was supported by grant 4-7531.50-03-FZR/607 from the Sächsisches Staatsministerium für Wissenschaft und Kunst, Dresden, Germany.

## References

/1/ Merroun, M. et al., Radiochim. Acta (submitted)

# CELLULAR LOCALIZATION OF URANIUM ACCUMULATED BY *A. FERROOXIDANS* CELLS USING TRANSMISSION ELECTRON MICROSCOPY AND ENERGY-DISPERSIVE X-RAY ANALYSIS

M. Merroun, S. Selenska-Pobell

*A combination of Transmission Electron Microscopy (TEM) and Energy-Dispersive X-ray (EDX) was used to study the cellular localization of uranium accumulated by the cells of A. ferrooxidans.*

Uranium and other actinides may be present initially in soluble or insoluble forms in natural and also in so called disposal sites. There they may be converted from one to the other form by microorganisms. Under appropriate conditions actinides can be mobilized or immobilized by direct (enzymatic) or indirect (nonenzymatic) microbial actions. In this work we used TEM and EDX to determine the cellular localization of uranium accumulated by *A. ferrooxidans* cells.

TEM analysis of *A. ferrooxidans* cells exposed to 0.5 mM uranium solution demonstrates electron-dense accumulates mainly within the extracellular polysaccharides (Fig. 1a). These electron-dense accumulates were identified as uranyl phosphates using EDX analysis (not shown), in agreement with EXAFS results [1]. Electron dense granules were observed also in the cytoplasm (Fig. 1c). EDX analysis of these granules showed that they contain high amounts of U and P (Fig. 2a). We suggest that these granules correspond to polyphosphate bodies. Inorganic polyphosphates (poly P), are linear polymers of inorganic phosphate ( $P_i$ ) residues linked by phosphoanhydride bonds. Chains length may vary from 3 to 1000  $P_i$  residues depending on the organisms, its growth and physiological conditions. It has been suggested that the intracellular chelation of heavy metals by polyphosphate is a passive mechanism for heavy metal tolerance.

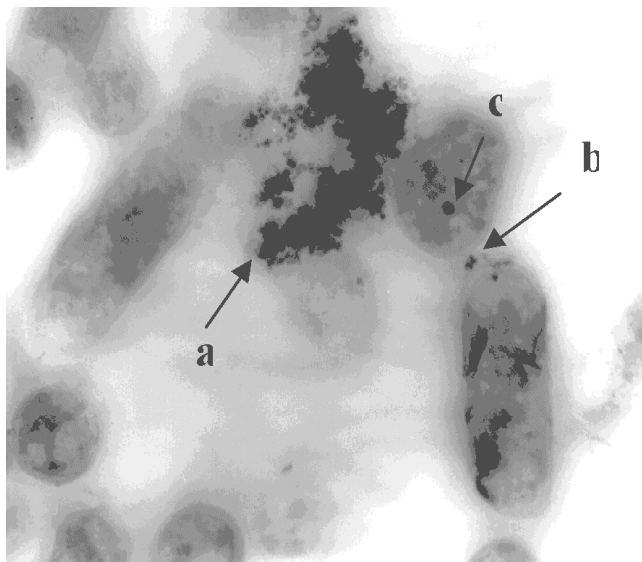


Fig. 1: Transmission electron micrograph of a thin section of *A. ferrooxidans* W1 challenged with uranium. The metal accumulated is located within the extracellular polysaccharides (a), on the cell wall (b), and at the level of intracellular polyphosphate bodies (c). Magnification 20 000 $\times$ .

A small part of the uranium accumulated by *A. ferrooxidans* cells is located on the cell wall (Fig. 1b) as

phosphate compounds (Fig. 2b). No U was detected in the control, untreated with uranium, cells.

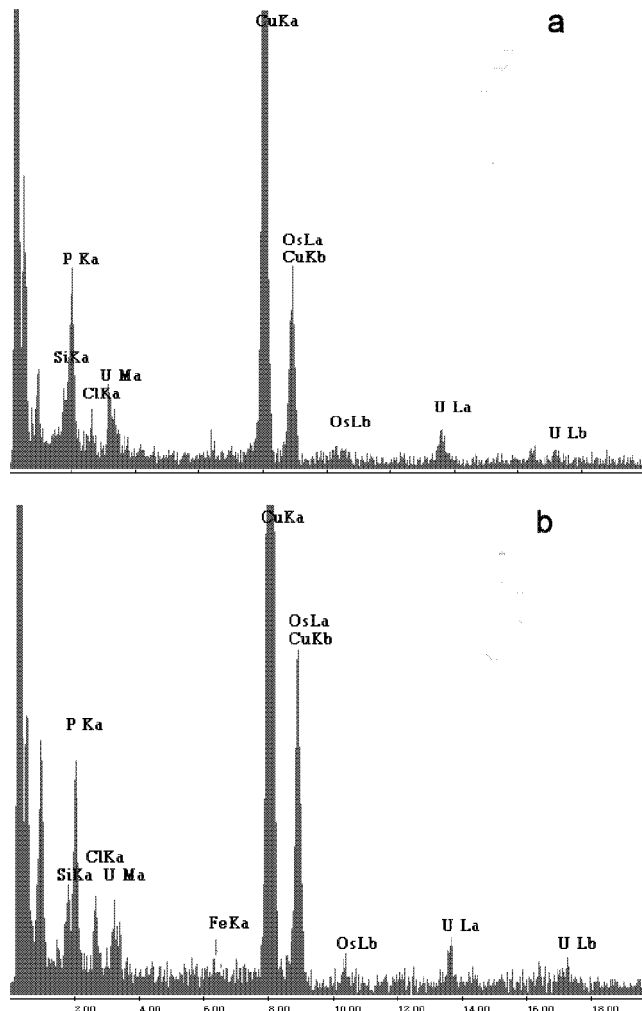


Fig. 2: Energy-dispersive x-ray (EDX) analysis of *A. ferrooxidans* samples with uranium: a) intracellular polyphosphate bodies and b) compounds at the cell wall.

Based on the combined information from TEM and EDX we conclude that the uranium accumulated by *A. ferrooxidans* cells is located mainly as organic phosphate compounds mainly within the extracellular polysaccharides and on the cell wall. Once the uranium enters the cells, this radionuclide is detoxified through sequestration by intracellular polyphosphate bodies.

## Acknowledgment

This study was supported by grant 4-7531.50-03-FZR/607 from the Sächsisches Staatsministerium für Wissenschaft und Kunst, Dresden, Germany.

## References

[1] Merroun, M. et al., Radiochim. Acta (submitted).

# FT-IR STUDIES OF THE PHOTOREACTIONS OF PHYTOCHROME ASSEMBLED WITH ISOTOPIC LABELED CHROMOPHORES

H. Foerstendorf, W. Gärtner<sup>1</sup>, F. Siebert<sup>2</sup>

<sup>1</sup>Max-Planck-Institut für Strahlenchemie, Mülheim, Germany; <sup>2</sup>Albert-Ludwigs-Universität, Freiburg, Germany

The photoreactions of the plant receptor phytochrome was investigated by FT-IR difference spectroscopy. The assembly of all-<sup>13</sup>C-labeled PΦB to the apoprotein allows the discrimination between chromophore and protein modes in the infrared spectra due to the isotope effect.

The active molecule of the plant photoreceptor phytochrome (Phy) is a soluble homodimer of two polypeptides each consisting of about 1,100 amino acids and containing a covalently linked linear tetrapyrrole chromophore (Fig. 1, PΦB). It shows a photoreversible photoreaction between two parent states Pr ( $\lambda_{\max}$  = 666 nm) and Pfr ( $\lambda_{\max}$  = 730 nm) /1/. During this photoreaction the chromophore undergoes a Z,E isomerization around its C<sub>15</sub>=C<sub>16</sub> double bond via several intermediates which can be trapped at low temperatures /2/.

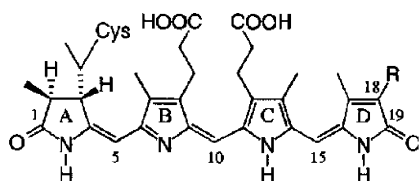


Fig. 1: PΦB-chromophore of phytochrome (R = -CH=CH<sub>2</sub>)

Light induced FT-IR difference spectroscopy is a powerful tool for investigating the photoreactions of biological systems. Although the obtained spectra are generally characterized by numerous bands, detailed information about structural changes occurring during the conversions can be derived. An indispensable prerequisite for the interpretation of the spectra is a correct assignment of the bands to distinct molecular groups. This can be achieved by comparing spectra of selective modified systems with those of the native protein. Recently, we assigned bands around 1725 cm<sup>-1</sup> to the outer carbonyl groups of the chromophore using isotopically labeled PΦB /3/.

In the difference spectra only modes are detected which change their frequencies upon the induced reaction, but the number of arising bands is still considerably high. A discrimination between spectral features originated from the chromophore and from the protein matrix, respectively, is therefore desirable. We reconstituted the Phy apoprotein with chromophores which were isolated from bacteria grown in a <sup>13</sup>C-medium and producing all-<sup>13</sup>C-PΦB. Due to the isotope effect considerable shifts of the chromophore bands are expected.

In the spectral range above 1500 cm<sup>-1</sup> distinct shifts of several bands are observed (indicated by arrows) in the spectra of the parent states (T=0 °C; Fig. 2) and of the first intermediate formed out of Pr, i.e. lumi-R (T= -140 °C; Fig. 3). These bands can be assigned to the chromophore whereas the strong band around 1640 cm<sup>-1</sup> is obviously due to the amide-I mode of the protein since it is not shifted. In the so-called fingerprint region below 1500 cm<sup>-1</sup> great parts of the Pfr-spectrum remain unaltered suggesting strong contributions from amino acid residues of the protein. In contrast, in this region the lumi-R-spectrum is obviously characterized by bands which have to be as-

signed to chromophore modes since patterns of band structures are completely shifted to lower frequencies.

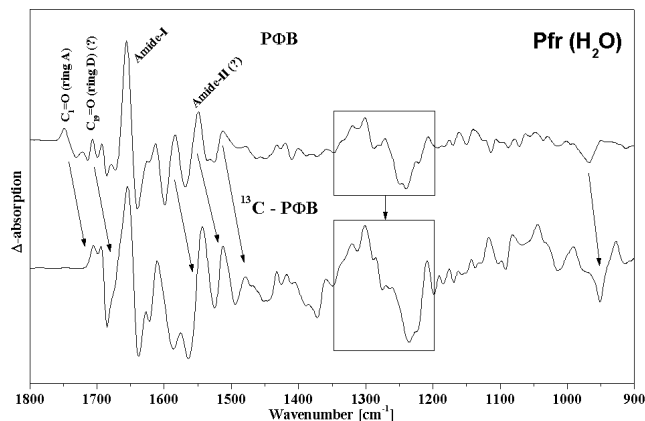


Fig. 2: Pfr/Pr spectra of Phy-PΦB (upper trace) and Phy-<sup>13</sup>C-PΦB (lower trace). Positive bands represent Pfr, negative Pr.

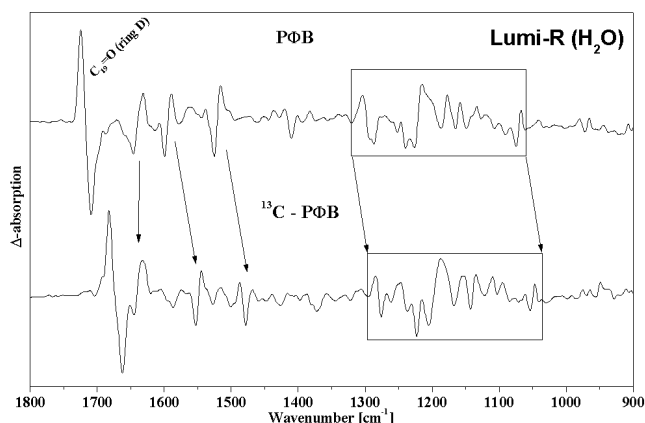


Fig. 3: Lumi-R/Pr spectra of Phy-PΦB (see Fig. 2)

We conclude that in the early stage of the photoreaction molecular changes mainly depend on the chromophore and its environment whereas significant conformational changes of the protein occur in the later steps of the photoconversion.

The incorporation of unspecific labeled <sup>13</sup>C-PΦB into the Phy apoprotein provides the identification of chromophore modes especially in the spectra of the early intermediates. This will considerably facilitate the interpretation of infrared spectra of phytochromes in future times.

## Acknowledgment

This work was supported by the Deutsche Forschungsgemeinschaft (SI 287/20-1).

## References

- 1/ Casal, J.J., Photochem. Photobiol. **71**, 1-11 (2000)
- 2/ Sineshchekov, V., Biochim. Biophys. Acta **1228**, 125-164 (1995)
- 3/ Foerstendorf, H. et al. Biochemistry **40**, 14952-14959 (2001)

# **Modeling of Radionuclide Transport**

# INTEGRATION OF THE METAL ION CHARGE NEUTRALIZATION MODEL FOR HUMIC ACID COMPLEXATION INTO THE GEOCHEMICAL SPECIATION CODE EQ3/6

V. Brendler

Geochemical modeling often requires the consideration of humics as major complexing agent and colloid. The metal ion charge neutralization model can handle respective interactions and has therefore been integrated into the speciation software EQ3/6. An application showing the influence of the pH-dependence of the loading capacity on actinide speciation is given.

One of the most prominent models used to describe interactions between humics and actinides is the metal ion charge neutralization (MICN) model /1/. Essential parameters required by the model are the proton exchange capacity (PEC) giving the total of available binding sites, and the loading capacity (LC) describing the part of the binding sites actually accessible for ligands (normalized to the charge of the ligand). LC is a phenomenological parameter and thus a function of pH, ionic strength, ligand and others.

The EQ3/6 geochemical speciation package /2/ is well suited for thermodynamic and kinetic modeling of complex and heterogeneous systems. But so far the software does not consider any humics-metal interactions, despite that such interaction can not be neglected in many natural systems. Therefore the MICN approach has been integrated into EQ3/6. This required changes in Fortran code of the modules for the data input, the addition of the computation of LC as  $f(\text{pH})$  and the determination of the metal complex concentration. The program was compiled both as UNIX version (f77 compiler) and MS Windows NT version (Lahey LF 90 compiler). A major goal of the development was to reach a flexible solution with minimum impact on the existing input file and database structure. So unused options in the EQ3/6 input files now trigger functions such as the mode of the humics hydrolysis (see below), or the type of the pH function of LC.

Humics species were included into the EQ3/6 thermodynamic database by defining pseudo-species based on fictitious elements because the very nature of humics prevent an exact stoichiometry and formation reaction based on simpler organic molecules. The humics species set exists twice: one version is based on a formally uncharged humics molecule  $\text{Hx}(\text{aq})$ , the other one ( $\text{HhH}_2$ ) considers two deprotonation steps. An input option allows the switch between these two alternative formulations.

A verification of the changed EQ3/6 version was done through speciation modeling of the systems U(VI)-humic acid and Np(V)-humic acid. In a first step published LC values for the humic acid-actinide system were fitted to a linear function as the simplest possible approach. Fig. 1 shows the results for Np(V). Then the obtained pH-LC relationship was used to compute the actinide speciation pattern as given in Fig. 2, again for Np(V). Similar results for U(VI) lead to the conclusions that a) the thermodynamic data sets for the interactions between actinides and humic acids are sparse and scattered, and b) LC as function of pH is not well defined, certainly caused by its very nature

of being an empirical correction factor subsuming many different effects. To obtain a more comprehensive picture of the situation a development of a respective database has been initiated.

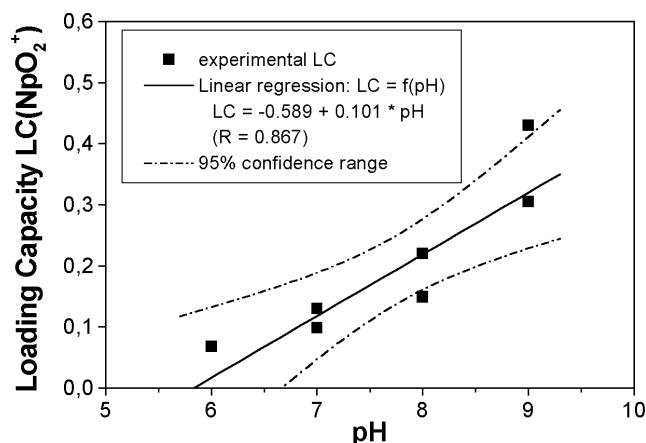


Fig. 1: Loading capacity LC of humic acids with respect to neptunyl(V) ions: measured and modeled values as  $f(\text{pH})$

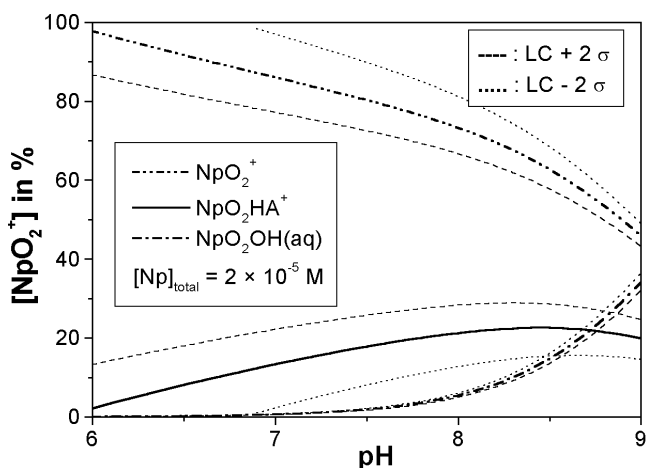


Fig. 2: Np(V) speciation at humic acid concentrations of 100 mg/L in 0.1 M  $\text{NaClO}_4$  computed with the updated EQ3/6 version

## Acknowledgement

Funding by the German Federal Ministry of Economics and Technology (BMWi) under contract No. PtWt+E 02E92999 is gratefully acknowledged.

## References

- Kim, J.I., Czerwinski, K.R., Radiochim. Acta **73**, 5-10 (1996)
- Wolery, T.J., Report UCRL-MA-110662 Part I, Lawrence Livermore National Laboratory (1992)

## FURTHER DEVELOPMENTS OF THE RES<sup>3</sup>T SORPTION DATABASE

V. Brendler

RES<sup>3</sup>T - the Rossendorf Expert System for Surface and Sorption Thermodynamics currently under development has been expanded towards the provision of comprehensive sorption data sets suitable for complex natural systems of rocks and soils. Also a statistical evaluation of the available SCM (Surface Complexation Model) data is now implemented. Finally, a normalization of SCM parameters to a standard site density has been incorporated.

### Selection of data sets

The mineral-specific sorption database currently under development /1,2/ now allows users to easily extract comprehensive data sets as necessary to model complex scenarios involving natural water interacting with rocks and soils. The user is supplied with all records relevant for the combination of given lists of relevant minerals and ligands (contaminants and matrix elements). Next, a specific SCM subtype must be selected. The resulting data assembly can now be checked and condensed based on criteria such as consistency, accuracy and trustworthiness. Whereas at the moment the data collection finally arrived at can only be printed or exported in ASCII format, in future the user may choose to export directly in an input file for geochemical speciation codes such as MINTEQA2, GEMS, PHREEQC-2 or HARPHRQ and reactive transport software such as CHEMTARD, HYDROBIOGEOCHEM or OS3D/GIMRT. In case of such data exports, the output format will automatically be adapted to the specific requirements of the different software packages.

### Statistical evaluation

Based on the large data accumulation accessible via RES<sup>3</sup>T, a statistical evaluation of the currently available SCM data records was performed. It revealed that at present the information supply is very unbalanced concerning the requirements of risk assessment and site remediation. Most SCM data are gathered for the contaminants uranium, copper, cadmium, thorium, and lead, but nearly no data are available for other actinides (especially under reducing conditions). Concerning the solid phases, iron (hydr)oxides, clays, aluminum (hydr)oxides, quartz varieties, and manganese (hydr)oxides are well represented, see Fig. 1, whereas important rock forming mineral groups such as feldspars, mica, pyroxenes, amphiboles, or olivines have not been investigated to a satisfactory extent.

### Normalization of surface data

As clearly pointed out by Kulik in /3/ the establishment of standard and reference states for surface complexation data is essential for a proper thermodynamic handling of such reactions. Therefore a respective normalization procedure has been integrated into RES<sup>3</sup>T, allowing a comparison of the various SCM parameters for given combinations of SCM subtype and mineral. Following /3/ and setting the reference site density to 12.05 sites / nm<sup>2</sup>, the 1<sup>st</sup> protolysis constants for goethite, hematite, ferrihydrite, SiO<sub>2</sub>(am),  $\gamma$ -alumina, and TiO<sub>2</sub> have been normalized. The results for goethite are shown in Fig. 2. As expected, the data spread is reduced by this normalization procedure, especially for the Constant Capacitance and Diffuse Double Layer models. In

general, the normalization effect is much less pronounced for the Triple Layer model, however, where also the original measured values exhibit the broadest range.

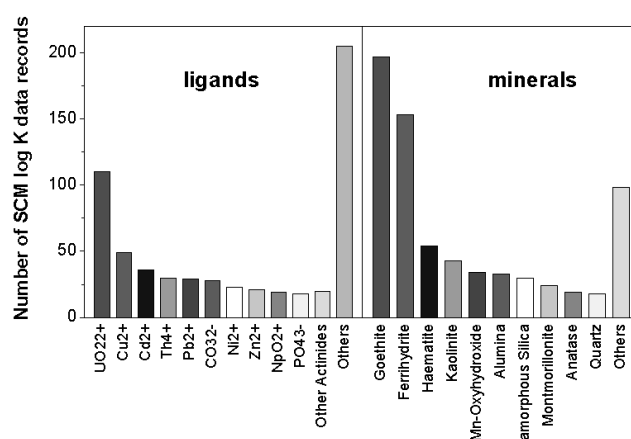


Fig. 1: Distribution of published SCM data records (log K values for surface complex formation) between major ligands and mineral phases

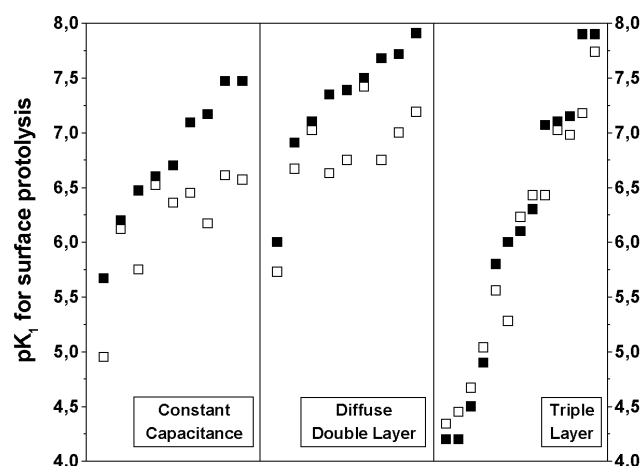


Fig. 2: 1<sup>st</sup> surface protonation constants of goethite: originally published values (closed symbols, sorted in ascending order) and values normalized to a sorption reference state (open symbols)

### Acknowledgement

Funding by the German Federal Ministry of Economics and Technology (BMWi) under contract No. PtWt+E 02E9471 is gratefully acknowledged.

### References

- /1/ Brendler V. et al., Report FZR-318 (2001), p.41
- /2/ Brendler V. et al., J. Contam. Hydrol. (2002), accepted
- /3/ Kulik D., J. Contam. Hydrol. (2002), accepted

# MODELING GYPSUM DISSOLUTION IN A COLUMN EXPERIMENT: COMPARISON OF TWO REACTIVE TRANSPORT CODES

J. Mibus, R. Kuchler<sup>1</sup>

<sup>1</sup> Forschungszentrum Rossendorf e.V., Institute of Safety Research

A gypsum leaching column experiment in unsaturated sand was used as a test case for a comparative assessment of two reactive transport codes. A suitable kinetic approach proved essential for adequate modeling of the experimental data.

Reactive solutes in the soil and groundwater zone are subject to both physical transport and chemical reactions. Experimental and numerical simulation of these reactive transport processes on a laboratory scale is an important tool for analyzing and understanding migration in the subsurface. The performance of a coupled transport and speciation code may be assessed by comparison with experimental data and with another, preferably more sophisticated, model.

Leaching gypsum in a variably saturated sand matrix is the benchmark problem used /1/. A column (length 1.0 m, inner diameter 0.1 m) filled with dried fine sand and 0.2 wt.-% gypsum (grain size 0.2 to 0.3 mm) was flown through unsaturated with Milli-Q water applying a Darcy velocity of  $8.3 \cdot 10^{-8} \text{ m s}^{-1}$  for 90 days. The electrolytic conductivity was measured at vertical positions  $x = 0.1, 0.3, \dots 0.9 \text{ m}$  ( $x$  counts positive upward) and recalculated for free calcium concentration.

A computer code POLLUTRANS /1/ (hereinafter referred to as PT) was developed to model the experimental results. The commonly available code HydroBioGeoChem /2/ (hereinafter HBGC) was also utilized. Both codes solve the transport equation for variably saturated media and can deal with mixed kinetic/equilibrium reactions.

Feature	PT	HBGC
<i>Transport</i>		
numerical approximation	finite diff.	finite elem.
dimension (capable)	2D	3D
vadose zone transport	+	+
sequential iterative coupling	+	+
<i>Chemical reactions</i>		
aqueous complexation	+	+
redox equilibria	+	+
precipitation/dissolution	+	+
kinetics linear/nonlinear	+/+	+/-
adsorption/surface complex.	-/-	+/+
biochemical reactions	-	+

Tab. 1: Main features of both reactive transport codes

In both cases a 1-D model was set up with a spatial resolution of  $\Delta x = 0.01 \text{ m}$  and a temporal resolution of  $\Delta t = 0.01 \text{ h}$  and  $0.1 \text{ h}$  in PT and HBGC respectively. A longitudinal dispersivity of  $\alpha_L = 0.01 \text{ m}$  was assumed. A tracer concentration of  $c_{i|t=0} = 10^{-10} \text{ M}$  was specified as initial condition. At the column inflow a Cauchy boundary condition (given total flux) and at the outflow a Neumann B.C. (zero gradient flux) was defined.

In PT a kinetic rate law  $R$  for gypsum dissolution from /3/ was extended to account for the effect of the reactive surface as shown in equation (1). The parameter  $\eta = (m(t)/m_0)^\beta$  describes the decrease in gypsum

mass and hence in reactive surface as leaching progresses. The rate constant  $k$  was taken from /3/.

$$R = \eta(x,t) \frac{A_{\text{gypsum}}}{V_{\text{solution}}} \cdot k \left( 1 - \frac{a_{\text{Ca}^{2+}} \cdot a_{\text{SO}_4^{2-}}}{K_{\text{SP,gypsum}}} \right) \quad (1)$$

In HBGC, however, only a kinetic approach at a less variant rate is applicable. The initial rate (i.e.  $\eta = 1$ ) of  $3 \cdot 10^{-4} \text{ mol l}^{-1} \text{ h}^{-1}$  was used throughout the model time. The equilibrium constants for gypsum and  $\text{CaSO}_4(\text{aq})$  were the same as in /3/. Activity coefficients were calculated according to the Davies equation.

Both models exhibit a satisfactory convergence behavior. In Fig. 1 the modeled concentration curves are compared with the experimental values.

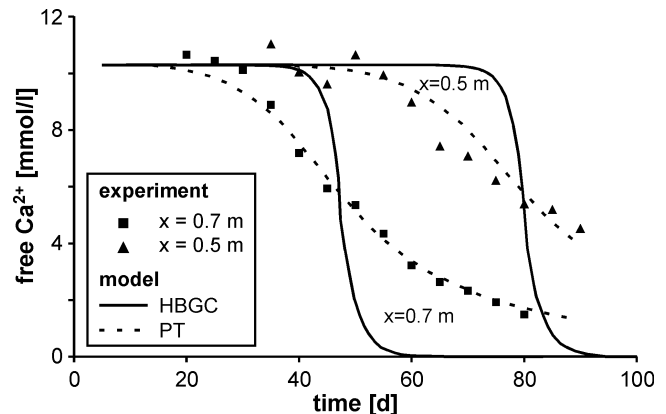


Fig. 1: Measured and modeled Ca concentration as a function of time

The successive exhaustion of gypsum in the monitored vertical positions causes the observed decrease in concentration. The gradually declining shape is a result of (1) hydrodynamic dispersion and (2) the continuous decrease of the dissolution rate due to the reduced surface. Dispersivity does not vary much in unigranular sand. Hence in PT the parameter  $\beta$  was changed to fit the curve shape, resulting in good agreement with the experiment. In HBGC with stiff reaction rates this fit is not possible. Although it can describe the process in principle, no exact conformity is obtained.

In the future HBGC will have to be extended by more realistic kinetic approaches. Its suitability for modeling adsorption phenomena will be explored.

## References

- /1/ Kuchler, R. et al., Report FZR-342 (2002)
- /2/ Yeh, G.T. et al., Report ORNL/TM-13668, Oak Ridge National Laboratory, Oak Ridge, TN (1998)
- /3/ Jeschke, A.A. et al., Geochim. Cosmochim. Acta **65** 27 (2001)

# **Development of Nanoscopic Methods**

# WAVELET ANALYSIS OF EXAFS DATA – FIRST STUDIES

H. Funke, M. Chukalina<sup>1</sup>

<sup>1</sup>Institute of Microelectronics Technology RAS, Chernogolovka, Russia

The wavelet transform is used in completion to the Fourier transform to analyze EXAFS data. The method of operation and the expected advantage of the wavelet analysis is demonstrated at a simple model example.

A typical EXAFS analysis begins with the discussion of the Fourier transform (FT) of the ( $k^3$ -weighted) EXAFS data. This first estimation can give a guess upon, how many co-ordination shells at (approximately) which distance are entered by the EXAFS spectrum. This can be analyzed afterwards by e.g. several fitting methods.

Here, the wavelet transform (WT) is proposed to complement the FT. While the FT analyzes the distances of the back scattering atoms contained in the EXAFS signal, the WT shows additionally at which energies the back scattering takes place.

Originally, wavelet analysis forms a tool for the evaluation of complex time-frequency signals. The essential advantage of the WT is the fact that the time-frequency window is flexible and does in fact adapt in such way that there is always about the same number of periods of the frequency analyzed in the time window.

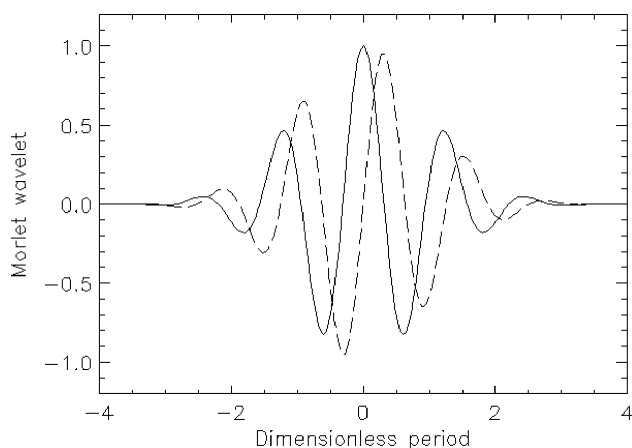
Wavelets are window functions  $\psi(t)$  with zero mean:

$$\int_{-\infty}^{\infty} dt \psi(t) = 0$$

In the following the Morlet-wavelet is chosen. It is obtained by taking a complex sine wave, and by localizing it with a Gaussian (bell-shaped) envelope:

$$\psi(t) = \exp(ik_0 t) \exp\left(-\frac{t^2}{2}\right), \quad \kappa_0 = 5,$$

Its graph of the real- and imaginary part has the form:



The WT is a window operation like a windowed FT. The kernel of the WT being obtained by translation (parameter  $b$ ) and dilation (parameter  $a$ ) of the chosen basis wavelets. The WT of a signal  $f(t)$  is defined as:

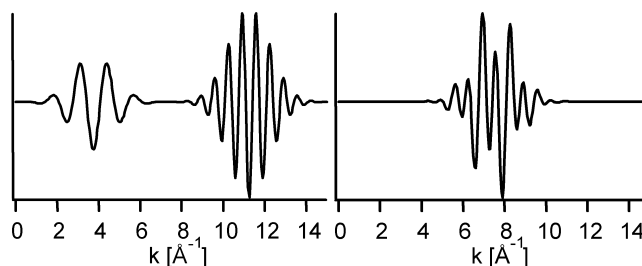
$$W_f^\psi(a, b) = \frac{1}{\sqrt{|a|}} \int_{-\infty}^{\infty} dt f(t) \psi\left(\frac{t-b}{a}\right),$$

and its inverse transform is ( $c=\text{const.}$ ):

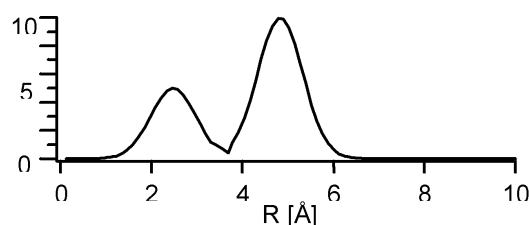
$$f(t) = \frac{1}{c^2} \int_a \int_b da db W_f^\psi(a, b) \frac{1}{a^2} \psi\left(\frac{t-b}{a}\right).$$

The transition of wavelet based data analysis methods from the time-frequency to the wavenumber( $k$ )-distance( $r$ ) regime in the EXAFS evaluation procedure is simply done by the relation:  $2\pi\omega t \Rightarrow 2kr$ .

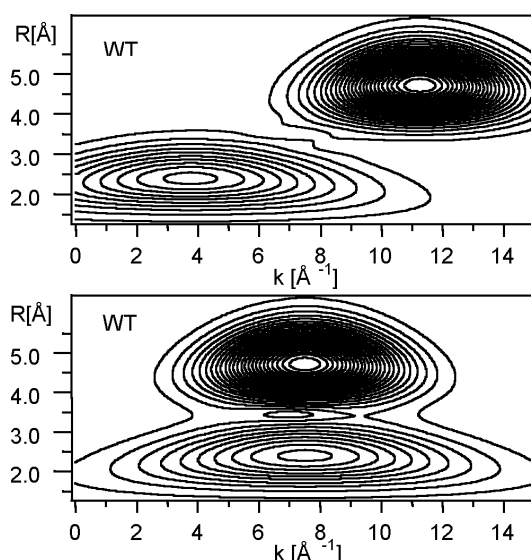
Two sinus waves, enveloped by gaussians, are considered to demonstrate the possibilities of the WT. At left the signals with separated centers and at right the same signals with coinciding centers are shown.



Both "absorption"-functions generate the same FT:



In contrast to the FT, their WT shows both the distances, which also follows from the FT, **and** the position of the centers of the two components of the signal. The magnitude of the WT is plotted for both model functions:



The next step is the application of the presented wavelet analysis procedure to model- and real EXAFS spectra. The aim is to extract more information about the  $k$ -dependence of the absorption signals.

## References

/1/ Mallat, S., *A wavelet tour of signal processing*, Academic Press (1999)

# PROGRESS REPORT ON THE REGULARISATION METHOD FOR EXAFS DATA ANALYSIS

M. Kunicke<sup>1</sup>, H. Funke, T. Reich, Yu. A. Babanov<sup>2</sup>

<sup>1</sup>FZR, Department Communication and Data Processing; <sup>2</sup>Institute of Metal Physics, Ekaterinburg, Russia

The development of a program for the determination of three partial pair correlation functions from one EXAFS spectrum using the regularization method has been continued. Some new results are presented to demonstrate the convergence of the procedure.

The most general EXAFS integral equation in single scattering approximation and, for simplicity, for one type of backscatterer is written as /1/:

$$k\chi(k) = 4\pi\rho_0 c \int_0^{\infty} f(k,r) e^{-\frac{2r}{\lambda(k)}} \sin(2kr + \psi(k,r)) g(r) dr$$

( $\chi(k)$  is the normalized oscillating part of the X-ray absorption spectrum,  $\rho_0$  the atomic density of the compound,  $c$  the concentration of the backscatterer,  $f(k,r)$  the backscattering amplitude,  $\psi(k,r)$  the total phase shift,  $\lambda(k)$  the mean free path of the photoelectron. The functions  $f(k,r)$ ,  $\psi(k,r)$ ,  $\lambda(k)$  are commonly obtained from the program FEFF-8).

The searched partial pair correlation function (PCF) is  $g(r)$ .

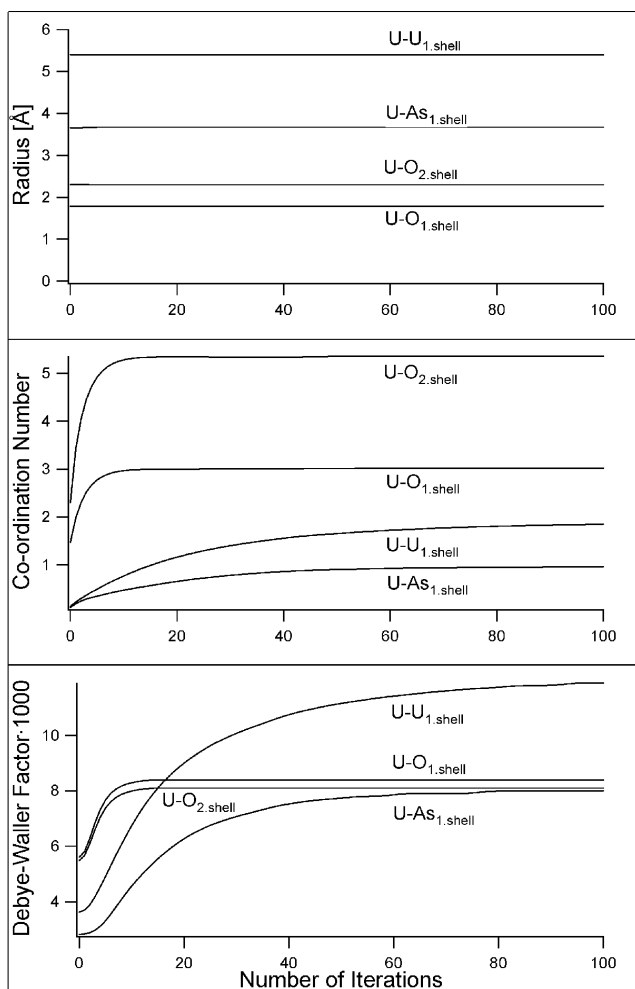


Fig. 1: Development of the searched physical values as a function of the number of iterations

The regularization method has been shown to be an attractive method to solve similar ill-posed problems /2/. This method was applied to EXAFS data analysis of one-component and binary crystalline systems /1/. The aim of the present collaboration is the development of an analog algorithm applicable to liquid and amorphous systems. First results were presented in /3/, see also /4/.

The instability of the solution had remained an open problem. Three numerical amendments were introduced into the program to obtain stable solutions and thus a truncation condition for the iteration process was established.

- 1) The number of grid points, in which the functions  $f(k,r)$ ,  $\psi(k,r)$ ,  $\lambda(k)$  were calculated directly from FEFF8, was increased and equilibrated.
- 2) The inverse of the matrix is calculated by the lower-upper triangular decomposition (LUD) method /5/.
- 3) Some internal numerical procedures were replaced by the equivalent algebraic expressions.

Fig. 1 illustrates the development of stability of the searched physical values, i.e. radius, co-ordination number and Debye-Waller factor, for the reference sample uranyl arsenate ( $\text{UO}_2(\text{HAsO}_4) \times 4\text{H}_2\text{O}$ ) /3/.

Without going into details, it is marked that the residual of the EXAFS equation also converges.

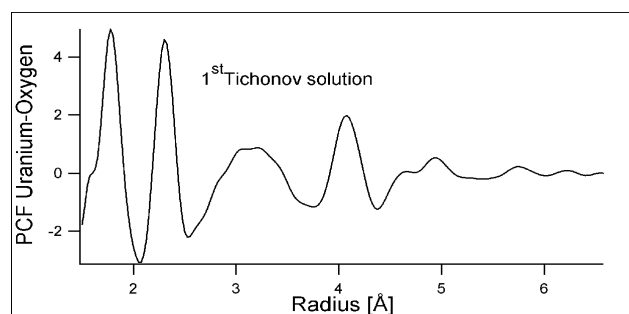


Fig. 2: Pair correlation function uranium-oxygen in the first Tichonov approximation

The immediate stable determination of the distances of the central atom to the backscattering shells comes from the strong development of the first peaks in the PCF for the individual elements. The PCF for the backscattering by oxygen as example is shown in Fig. 2. The distances of the first two shells are obtained correctly by the first Tichonov approximation. With the help of a special iteration procedure /1,3/, which is based on the Tichonov approximation, a stable result is achieved.

## References

- /1/ Babanov, Yu.A., Vasin, V.V., Ageev, A.L., Ershov, N.V., Phys. Stat. Sol. (b) **105**, 747 (1981); **108**, 103 (1981)
- /2/ Tikhonov, A.N., Arsenin, V.Ya., *Solution of Ill-Posed Problems*, John Wiley, New York (1981)
- /3/ Babanov, Yu.A. et al., Proceedings of the 2<sup>nd</sup> Euro-conference and NEA Workshop on Speciation, Techniques, and Facilities for Radioactive Materials at Synchrotron Light Sources, Grenoble, France, Sept. 10-12, 2000
- /4/ Babanov, Yu.A., Zayarnaja, T.Ye., Report FZR-318 (2001), p. 45-46
- /5/ *Numerical Recipes*, Vol. 1, chapter 2.3, Cambridge University Press (1999)

# EXAFS ANALYSIS OF URANIUM SPECIATION IN PLANTS USING THE DIFFERENCE TECHNIQUE

A. Roßberg, T. Reich, A. Günther, G. Bernhard

An EXAFS spectrum is the sum of the signals of scattering contributions from single atoms and multiple scattering (MS) between atoms. The scattering contributions with high intensity are the major and such with low intensity are the minor components in an EXAFS spectrum. A chi-squared fit algorithm is not sensitive enough to the minor components. A difference technique has been developed /1/ to isolate the minor components from the whole EXAFS spectrum to increase the accuracy in determining of their EXAFS structural parameters.

## Introduction

Two plants were grown in a solution of  $1.0 \cdot 10^{-3}$  M  $UO_2(NO_3)_2$  at pH 3 and pH 5. The plants were washed, separated into roots (r) and shoot axis (s). The U  $L_{III}$ -edge EXAFS spectra of the fresh samples were recorded in fluorescence mode at ROBL.

## Data treatment and results

The raw U  $L_{III}$ -edge  $k^3$ -weighted EXAFS spectra of the samples and their corresponding Fourier transforms (FT) are shown in Fig. 1. Theoretical phases and amplitudes were calculated with FEFF8 using the crystal structure of m-autunite ( $Ca[UO_2PO_4]_2 \cdot 6H_2O$ ) /2/.

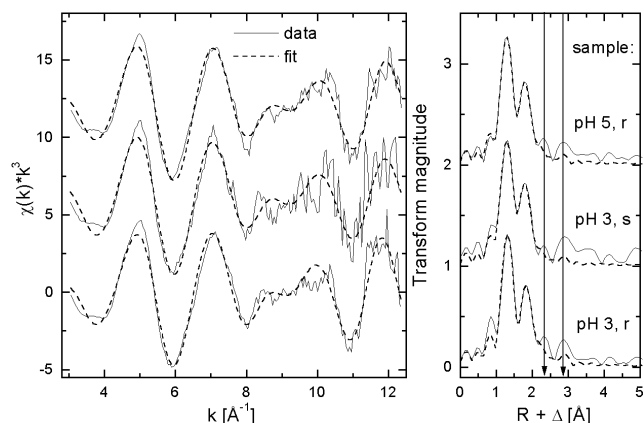


Fig. 1: Raw U  $L_{III}$ -edge  $k^3$ -weighted EXAFS spectra of the plant samples (left) and their corresponding FT (right). Fit of the major components, see text.

Two minor contributions of backscatters are visible in the FT at a radial distance of  $2.3 + \Delta \text{Å}$  (a) and  $2.9 + \Delta \text{Å}$  (b), Fig. 1. To isolate the minor components the following four steps, were necessary. 1) Fit of the major components, i.e. the two axial oxygen atoms ( $O_{ax}$ ), the equatorial oxygen atoms ( $O_{eq}$ ), and the MS path U- $O_{ax(1)}$ -U- $O_{ax(2)}$  along the uranyl chain (Tab. 1).

Sample	pH 3, r	pH 3, s	pH 5, r	Aut.
<b><math>O_{ax}</math></b>				
R [Å]	1.79	1.77	1.77	1.89 <sup>a)</sup>
$\sigma[\text{Å}]^2 \cdot 10^3$	2.1	2.8	2.6	
<b><math>O_{eq}</math></b>				
N	3.2	4.2	4.0	4.0
R [Å]	2.30	2.29	2.28	2.33
$\sigma[\text{Å}]^2 \cdot 10^3$	2.6	4.3	4.0	
$\Delta E_0$	-16.7	-20.0	-20.3	

For  $O_{ax}$  the coordination number was held constant at 2. a) The average U- $O_{ax}$  distance (U- $O_{ax(1)}$  = 1.789 Å, U- $O_{ax(2)}$  = 1.991 Å).

Tab. 1: EXAFS structural parameters of the major components and x-ray structural parameters of m-autunite (aut.). r – root, s - shoot axis.

2) Subtraction of this fit from the experimental data to get the residual. The residual EXAFS contains the minor components a) and b) and some residual back-

ground. 3) Fourier Filtering of the residual EXAFS in the region, which contains a) and b) ( $1.9-3.9 + \Delta \text{Å}$ , Fig. 2).

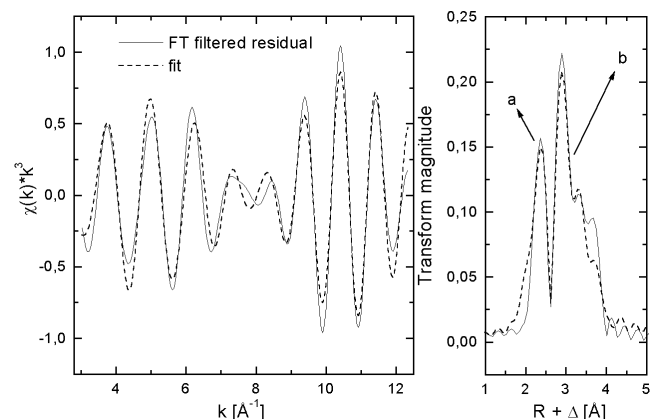


Fig. 2: The  $k^3$ -weighted U  $L_{III}$ -edge EXAFS spectra (left) and the corresponding FT (right) of the FT filtered residual for sample at pH 3, root.

4) Fit of the minor components. The FT filtered residual EXAFS is equal to the sum of the EXAFS signal of an O atom (component a)), phosphorus (component b)), and the twofold degenerated 3-legged MS path U- $O_{eq}$ -P (component b)) (Fig. 2, Tab. 2).

Sample	pH 3, r	pH 3, s	pH 5, r	aut.
<b>O</b>				
N	0.90	0.76	0.59	-
R [Å]	2.86	2.82	2.87	-
<b>P</b>				
N	4.5	5.4	5.0	4.0
R [Å]	3.63	3.62	3.60	3.59
$\sigma[\text{Å}]^2 \cdot 10^3$	3.9	3.3	5.3	
<b>MS U-O-P</b>				
R [Å]	3.75	3.73	3.72	3.69 <sup>a)</sup>
$\sigma[\text{Å}]^2 \cdot 10^3$	3.7	3.9	6.6	

$\Delta E_0$  was taken from the fit of the major components (Tab. 1) and was held constant. a) This value is calculated with ATOMS. The coordination number (N) of the MS was coupled with N of phosphorus.

Tab. 2: EXAFS structural parameters for the minor components and x-ray structural parameters of m-autunite (aut.).

The EXAFS structural parameters of the plant samples are similar to x-ray structural parameters observed for m-autunite. The difference technique was also applied to isolate EXAFS structural parameters for phosphorus in the system uranium/bacteria /3/.

## References

- 1/ Teo, B.K., *EXAFS: Basic Principles and Data Analysis*. New York, 139 (1986)
- 2/ Markow, E.S. et al., *Doklady Akademii Nauk SSSR* **132**, 637 (1960)
- 3/ Merroun, M. et al., *Radiochim. Acta*, submitted

# RADIUM DETERMINATION AFTER CHEMICAL SEPARATION AND BY ANALYSING LIQUID SCINTILLATION SPECTRA – A COMPARISON

L. Baraniak, C. Nebelung, M. Thieme<sup>1</sup>

<sup>1</sup> Technische Universität Dresden, Institute of Materials Science, Dresden, Germany

A comparison is given between <sup>226</sup>Ra measurements immediately after separation from its daughter products and <sup>226</sup>Ra determinations by analyzing  $\beta$ -corrected alpha liquid scintillation spectra. The mean <sup>226</sup>Ra yield of 26 samples determined after the two step standard separation was 93.3±1.9% compared with 102.7±3.0% calculated by liquid-scintillation peak fitting.

**Introduction:** In <sup>226</sup>Ra activity determination the influence of the decay products,  $\alpha$ - and  $\beta$ -emitting nuclides of Rn, Po, Bi and Pb in the mass range from 210 to 222, has to be taken into account. The first decay product <sup>222</sup>Rn is gaseous. The equilibrium between <sup>226</sup>Ra and its daughter products is disturbed after sampling. We measured the <sup>226</sup>Ra activity by analyzing the alpha liquid scintillation (LS) spectra recorded with the LS counter (Wallac system 1414, Perkin-Elmer) which separates alpha and beta counts. Since the peak shape is not pure Gaussian, the alpha spectra are fitted by a Gauss function with an exponential correction term /1/. The results are compared with those of the LS measurements after separation by the chemical standard procedure /2/.

**Results:** (1) The radium content of 26 samples with a nominal activity of 40.00 Bq <sup>226</sup>Ra (Amersham standard) was measured after separation (Fig. 1). The <sup>226</sup>Ra content was calculated from the alpha counts corrected for decay products grown in the time between separation and measurement /3/. It amounts to (37.32±0.75) Bq equivalent to a chemical yield of (93.29±1.88)%.

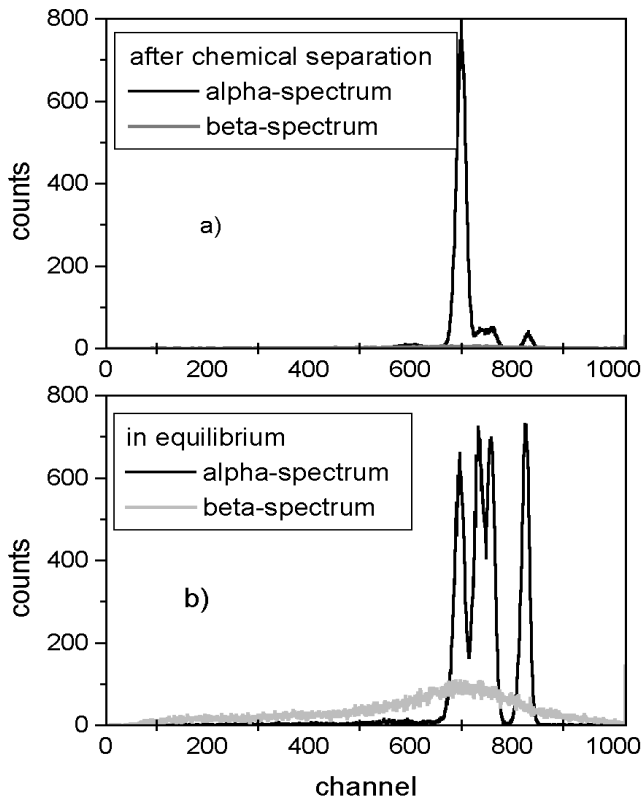
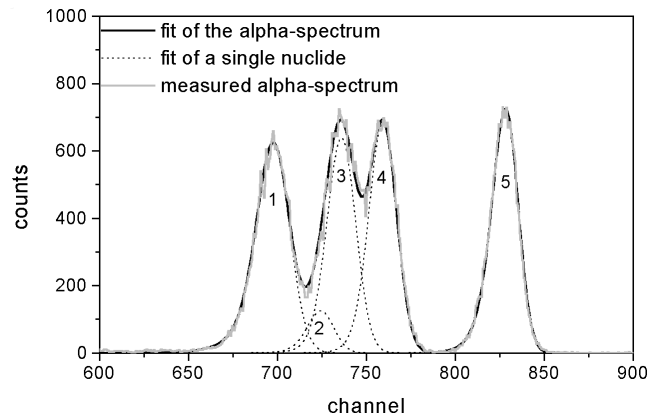


Fig. 1: Liquid-scintillation spectrum of <sup>226</sup>Ra after chemical separation

(2) In a second series of 20 samples 10,67 Bq <sup>226</sup>Ra was measured 5 weeks after preparation, i.e., when

the <sup>226</sup>Ra was in equilibrium with its short-lived decay products <sup>222</sup>Rn, <sup>218</sup>Po, <sup>214</sup>Pb, <sup>214</sup>Bi and <sup>214</sup>Po. The daughter products of the long-lived <sup>214</sup>Pb (half-life 22.3 a), <sup>210</sup>Bi and <sup>210</sup>Po, contribute only little to the total activity. The <sup>226</sup>Ra counts were calculated by analyzing the spectra from the 4.78-MeV-peak (Fig. 2). The peak fitting analysis of 20 spectra resulted in a mean <sup>226</sup>Ra content of (24.05±0.43)% equivalent to (10.96±0.33) Bq <sup>226</sup>Ra, which is 2.7% more than the initial activity. But it is within the relative standard deviation of the final result (±3.0%).



Peak	FWHM Channel	Netto Counts	AreaFit %	CenterMax Channel
1 <sup>226</sup> Ra	22.38	14293	24.26	697.20
2 <sup>210</sup> Po	17.71	2400	4.09	724.05
3 <sup>222</sup> Rn	19.16	13781	23.48	735.70
4 <sup>218</sup> Po	18.49	14392	24.52	758.97
5 <sup>214</sup> Po	17.65	13881	23.65	827.86

Fig. 2: Peak fitting results of the alpha liquid scintillation spectrum of a <sup>226</sup>Ra sample in equilibrium

**Conclusions:** The comparison of the two methods makes it evident that <sup>226</sup>Ra can be determined much better by liquid scintillation spectrometry because <sup>226</sup>Ra is quantitatively measured (no yield correction) with nearly the same precision as the chemical standard procedure and the sole preparation of the LS sample is much easier and not so time-consuming as the two-step separation.

## References

- /1/ Nebelung, C., Nitsche, H., *Stillegung und Rückbau: Direktmessung alpha-aktiver Nuklide in Bauschutt zur Freigabeentscheidung, Schlußbericht BMBF Fördervorhaben 02 S 7655* (1999)
- /2/ Chalupnik, S., Lebecka, J.M., *Proc. Liquid Scintillation Spectrometry, Radiocarbon 1992*, p. 397
- /3/ Baraniak, L. et al., *Transportvorgänge des Radiums in Sedimenten im Bereich der Lagerstätte Königstein*, Studie 1/3.1/25579/1594/94 (1995) p. 23

# ESTABLISHMENT OF A LABORATORY FOR SPECTROSCOPIC INVESTIGATION OF RADIOACTIVE SAMPLES AT THE ELBE-FEL FACILITY. INTENTIONS AND PERSPECTIVES

H. Foerstendorf, H. Friedrich, K.H. Heise

*The Institute of Radiochemistry is setting up a radionuclide laboratory for optical spectroscopy at the free electron laser facility of the ELBE electron accelerator (ELBE-FEL). The quality of the infrared light source opens up new fields of analytical research in radiochemistry. Some aspects of future applications are introduced.*

At the Forschungszentrum Rossendorf (FZR) a superconducting electron linear accelerator of high brilliance and low emittance (ELBE) has been built in the last three years. The electron beam will be used to drive a free electron laser (FEL) for generation of intensive coherent infrared light which will be tunable in the frequency range from 5 – 150  $\mu\text{m}$  (Fig. 1).

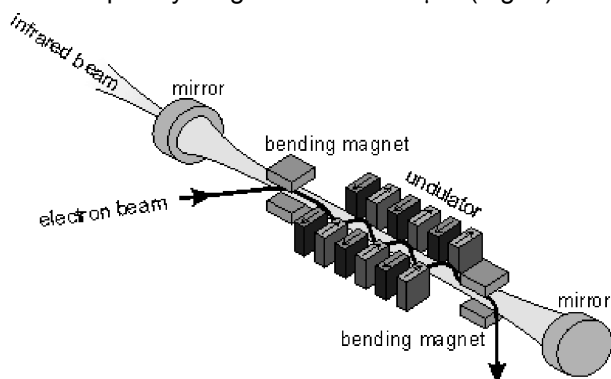


Fig. 1: The principle of a free electron laser [from: R. Wunsch, FZR]

Depending on the operating frequency of the injector, the FEL will emit pulses in the ps time range, allowing investigation of dynamic processes, such as pump-probe experiments or time-resolved experiments with synchronized external laser systems. The energy of the infrared light pulses is estimated to be about 2 and 10  $\mu\text{J}$  for 20 and 40 MeV electron energy, respectively.

The Institute of Radiochemistry (FWR) is installing a laboratory for optical spectroscopy at the ELBE-FEL facility. The special feature of this laboratory will be its classification as a laboratory for radionuclides which will allow the handling of radioactive samples, taking all aspects of radiation protection into account. At the first stage of implementation the FWR will establish a control zone consisting of one user cave and a sluice allowing investigation of preferably sealed samples. As a second step the laboratory is planned to be expanded to include a neighbouring cave that will make it possible to carry out experiments on sensitive samples of higher activity which have to be kept in an inert gas atmosphere (Fig. 2).

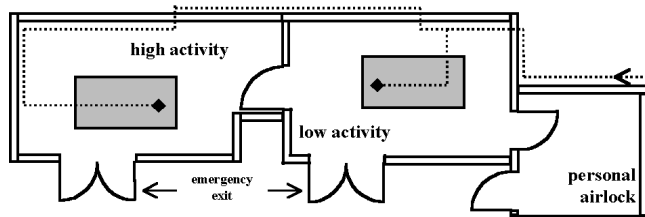


Fig. 2: Floor plan of the FEL laboratories of FWR at the ELBE-FEL facility. The dotted line shows a proposed infrared beamline.

At present the future users of the ELBE-FEL facility decide on the layout of the infrared beamline

throughout the optic laboratories. It is necessary to find a compromise between the dimension of the infrared beam diameter and its divergence on top of the optical tables in the caves which varies with the chosen wavelength.

Infrared spectroscopy is widely used for determination of molecular structures and for investigation of molecular changes and interactions occurring during the course of chemical reactions. The extraordinary quality of the infrared light provided by the FEL opens new perspectives for analytical research in radiochemistry. This may be especially true for investigations on solid surfaces where reflection techniques have to be applied. The reflected infrared light is generally of weak intensity resulting in a poor signal. With regard to the high intensity of the FEL an increased signal-to-noise ratio and a decreased detection limit can now be expected.

Thermal beam deflection (mirage effect) spectroscopy represents another appropriate technique for analyzing solid surfaces. It is highly sensitive and therefore especially suitable for low sample concentrations. Some first experiments were carried out at the CLIO-FEL facility, Orsay, F, with heavy metal ion complexes /1/.

The combination of high brilliance and pulse rate of the coherent light source allows the application of nonlinear second-order techniques such as sum frequency generation (SFG). Since this application is restricted to media lacking inversion symmetry, it is of special interest for interface studies where such symmetries are broken. Because of its inherent surface sensitivity this technique directly measures the vibrational spectrum of molecules at an interface /2/. Contributions of the bulk are not present in the spectra. Binding studies of metal complexes at mineral surfaces will be feasible under natural conditions in an aqueous medium. A special challenge will be the application of SFG to biological interfaces – e.g. lipid monolayers or membranes – serving as model systems for the deduction of processes occurring on cell surfaces.

Vibrational spectroscopy using FEL light represents an extraordinary complementation of the analytical methods already established at the FWR. A deeper insight into interactions between heavy metal ion complexes and mineral interfaces or humic substances can be expected from spectral data obtained by linear and non-linear infrared spectroscopy.

## Acknowledgments

The cooperation with the Institute of Nuclear and Hadron Physics, FZR, is gratefully acknowledged.

## References

- /1/ Seidel, W., FZR, Institute of Nuclear and Hadron Physics, Annual Report 2000
- /2/ Richmond, G.L., Annu. Rev. Phys. Chem. **52**, 357-389 (2001)

# THE USE OF THERMAL OPTICAL DETECTION BY FEL-IR MEASUREMENT OF SOLUTIONS

K.H. Heise, R. Nicolai, W. Seidel<sup>1</sup>, A. Schamlott<sup>1</sup>, J.-M. Ortega<sup>2</sup>, F. Glotin<sup>2</sup>, R. Prazeres<sup>2</sup>

<sup>1</sup>Institute of Nuclear and Hadron Physics; <sup>2</sup>LURE, Centre Universitaire Paris-Sud, Orsay, France

*Thermal-optical detection methods are normally used for IR measurement of solids. We adapted this method to the IR measurement of solutions and explain this novel application by example of uranyl nitrate solution.*

When an IR beam impinges on the surface of a sample, the optical density of atmosphere supside the surface changes. The change of optical density is subject to IR absorption and depends on the wavelength of IR beam. Measurement of the change in optical density at various wavelength over a sample is the basis of thermal optical IR detection by solid samples.

Fig. 1 shows the principles of this detection method: The tunable IR beam from FEL impinges at right angles on the surface of a solid sample. A second, bunched light beam, usually generated by a stabilized He-Ne laser, either touches on the surface of the sample ( $\Theta = 0^\circ$ ) or impinges on the surface of the sample at another angle of incidence of the IR-beam ( $\Theta < 90^\circ > 0^\circ$ ). The shift of the angle of the He-Ne laser beam to  $\Theta'$  by refraction, known as "mirage effect" /1/, or by deflection /2/ with  $\Theta \neq \Theta'$  is measured with the aid of a high resolution position detector.

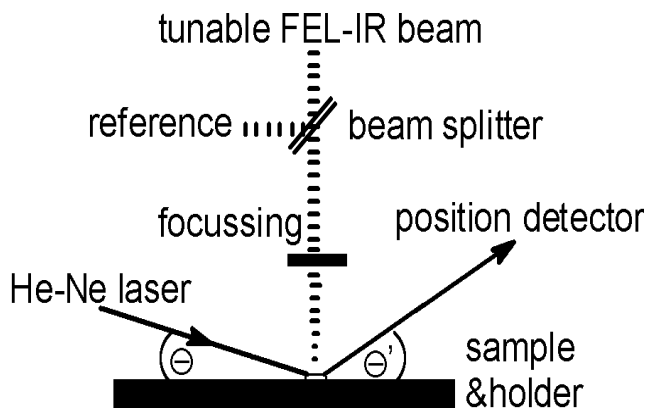


Fig. 1: Diagram of thermal-optical IR detection by FEL

We have implemented this technique at the CLIO-FEL (LURE/Orsay, France) with a multi-sector detector and reported in /3/ and /4/ about our results by FEL-IR measurement of solid samples.

Measurements of solutions, however, required the use an IR cell. This means that such measurements are impossible to carry out, using this technique.

For solutions we used thermal optical detection by quick-freeze in order to obtain a solid sample. For this purpose we used a powerful, small Peltier element (7.5 W per 15x15 mm<sup>2</sup>), which together served as sample holder. When we applied a small drop of a solution to the cold site of Peltier, the drop was quick frozen in a split second. This frozen drop had a nearly ideal surface for the thermal optical measurements. However, atmospheric moisture may also distinctly interfere by ice formation on the surface of the frozen sample. This has to be prevented by dried air. By way of example Fig. 2 shows a detail of the FEL-IR spectrum of quick frozen 1 molar UO<sub>2</sub>(NO<sub>3</sub>)<sub>2</sub> x 6H<sub>2</sub>O solution at -35°C by deflection (left) in comparison with the FTIR spectrum (right) of the same solu-

tion at +20°C (Perkin-Elmer FTIR spectrometer Mod 2000, ZnSe cell). Both spectra show the significant uranyl vibration, the FEL-IR spectrum at 941 cm<sup>-1</sup>, the FTIR spectrum at 961 cm<sup>-1</sup>. The minor deviation of 20 cm<sup>-1</sup> between the two spectra is attributed to an error in calibration of the FEL-IR beam. Resolution too is still unsatisfactory as there are not enough reading points.

## Outlook

The aim of our next experiments is to improve the resolution of the spectra and obviously to improve the sensitivity so as to facilitate measurements in range of environmental concentrations. Various improvements of instrumentation are necessary, such as an improvement of the sample holder so as to avoid ice coating on the frozen sample. We will also arrange improvements of the quality and stability of the IR beam.

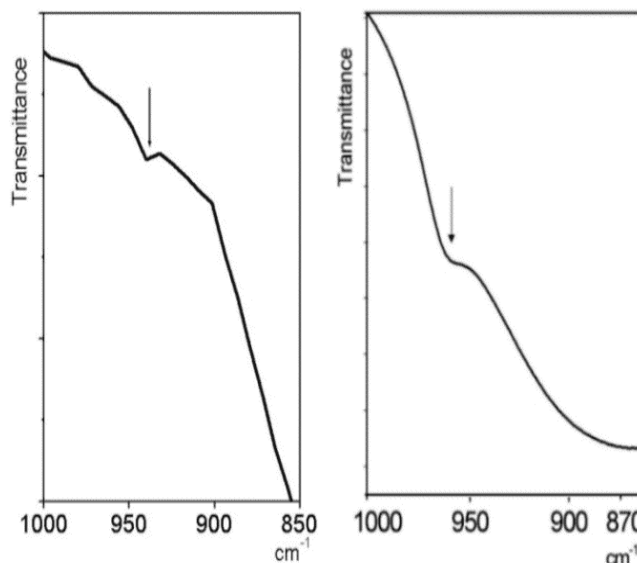


Fig. 2: Infrared spectra of 1M UO<sub>2</sub>(NO<sub>3</sub>)<sub>2</sub> x 6 H<sub>2</sub>O solution; left: FEL-IR spectrum (quick-frozen drop); right: FTIR-IR spectrum (solution /ZnSe cell)

## Acknowledgment

We thank LURE, Orsay, France, for financial support by the EC endowment funds, index no. IC 008-01.

## References

- /1/ Boccara, A.C. et al. Appl. Phys. Lett. **36**, 130 (1980)
- /2/ Olmstaed, M.A. et al. Appl. Phys. **A32**, 141 (1983)
- /3/ Seidel, W. et al., FZR, Institute of Nuclear and Hadron Physics, Annual Report 2000
- /4/ Seidel, W. et al., CLIO Workshop on Application of FEL. Orsay, France, February 2002

## AN X-RAY ABSORPTION SPECTROELECTROCHEMICAL CELL FOR RADIOACTIVE SOLUTIONS

D. Rettig, S. Herrmann<sup>1</sup>, F. Mitschke<sup>1</sup>, V. Brendler, G. Geipel, T. Reich, W. Vonau<sup>1</sup>, G. Bernhard  
<sup>1</sup>Kurt-Schwabe-Institut für Meß- und Sensortechnik e.V. Meinsberg, Germany

*A spectroelectrochemical cell was designed and constructed for measurement of X-ray absorption spectra under electrochemical control of the redox potential of actinide-containing solutions. A first inactive test demonstrated the feasibility of an Ag anode as a non-gassing auxiliary electrode in chloride solutions.*

A detailed knowledge about the structure and equilibrium speciation of redox-active actinide-containing entities can be gained by X-ray absorption experiments (EXAFS and XANES) under controlled electrochemical redox conditions. However, radioactive safety regulations for these experiments require the hermetic inclusion of the electrolyte in a cell without any gas vent ports. Such a cell should be made of plastic with high transmission characteristics for X-rays. After filling the cell with the electrolyte and inserting the electrodes, the cell will be closed in Rossendorf and shipped in a container. The cell will be operated in the glove box at the Rossendorf Beamline at the ESRF in Grenoble without opening.

A section drawing of the spectroelectrochemical cell is shown in Fig. 1. The PTFE cell body (1) is enclosed in a steel cladding (2). The lower part of the cell body contains an oval cylindrical electrolyte compartment (3) with thin windows for the beam (4) and space for a magnetic stirrer. The cell is sealed twice: by the interior lid arrangement (5) with a special type of miniaturized electrodes (6) inserted, and by the outside lid arrangement (7) with the connectors (8) tightly fitted in.

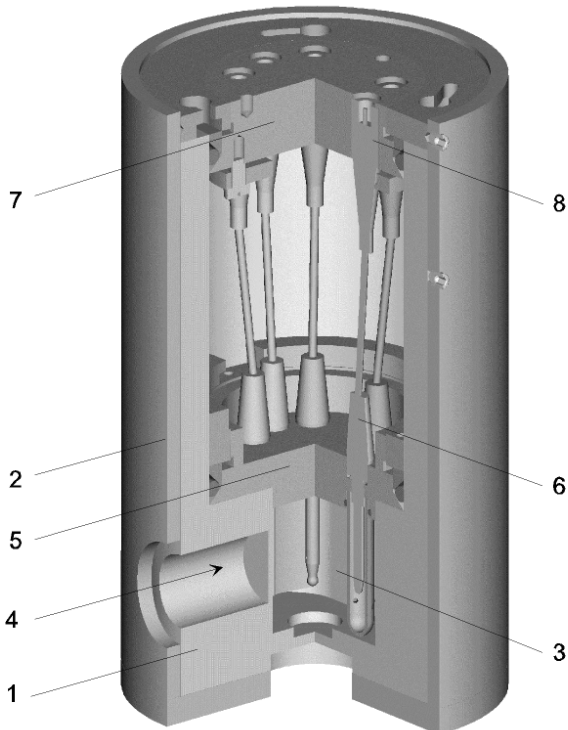
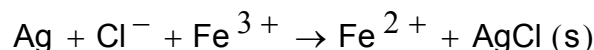


Fig. 1: Spectroelectrochemical cell

The electrochemical functions of the cell were tested with an inactive Fe(III)/Fe(II) redox sample in an acid chloride solution. The electrode system consisted of a Pt gauze working electrode, an Ag rod auxiliary and an Ag/AgCl reference electrode, both without separators, and a Pt redox electrode. The Ag rod forms a

non-gassing anode under AgCl formation. The redox electrode with the reference electrode forms a cell of the voltage  $U_r$  free of any liquid junction. The overall cell reaction is:



The redox voltages  $U_r$  achieved after the potentiostatic reduction (at 0 V of the working electrode vs. Ag/AgCl) in PTFE and glass cells are presented in Fig. 2. The electric charge  $Q$  is related to the charge  $Q_0$  for the theoretical complete reduction of Fe(III) to Fe(II). Results of a thermochemical calculation with the EQ3/6 code, taking 11 Fe containing species into consideration, are also presented.

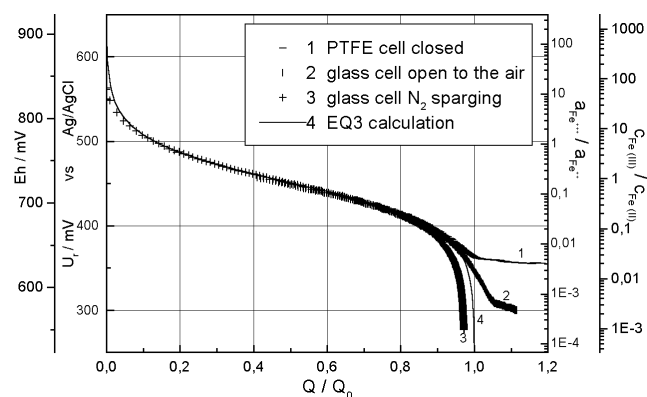


Fig. 2: Dependence of the redox potential  $U_r$  on the electric charge  $Q$  used.  $E_h$  and the activity ratios of the species and of the concentration ratios of the components are calculated from  $U_r$  and  $Q/Q_0$ . Initial concentration:  $\text{H}^+=0.1$ ;  $\text{Na}^+=0.1$ ;  $\text{Cl}^-=0.20192$ ;  $\text{Fe}^{3+}=0.00064$  [mol/l]

The deviations of the experimental curves from the theoretical ones can be explained by two effects: 1. Self-discharge according to the cell reaction will contribute to the reduction of  $\text{Fe}^{3+}$  and make the charge passing the outside circuit smaller. 2. Oxygen from the outside air can penetrate into the open glass cell and into the PTFE cell by permeation through the plastic wall, making a higher charge necessary for reduction. In addition, the redox potential may be disturbed by oxygen, especially at very small Fe(II) concentrations. However, the latter effect can be avoided by setting the polarization potential more negative, e.g., at -0.2 V vs. Ag/AgCl.

In summary, the potentiostatic Fe(III) reduction in an encapsulated plastic cell was achieved, using an Ag electrode in a chloride solution. In future experiments the deviations from theory will be reduced, substituting PTFE by a plastic of lower oxygen permeability and using a special anode compartment with a separator. For electrolytes without chlorides, other types of reference and auxiliary electrodes are necessary.

## **II. PUBLICATIONS, PATENTS, LECTURES AND POSTERS**

## PUBLICATIONS

- Arnold, T., Zorn, T., Zänker, H., Bernhard, G., Nitsche, H.  
Sorption Behaviour of U(VI) on Phyllite: Experiments and Modeling.  
*Journal of Contaminant Hydrology* **47**, 219-231 (2001)
- Arnold, T., Krawczyk-Bärsch, E., Walter, M., Geipel, G., Bernhard, G.  
Sorption of U(VI) on Muscovite: Comparing SCM Modeling with Spectroscopic and Microscopic Results.  
*European Journal of Mineralogy* **13**, 17 (2001)
- Bernhard, G., Friedrich, H., Nitsche, H.  
Radiochemisches Laborgebäude für die Actiniden Forschung; Technik, Strahlenschutz, Methoden  
*Atw* **46**, 653-658 (2001)
- Bernhard, G., Geipel, G., Reich, T., Brendler, V., Amayri, S., Nitsche, H.  
Uranyl(VI) Carbonate Complex Formation: Validation of the  $\text{Ca}_2\text{UO}_2(\text{CO}_3)_3(\text{aq.})$  Species  
*Radiochim. Acta* **89**, 511-518 (2001)
- Bolvin, H., Wahlgreen, U., Moll, H., Reich, T., Geipel, G., Fanghänel, T., Grenthe, I.  
On the structure of Np(VI) and Np(VII) species in alkaline solution studied by EXAFS and quantum chemical methods  
*J. Phys. Chem. A* **105**, 11441-11445 (2001)
- Foerstendorf, H., Benda, C., Gärtner, W., Storf, M., Scheer, H., Siebert, F.  
FTIR studies of phytochrome photoreactions reveal the C=O bands of the chromophore: Consequences for its protonation states, conformation, and protein interaction  
*Biochemistry* **40**, 14952-14959 (2001)
- Funke, H., Bernhard, G., Claussner, J., Jansen, K., Matz, W., Nitsche, H., Oehme, W., Reich, T., Röllig, D.  
Technical Description of the Radiological Safety System for X-Ray Absorption Spectroscopy Experiments on Radioactive Samples at the Rossendorf Beamline  
*Kerntechnik* **66**, 195-201 (2001)
- Gabriel, U., Charlet, L., Schlaepfer, C.W., Vial, J.C., Brachmann, A., Geipel, G.  
Uranyl Surface Speciation on Silica Particles studied by Time-Resolved Laser-Induced Fluorescence Spectroscopy  
*Journal of Colloid and Interface Science* **239**, 358-369 (2001)
- Gerasopoulos, E., Zanis, P., Stohl, A., Zerefos, C.S., Papastefanou, C., Ringer, W., Tobler, L., Hübener, S., Gäggeler, H.W., Kanter, H.J., Tositi, L., Sandrini, S.  
A climatology of  $^7\text{Be}$  at four high-altitude stations at the Alps and the Northern Apennines  
*Atmospheric Environment* **35**, 6347-6360 (2001)
- Guerman, K., Reich, T., Sergeant, C., Ortega, R., Tarasov, V., Simonoff, M.  
Technetium metal and pyrometallurgically formed sediments: Study and speciation by Tc NMR and EXAFS/XANES  
Workshop Proceedings: Pyrochemical Separations; Avignon, France; p.233-241 (2001)
- Hennig, C., Panak, P., Reich, T., Roßberg, A., Raff, J., Selenska-Pobell, S., Matz, W., Bucher, J.J., Bernhard, G., Nitsche, H.  
EXAFS Investigation of Uranium (VI) Complexes formed at *Bacillus cereus* and *Bacillus sphaericus* surfaces  
*Radiochem. Acta* **89**, 625-631 (2001)
- Hennig, C., Reich, T., Funke, H., Roßberg, A., Rutsch, M., Bernhard, G.  
EXAFS as a tool for bond-length determination in the environment of heavy atoms  
*J. Synchrotron Rad.* **8** 695-697 (2001)
- Hennig, C., Reich, T., Funke, H., Roßberg, A., Dienel, S., Oehme, W., Strauch, U., Bernhard, G.  
EXAFS measurements of radioactive samples at low temperature  
Project-Group ESRF-Beamline (ROBL-CRG)  
Report FZR-322, FZ Rossendorf, p.22-26 (2001)
- Hübener, S., Taut, S., Vahle, A., Dressler, R., Eichler, B., Gäggeler, H.W., Jost, D.T., Piguet, D., Türler, A., Bröchle, W., Jäger, E., Schädel, M., Schimpf, E., Kirbach, U., Trautmann, N., Yakushev, A.B.

Physico-Chemical Characterization of Seaborgium as Oxide Hydroxide  
Radiochim. Acta **89**, 737 (2001)

Krawczyk-Bärsch, E., Arnold, T., Hüttig, G., Zänker, H., Brandt, F., Bosbach, D., Bernhard, G.  
The Effect of Secondary Iron Mineral and Colloid Formation on Uranium Sorption during the Dissolution of Chlorite  
11<sup>th</sup> Annual V.M. Goldschmidt Conference; Abstract No. 3161. LPI Contribution No. 1088, Lunar and Planetary Institute, Houston (2001)

Krawczyk-Bärsch, E., Arnold, T., Bernhard, G.  
Das Sorptionsverhalten von U(VI) am Granit von Eibenstock (Erzgebirge) und seinen mineralogischen Komponenten  
European Journal of Mineralogy **13**, 103 (2001)

Merroun, M., Selenska-Pobell, S.  
Interactions of three eco-types of *Acidithiobacillus ferrooxidans* strains with U(VI)  
BioMetals **14**, 171-179 (2001)

Moll, H., Reich, T., Szabó, Z.  
The hydrolysis of uranium(VI) investigated using EXAFS and <sup>17</sup>O-NMR  
ESRF Highlights 2000, 21-22 (2001)

Nebelung, C.  
Schnelles Freimeßverfahren für alpha-aktive Nuklide in Bauschutt durch Direktmessung von großflächigen dünnen Meßpräparaten - Automatisierung des Verfahrens  
Schlußbericht BMBF Fördervorhaben 02 S 7768 6 (2001)

Pompe, S., Schmeide, K., Brendler, V., Heise, K.H., Bernhard, G.  
Untersuchungen über das Komplexierungsverhalten von Huminsäuren und deren Einfluß auf die Migration von radioaktiven und nichtradioaktiven Stoffen unter geogenen Bedingungen  
Report FZKA-PTE Nr.7, FZ Karlsruhe, p.473-480 (2001)

Reich, T., Roßberg, A., Hennig, C., Reich, G.  
Characterization of chromium complexes in chrome tannins, leather, and gelatin using extended X-ray absorption fine structure (EXAFS) spectroscopy  
J. Am. Leather Chem. Assoc. **96**, 133-147 (2001)

Reich, T., Roßberg, A., Geipel, G., Baraniak, L., Funke, H., Hennig, C., Bernhard, G.  
Moleküle unter der Lupe – Strukturuntersuchungen in der Radioökologie mit Hilfe von Synchrotronstrahlung  
Report FZR-327, p.37-41 (2001)

Reich, T., Geipel, G., Funke, H., Hennig, C., Roßberg, Bernhard, G.  
XANES and EXAFS measurements of plutonium hydrates  
Project-Group ESRF-Beamline (ROBL-CRG)  
Report FZR-322, p.27-32 (2001)

Seifert, S., Künstler, J.-U., Gupta, A., Funke, H., Reich, T., Hennig, C., Roßberg, A., Pietzsch, H.-J., Alberto, R., Johannsen, B.  
EXAFS analyses in radiopharmaceutical research; Stability studies of technetium (I) carbonyl complexes in solution  
ESRF Highlights 2000, 22-23 (2001)

Seifert, S., Künstler, J.-U., Gupta, A., Funke, H., Reich, T., Pietzsch, H.J., Alberto, R., Johannsen, B.  
Reactivity of technetium(I) thioether carbonyl complexes towards histidine – an EXAFS study in solution  
Inorg. Chim. Acta **322**, 79-86 (2001)

Selenska-Pobell, S., Flemming, K., Kampf, G., Radeva, G., Satchanska, G.  
Bacterial Diversity in soil Samples from two Uranium Waste Piles as Determined by Rep-APD, RISA and the 16S rDNA Retrieval  
Antonie van Leeuwenhoek **79**, 149-161 (2001)

Sémon, L., Boehme, C., Billard, I., Hennig, C., Lützenkirchen, K., Reich, T., Roßberg, A., Rossini, I., Wipff, G.  
Do perchlorate and triflate anions bind to the uranyl cation in an acidic aqueous medium? A combined EXAFS and quantum mechanical investigation  
Chem. Phys. Chem. **2**, 591-598 (2001)

Stumpf, Th., Rabung, Th., Klenze, R., Geckeis, H., Kim, J.I.  
A Spectroscopic Study of the Cm(III) Sorption onto  $\gamma$ -Alumina  
J. Colloid Interface Sci. **238**, 219-224 (2001)

Stumpf, Th., Bauer, A., Coppin, F., Kim, J.I.  
Time-Resolved Laser Fluorescence Spectroscopy (TRLFS) Study of the Sorption of Cm(III) onto Smectite and Kaolinite  
Environ. Sci. Technol. **35**, 3691-3694 (2001)

Stumpf, Th., Bolte, M.  
Tetraaquatrinitratoeuropium(III)dihydrate  
Acta Cryst. **E57**, i10-i11 (2001)

Stumpf, Th., Bolte, M.  
Dihydrotetra(4-picoline)siliconchloride-hexakis-chloroform  
Acta Cryst. **E57**, o209-o211 (2001)

Teterin, Yu.A., Nefedov, V.I., Nikitin, A.S., Teterin, A.Yu., Ivanov, K.E., Maslakov, K.I., Utkin, I.O., Bubner, M., Reich, T., Pompe, S., Heise, K.H., Nitsche, H.  
Interaction of  $\text{UO}_2^{2+}$  and  $\text{Fe}^{3+}$  ions with natural humic acid  
Russian J. Inorg. Chem. **46**, 886-891 (2001); Zh. Neorg. Khimii **46**, 900-995 (2001)

Tsushima, S., Reich, T.  
A theoretical study of uranyl hydroxide monomeric and dimeric complexes  
Chem. Phys. Lett. **347**, 127-132 (2001)

Vallet, V., Wahlgren, U., Schimmelpfennig, B., Moll, H., Szabó, Z., Grenthe, I.  
Solvent effects on uranium(VI) fluoride and hydroxide complexes studied by EXAFS and quantum chemistry  
Inorg. Chem. **40**, 3516-3525 (2001)

Wahl, R., Mertig, M., Raff, J., Selenska-Pobell, S., Pompe, W.  
Formation of Highly Ordered Palladium and Platinum Nanoclusters on the S-Layer of *Bacillus Sphaericus* NCTC 9602  
Advanced Materials **13**, 736-740 (2001)

Wahl, R., Raff, J., Selenska-Pobell, S., Mertig, M., Pompe, W.,  
A Fast Screening Method for Surface Layers on Gram-positive Bacilli  
Biotechnology Letters **23**, 1485-1490 (2001)

Walter, C., Geipel, G.,  
Laser Induced Breakdown Detection of Colloids  
Report FZKA 6629, FZ Karlsruhe, p.97 (2001)

Yakushev, A.B., Buklanov, G.V., Chelnokov, M.L., Chepigin, V.I., Dimitriev, S.N., Gorshkov, V.A., Hübener, S., Lebedev, V.Ya., Malyshev, O.N., Oganessian, Yu.Ts., Popeko, A.G., Sokol, E.A., Timokhin, S.N., Türler, A., Vasko, V.M., Yerechin, A.V., Zvara, I.  
First Attempt to Chemically Identify Element 112  
Radiochim. Acta **89**, 743 (2001)

Zeevaert, Th., Bousher, A., Brendler, V., Hedemann Jensen, P., Nordlinder, S.  
Evaluation and Ranking of Restoration Strategies for Radioactively Contaminated Sites  
J. of Environmental Radioactivity **56**, 33-50 (2001)

## PATENTS

Rettig, D., Merker, P., Rudolph, A., Adam, R.  
Verfahren zur Herstellung von Aerosolen im Nanometerbereich  
Offenlegungsschrift DE 19942210 A1; Offenlegungstag: 05.04.2001

## LECTURES

Amayri, S., Geipel, G., Reich, T., Brendler, V., Bernhard, G.  
Erdalkaliuranylcarbonate,  $\text{M}_2[\text{UO}_2(\text{CO}_3)_3]\text{nH}_2\text{O}$ ; Synthese, physikalisch-chemische Charakterisierung und Bestimmung ihrer Löslichkeit

GDCh-Jahrestagung Chemie 2001, FG Nuklearchemie  
Würzburg, Germany, 23.-26.09.2001

Arnold, T.  
Sorption of U(VI) on Muscovite. Comparing SCM Modeling with Spectroscopic and Microscopic Results.  
DMG Tagung  
Potsdam, Germany, 9.-13.09.2001

Baraniak, L., Nebelung, C.  
Sorption von Uranium(VI), Radium und [<sup>14</sup>C]-Carbonat an tonigen Allertalsedimenten  
Projektbericht ERAM-Projekt  
Karlsruhe, Germany, 05.02.2001

Bernhard, G.  
Zur Speziation des Urans in Umweltkompartimenten  
Max-Planck-Institut für Biogeochemie  
Jena, Germany, 06.11.2001

Bernhard, G.  
Interaction of Microorganisms with Uranium (Actinides)  
Projectmeeting, University Politecnica Catalunya  
Barcelona, Spain, 29.-31. 10.2001

Bernhard, G.  
Wechselwirkung von Actiniden mit Mikroorganismen  
2<sup>nd</sup> Coordination Meeting PSI/LES-FZR/IR  
Villigen, Switzerland, 22.-23.10.2001

Bernhard, G.  
Institute of Radiochemistry, Forschungszentrum Rossendorf, Profile-Research Topics  
Workshop University of Gothenburg, Chalmers University, Institute of Radiochemistry  
Gothenburg, Sweden, 16.-18.10.2001

Bernhard, G.  
Umweltrelevante Speziation des Urans  
Johannes Gutenberg-Universität Mainz, Institut für Kernchemie  
Mainz, Germany, 18.07.2001

Bernhard, G.  
Zur Speziation des Uran in der Umwelt  
TU München, Institut für Radiochemie,  
München, Germany, 29.01.2001

Bernhard, G., Pompe, S., Schmeide, K., Heise, K.H., Brendler, V., Trautmann, N., Kuczewski, B., Seibert, A.,  
Kratz, J.V., Beck, H.P., Wagner, H., Gottfreund, T., Zeitz, M.  
Untersuchungen über die Komplexbildung und die Migration von Actiniden und nichtradioaktiven Stoffen mit  
Huminsäuren unter geogenen Bedingungen.  
5. Projektstatusgespräch "FuE-Vorhaben auf dem Gebiet der Entsorgung gefährlicher Abfälle in tiefen geologi-  
schen Formationen"  
Leipzig, Germany, 15.-16.05.2001

Brendler, V.  
Ladungsausgleichsmodell für Huminsäurekomplexe: Integration in EQ3/6  
Workshop BMWi-Projekt „Huminsäuren“  
Saarbrücken, Germany, 26.-27.04.2001

Brendler, V.  
Geochemische Modellierung mit dem Programmpaket EQ3/6  
Workshop at DGFZ  
Dresden, Germany, 12.05.2001

Brendler, V., Vahle, A., Arnold, T., Bernhard, G., Fanghänel, Th.,  
A Mineral-Specific Thermodynamic Sorption Database  
Migration 2001  
Bregenz, Austria, 16.-21.09.2001

Eichler, R., Brüchle, W., Dressler, R., Düllmann, C.E., Eichler, B., Gäggeler, H.W., Gregorich, K.E., Hoffman, D.C., Hübener, S., Jost, D.T., Kirbach, U., Laue, C.A., Nitsche, H., Patin, J.B., Schädel, M., Taut, St., Türler, A., Vahle, A., Wilk, P.A., Yakushev, A.B.

Die chemische Untersuchung des Elements Bohrium (Element 107)

GDCh-Jahrestagung Chemie 2001, FG Nuklearchemie

Würzburg, Germany, 23.-26.09.2001

Fanghänel, Th.

Application of Pitzer's ion-interaction approach for the calculation of excess properties of trace radionuclides in electrolyte solutions

OECD/NEA TDB Workshop on The Use of Thermodynamic Databases in Performance Assessment

Barcelona, Spain, 29.-30.04.2001

Fanghänel, Th.

Aquatic Chemistry and Thermodynamics of Actinides and Fission Products Relevant to Nuclear Waste Disposal

OECD/NEA TDB Workshop on The Use of Thermodynamic Databases in Performance Assessment

Barcelona, Spain, 29.-30.04.2001

Funke, H.

The Rossendorf beamline (ROBL) at the ESRF in Grenoble

Institute of Metal Physics, RAS

Ekaterinburg, Russia, 26.03.2001

Funke, H.

The radiochemistry experimental station at the Rossendorf beamline at the ESRF

Second International Workshop, JINR Synchrotron Radiation Source: Perspectives of Research

Joint Institute of Nuclear Research

Dubna, Russia, 03.04.2001

Funke, H.

X-ray absorption experiments at the Rossendorf beamline (ROBL) at the ESRF

Institute of Microelectronics Technology, RAS

Chernogolovka, Russia, 06.04.2001

Geipel, G.

Laser-induzierte spektroskopische Methoden zur Bestimmung der Speziation von Schwermetallen am Beispiel der Actinide

Hochschule für Technik und Wirtschaft

Dresden, Germany, 29.03.2001

Geipel, G., Bernhard, G., Acker, M., Nitsche, H., Fanghänel, Th.

Femtosecond-Laser-Induced Spectroscopy - A new Tool to Study Interactions of Actinides with Organic Ligands

Migration 2001

Bregenz, Austria, 16.-21.09.2001

Geipel, G.

Introduction into Workpackage 4 - Enhanced Transport

Boris Coordination Meeting

Karlsruhe, Germany, 17.-19.01.2001

Geipel, G.

Proposed Studies on Extracted Microbial Substances from Tomsk-7 site

Boris Coordination Meeting; UIC

Barcelona, Spain, 29.-31.10.2001

Geipel, G., Bernhard, G., Fanghänel, Th.

Complex Formation of Neptunium(V) with 2,3-Dihydroxybenzoic acid studied by Femtosecond-Laser-Induced Spectroscopy

2<sup>nd</sup> Coordination Meeting PSI/LES-FZR/IR

Villigen, Switzerland, 22.-23.10.2001

Geipel, G., Bernhard, G., Fanghänel, Th.

Complex Formation of Uranium(IV) with Phosphate and Arsenate studied by Spectroscopic Methods

Actinides 2001

Hayama, Japan, 04.-09.11.2001

Geipel, G., Bernhard, G., Fanghänel, Th.

Complex Formation of Neptunium(V) with 2,3-Dihydroxybenzoic acid studied by Femtosecond-Laser-Induced Spectroscopy

Japan Atomic Energy Research Institute

Tokai-mura, Japan, 12.11.2001

Günther, A., Geipel, G., Koban, A., Bernhard, G.

Uran(VI)-Komplexierungen mit Modellverbindungen aus der Pflanzenchemie

GDCh-Jahrestagung Chemie 2001, FG Nuklearchemie

Würzburg, Germany, 23.-26.09.2001

Heise, K.H.

Entsorgung tritiumhaltiger Abfallstoffe am Forschungsstandort Rossendorf

PtWT+E-Workshop über Endlagerung in tiefen geologischen Formationen

Karlsruhe, Germany, 21.03.2001

Hennig, C.

EXAFS-Spektroskopie zur Untersuchung der Nahordnung – technischer Aufbau und Experimente an der Rossendorfer Beamline in Grenoble

Mikrosymposium „Strukturuntersuchungen an polykristallinen und röntgenamorphen Festkörpern“

Berlin, Germany, 19.04.2001

Hennig, C., Dähn, R., Scheidegger, A., Reich, T.

Polarization dependent EXAFS investigations of uranium(VI) sorbed onto montmorillonite

Migration 2001

Bregenz, Austria, 16.-21.09.2001

Hübener, S., Taut, S., Vahle, A., Fanghänel, Th.

Untersuchungen zur Flüchtigkeit der Oxidhydroxide hexavalenter Actiniden

GDCh-Jahrestagung Chemie 2001, FG Nuklearchemie

Würzburg, Germany, 23.-26.09.2001

Keil, D., Schmeide, K.

Synthese und Verwendung uranophiler Calixarene

FCS Mikrosymposium, Technologie- und Gründerzentrum Bitterfeld-Wolfen GmbH

Wolfen, Germany, 27.11.2001

Krawczyk-Bärsch, E., Arnold, T., Hüttig, G., Zänker, H., Brandt, F., Bosbach, D., Bernhard, G.

The Effect of secondary Iron Mineral and Colloid Formation on Uranium Sorption during the Dissolution of Chlorite

11<sup>th</sup> Annual V.M. Goldschmidt Conference

Hot Springs, Virginia, USA, 20.-24.05.2001

Krawczyk-Bärsch, E., Arnold, T., Hüttig, G., Zänker, H., Brandt, F., Bosbach, D., Bernhard, G.

Formation of Iron Oxyhydroxide Particles during the Dissolution of Chlorite – Effect on Uranium Sorption

79. Tagung der Mineralogischen Gesellschaft

Potsdam, Germany, 09.-13.09.2001

Krawczyk-Bärsch, E., Arnold, T., Bernhard, G.

Das Sorptionsverhalten von U(VI) am Granit von Eibenstock (Erzgebirge) und seinen mineralogischen Komponenten

79. Tagung der Mineralogischen Gesellschaft

Potsdam, Germany, 09.-13.09.2001

Merroun, M.

Spectroscopic Characterization of Uranium Complexes Formed by *Acidithiobacillus ferrooxidans* Types

Äspo Project Meeting

Göteborg, Sweden, 17.10.2001

Mibus, J.

Geochemische Prozesse in Halden des Kupferschieferbergbaus im südöstlichen Harzvorland

Umweltforschungszentrum Leipzig-Halle, Sektion Hydrogeologie  
Halle/Saale, Germany, 29.10.2001

Moll, H., Geipel, G., Reich, T., Bernhard, G., Fanghänel, Th., Grenthe, I.  
Uranyl(VI) complexes with alpha-substituted carboxylic acids in aqueous solution  
Migration 2001  
Bregenz, Austria, 16.-21.09.2001

Moll, H.  
Interaction of Actinides with the Predominant Indigenous Bacteria in Äspö Aquifer  
Workshop University of Gothenburg, Department of Cell and Molecular Biology, Microbiology  
Göteborg, Sweden, 16.-18.10.2001

Moll, H.  
Uranyl(VI) complexes with alpha-substituted carboxylic acids in aqueous solution  
2<sup>nd</sup> Coordination Meeting PSI/LES-FZR/IR  
Villigen, Switzerland, 22.-23.10.2001

Pompe, S., Schmeide, K.  
Synthetische Huminsäuren und deren Einsatz  
Vortrag vor der AG Gleixner, MPI für Biogeochemie Jena  
Rossendorf, Germany, 30.01.2001

Pompe, S.  
Markierung und Modifizierung von Huminsäuren und deren Komplexbildung mit Neptunium(V)  
Workshop Forschungsvorhaben "Untersuchungen über die Komplexbildung und die Migration von Actiniden und  
nicht-radioaktiven Stoffen mit Huminsäuren unter geogenen Bedingungen"  
Saarbrücken, Germany, 26.-27.04.2001

Raff, J.  
Analysis of the S-Layer from the Uranium Mining Waste Pile Isolate *Bacillus Shaericus* JG-A12 and its Interac-  
tions with Metals  
Institutsseminar, Universität Leipzig, Institut für Biochemie  
Leipzig, Germany, 17.12.2001

Reich, T., Roßberg, A., Pompe, S., Schmeide, K., Baraniak, L., Hennig, C., Funke, H., Bernhard, G.  
EXAFS study of actinide interaction with natural organic materials  
ESRF/ILL Joint Workshop on Environmental Studies Using Neutron and Synchrotron Facilities  
Grenoble, France, 20.-21.02.2001

Reich, T.  
Research program and experimental possibilities for experiments with radionuclides at ROBL  
CRG-Club Meeting, ESRF  
Grenoble, France, 13.03.2001

Reich, T.  
Application of X-ray absorption spectroscopy to environmental actinide chemistry  
European Commission, Institute for Transuranium Elements  
Karlsruhe, 27.03.2001

Reich, T.  
Advanced techniques in chemical speciation  
ITU Summer School 2001 – Actinide science and applications  
Karlsruhe, Germany, 20.-23.07.2001

Reich, T., Hennig, C., Merroun, M., Panak, P., Raff, J., Roßberg, A., Funke, H., Selenska-Pobell, S., Bernhard, G.  
Structural investigation of bacteria interaction with uranium(VI) using EXAFS spectroscopy  
3<sup>rd</sup> European Workshop on X-ray Absorption in Biology  
Siena, Italy, 02.-03.09.2001

Reich, T.  
Strukturuntersuchung an Actiniden am Rossendorfer Synchrotronstrahlrohr ROBL  
GDCh-Jahrestagung Chemie 2001, FG Nuklearchemie

Würzburg, Germany, 23.-26.09.2001

Reich, T. Sachs, S. Schmeide, K., Bubner, M., Brendler, V., Funke, H., Geipel, G., Hennig, C., Roßberg, A., Heise, K.H., Bernhard, G.

Structural studies of actinide complexation with humic substances  
Actinides 2001

Hayama, Japan, 04.-09.11.2001

Reich, T.

Application of X-ray absorption spectroscopy to problems in radiochemistry  
Japan Atomic Energy Research Institute  
Tokai-mura, Japan, 12.11.2001

Sachs, S., Schmeide, K., Geipel, G., Reich, T., Heise, K.H., Bernhard, G.

Interaction of Neptunium(V) with Humic Acids of Different Functionalities  
Migration 2001

Bregenz, Austria, 16.-21.09.2001

Sachs, S.

NIR-Untersuchungen an Np(V)-Humaten modifizierter und nicht modifizierter Huminsäuren sowie erste Ergebnisse zur Synthese von Huminsäuren mit ausgeprägter Redoxfunktionalität

Workshop Forschungsvorhaben "Untersuchungen über die Komplexierung und die Migration von Actiniden und nichtradioaktiven Stoffen mit Huminsäuren unter geogenen Bedingungen "

Karlsruhe, Germany, 15.-16.11.2001

Sachs, S., Schmeide, K., Artinger, R., Heise, K.H., Bernhard, G.

Einfluss von Huminstoffen auf das Wechselwirkungsverhalten von Uran(VI) unter naturnahen Bedingungen.

TU Bergakademie Freiberg, Geo-Umweltkolloquium "Kontamination aus der Nutzung von Ressourcen, Probleme und Lösungen"

Freiberg, Germany, 07.12.2001

Schmeide, K., Pompe, S.

Huminsäureforschung im FZR/IfR - Synthetische Huminsäuren

Vortrag vor Vertretern der Hochschule Zittau-Görlitz

Rosendorf, Germany, 30.04.2001

Schmeide, K.

EXAFS-Untersuchungen an Pu(III)-Humaten sowie erste Ergebnisse zur Np(V)-Sorption an Granit in Ab- und Anwesenheit von Huminsäure

Workshop Forschungsvorhaben "Untersuchungen über die Komplexierung und die Migration von Actiniden und nichtradioaktiven Stoffen mit Huminsäuren unter geogenen Bedingungen "

Karlsruhe, Germany, 15.-16.11.2001

Schmeide, K., Sachs, S.

Contribution of the Forschungszentrum Rosendorf to the HUPA Project

Workshop Forschungsvorhaben "Humic Substances in Performance Assessment of Nuclear Waste Disposal: Actinide and Iodine Migration in the Far-Field (HUPA)"

Karlsruhe, Germany, 03.-04.12.2001

Selenska-Pobell, S.

Bacterial Diversity and Activity in Uranium Wastes

VAAM-2001 Tagung

Oldenburg, Germany, 25.-28.03.2001

Selenska-Pobell, S.

Biocere auf Basis bakterieller Membranproteine für metallbindende Filter zur Behandlung von industriellen Abwässern und kontaminiertem Grundwasser

Workshop Innoregio-Forschungsvorhaben, Max Planck Institut Dresden

Dresden, Germany, 07.06.2001

Selenska-Pobell, S.

Bakterielle Diversität und Aktivität in mit Uran belasteter Umgebung

Kolloquium, Forschungszentrum Karlsruhe, Institut für Technische Chemie

Karlsruhe, Germany, 18.07.2001

- Selenska-Pobell, S.  
Bacteria in Uranium Wastes and their Interactions with Uranium and other Metals  
Kolloquium, Institut für Molekulare Biologie Sofia  
Sofia, Bulgaria, 10.10.2001
- Selenska-Pobell, S.  
Bacteria in Terrestrial Deep Subsurface  
Boris Coordination Meeting  
Karlsruhe, Germany, 17.-18.10.2001
- Selenska-Pobell, S.  
Biologische Synthese von Metallclustern und Proteinen und deren technische Nutzung  
Nanoverbund Projekttreffen, TU Dresden  
Dresden, Germany, 22.10.2001
- Stumpf, Th., Bauer, A., Coppin, F., Kim, J.I.  
Time-Resolved Laser Fluorescence Spectroscopy (TRLFS) Study of the Sorption of Cm(III) onto Smectite and Kaolinite  
Migration 2001  
Bregenz, Austria, 16.-21.09.2001
- Stumpf, Th., Fanghänel, Th.  
Strukturaufklärung im Submikromolbereich: TRLFS-Untersuchungen zur Cm(III) Sorption an und zum Einbau in Calcit  
GDCh-Jahrestagung Chemie 2001, FG Nuklearchemie  
Würzburg, Germany, 23.-26.09.2001
- Stumpf, Th., Fanghänel, Th., Roßberg, A., Kim, J.I.  
Complexation of Cm(III) and Eu(III) by glycolic acid: TRLFS studies  
Actinides 2001  
Hayama, Japan, 04.-09.11.2001
- Stumpf, Th., Fanghänel, Th.  
A Time-Resolved Laser Fluorescence Spectroscopy (TRLFS) Study of the Interaction of Trivalent Actinides (Cm(III)) with Calcite  
Japan Atomic Energy Research Institute  
Tokai-mura, Japan, 12.11.2001
- Taut, S., Hübener, S., Eichler, B.  
Metal Adsorption Studies of the Heaviest Actinides  
European Isotope Separation On-Line Radioactive Nuclear Beam Facility; 5th Target and Ion-Source Task Group meeting merged with the 1st TARGISOL project meeting  
CERN, 29.-30.10.2001
- Taut, S., Hübener, S., Eichler, B.  
Untersuchung der Metalladsorption schwerer Aktiniden mittels Thermochromatographie  
Seminar des Labors für Radio- und Umweltchemie der Universität Bern und des Paul Scherrer Instituts  
Bern, Switzerland, 07.12.2001
- Zänker, H., Richter, W.  
Die Sorption des Uran(VI) und anderer radiotoxischer Schwermetalle an Kolloidpartikeln im Flutungswasser des Uranbergwerks Königstein  
Institut für Geowissenschaften, Universität Jena  
Jena, Germany, 19.04.2001
- Zänker, H., Richter, W., Brendler, V., Moll, H., Hüttig, G.  
Inorganic Colloids in Mine Waters  
Annual Meeting of the Geological Society of America  
Boston, USA, 03.-08.11.2001
- Zänker, H., Jenk, U.  
Adsorption of Radiotoxic Heavy Metals by Colloid Particles – Evidence from the Mine Waters of the Königstein Mine  
8<sup>th</sup> Intern. Conf. on Radioactive Waste Management and Environmental Remediation (ICEM '01)  
Bruges, Belgium, 30.09.-04.10.2001

Zänker, H., Richter, W.  
Die Sorption des U(VI) und anderer radiotoxischer Schwermetalle an Kolloidpartikeln im Flutungswasser eines stillgelegten Uranbergwerks  
7. Kolloquium DFG-Schwerpunktprogramm 546 „Geochemische Prozesse mit Langzeitfolgen im anthropogen beeinflussten Sickerwasser und Grundwasser“  
Berlin, Germany, 14.-15.09.2001

Zänker, H., Richter, W., Schreyer, J., Jenk, U.  
Die Anlagerung von radiotoxischen Schwermetallen an Kolloidpartikel im Flutungswasser einer stillgelegten Urangrube  
GDCh-Jahrestagung Chemie 2001, FG Nuklearchemie  
Würzburg, Germany, 23.-26.09.2001

Zänker, H., Richter, W., Moll, H., Brendler, V., Hüttig, G.  
Anorganische Kolloide in Bergwerkswässern  
2<sup>nd</sup> Coordination Meeting PSI/LES-FZR/IR  
Villigen, Switzerland, 22.-23.10.2001

## POSTERS

Arnold, T., Krawczyk-Bärsch, E., Brendler, V., Bernhard, G.,  
Sorption of U(VI) on Granite: Comparison of Experimental and Predicted U(VI) Sorption Data  
Migration 2001  
Bregenz, Austria, 16.-21.09.2001

Bauer, A., Coppin, F., Stumpf, Th., Berger, G., Castet, S., Loubet, M.  
Adsorption of Lanthanides on Smectite and Kaolinite  
Migration 2001  
Bregenz, Austria, 16.-21.09.2001

Funke, H., Böttger, H., Reich, T., Hennig, C., Roßberg, A.  
A splice program to connect two different EXAFS spectra of the same sample  
11<sup>th</sup> ESRF Users' Meeting  
Grenoble, France, 19.02.2001

Heise, K.H., Nicolai, R., Fanghänel, Th., Seidel, W., Schamlott, A. Ortega, J.M., Glotin, F., Prazeres, R.  
Infrarot-Spektroskopie am Freie Elektronen Laser  
GDCh-Jahrestagung Chemie 2001, FG Nuklearchemie  
Würzburg, Germany, 23.-26.09.2001

Hennig, C., Reich, T., Funke, H., Roßberg, A., Rutsch, M., Bernhard, G.  
Structure parameter analysis of Cu[UO<sub>2</sub>AsO<sub>4</sub>]<sub>2</sub> nH<sub>2</sub>O using EXAFS spectroscopy  
11<sup>th</sup> ESRF Users' Meeting  
Grenoble, France, 19.02.2001

Hennig, C., Reich, T., Schell, N., Prokert, F., Reck, G., Kraus, W.  
Combination of EXAFS and powder diffraction for solving heavy-atom structures  
Aussois Science Days Seminar – Experiments Division Internal Meeting  
Aussois, France, 09.-11.05.2001

Hofmann, T., Baumann, T., Bundschuh, T., v. d. Kammer, F., Leis, A., Schmitt, D., Schäfer, T., Totsche, K.-U.,  
Zänker, H.  
Die Bedeutung von Kolloiden in der aquatischen Umwelt  
Jahrestagung der Wasserchemischen Gesellschaft in der GDCh  
Bad Wildungen, Germany, 21.-23.05.2001

Krawczyk-Bärsch, E., Arnold, T., Hüttig, G., Zänker, H., Brandt, F., Bosbach, D., Bernhard, G.  
Formation of Iron Oxyhydroxide Particles during the Dissolution of Chlorite - Effect on Uranium Sorption  
79. Tagung der Mineralogischen Gesellschaft  
Potsdam, Germany, 09.-13.09.2001

Merroun, M., Hennig, C., Reich, T., Geipel, G., Bernhard, G., Selenska-Pobell, S.  
EXAFS Investigation of Uranium(VI) Complexes Formed at *Acidithiobacillus ferrooxidans* Types

11<sup>th</sup> ESRF Users' Meeting, ESRF/ILL Joint Workshop on the Environmental using Neutron and Synchrotron Facilities  
Grenoble, France, 16.-21.02.2001

Merroun, M.  
Spectroscopic Characterization of Uranium(VI) Complexes Formed on *Acidithiobacillus ferrooxidans* Cells  
VAAM-2001 Tagung  
Oldenburg, Germany, 25.-28.03.2001

Merroun, M., Geipel, G., Nicolai, R., Heise, K.H., Hennig, C., Reich, T., Bernhard, G., Selenska-Pobell, S.  
Spectroscopic properties of uranium (VI) complexes formed at the cells of *acidithiobacillus ferrooxidans*  
Migration 2001  
Bregenz, Austria, 16.-21.09.2001

Moll, H., Zänker, H., Richter, W., Brendler, V., Reich, T., Hennig, C., Rossberg, A., Funke, H., Kluge, A.  
Acid Rock Drainage Samples from an abandoned Zn-Pb-Ag Mine investigated by XAS  
11<sup>th</sup> ESRF Users' Meeting, ESRF/ILL Joint Workshop on the Environmental using Neutron and Synchrotron Facilities  
Grenoble, France, 16.-21.02.2001

Nebelung, C.  
"Rückbau von Nuklearanlagen - Minimierung des Sondermülls. Schnelle Bestimmung von Alpha-Strahlern".  
Hannovermesse  
Hannover, 23.04. - 28.04.2001

Nebelung, C., Henniger, J.  
Schnelles Freimeßverfahren auf alpha-aktive Nuklide  
GDCh-Jahrestagung Chemie 2001, FG Nuklearchemie  
Würzburg, Germany, 23.-26.09.2001

Raff, J.  
A Novel Surface Layer Protein of the Uranium Waste Pile Isolate *Bacillus sphaericus* JG-A 12 and its Interaction with Metals  
VAAM-2001 Tagung  
Oldenburg, Germany, 25.-28.03.2001

Reich, T., Geipel, G., Funke, H., Hennig, C., Roßberg, A., Bernhard, G.  
EXAFS-Strukturuntersuchung an Neptunium- und Plutoniumhydraten  
GDCh-Jahrestagung Chemie 2001, FG Nuklearchemie  
Würzburg, Germany, 23.-26.09.2001

Richter, W., Zänker, H., Hüttig, G.  
Kolloidchemische Untersuchungen unter anoxischen Bedingungen  
7. Kolloquium des DFG-Schwerpunktprogramms 546 „Geochemische Prozesse mit Langzeitfolgen im anthropogen beeinflussten Sickerwasser und Grundwasser“  
Berlin, 14.-15.09.2001

Roßberg, A., Reich, T.  
The validation of iterative transformation factor analysis algorithm to resolve multicomponent EXAFS spectra of uranium(VI) complexes with acetic acid as a function of pH  
11<sup>th</sup> ESRF Users' Meeting  
Grenoble, France, 19.02.2001

Roßberg, A., Reich, T., Baraniak, L., Rutsch, M., Bernhard, G.  
The first application of the iterative transformation factor analysis to extract pure component spectra and composition profiles from EXAFS-spectra of mixtures  
Migration 2001  
Bregenz, Austria, 16.-21.09.2001

Sachs, S., Schmeide, K., Geipel, G., Reich, T., Heise, K.H., Bernhard, G.  
Interaction of neptunium(V) with humic acids of different functionalities  
Migration 2001  
Bregenz, Austria, 16.-21.09.2001

- Sachs, S., Bubner, M., Schmeide, K., Heise, K.H., Bernhard, G.  
Synthetische Huminsäuren und ihre Anwendung zur Untersuchung des Radionuklidtransports in der Umwelt  
GDCh-Jahrestagung Chemie 2001, FG Nuklearchemie  
Würzburg, Germany, 23.-26.09.2001
- Schmeide, K., Sachs, S., Reich, T., Hennig, C., Heise, K.H., Bernhard, G.  
Neptunium(V) sorption onto granite and its mineral constituents in the absence and presence of humic acid  
Migration 2001  
Bregenz, Austria, 16.-21.09.2001
- Selenska-Pobell, S.  
Molecular Bacterial Diversity in Water and Soil Samples of Uranium Waste Piles  
VAAM-2001 Tagung  
Oldenburg, Germany, 25.-28.03.2001
- Selenska-Pobell, S.  
Distribution Ecology of Bacteria in Water and Soil Samples of Uranium Mining Waste Piles  
ISME-9  
Amsterdam, Netherlands, 26.-31.08.2001
- Selenska-Pobell, S.  
Diversity and Activity of Bacteria in Uranium Waste Piles  
ISME-9  
Amsterdam, Netherlands, 26.-31.08.2001
- Selenska-Pobell, S.  
Bacterial Diversity in Drain Waters of Uranium Mining Waste Piles  
ISME-9  
Amsterdam, Netherlands, 26.-31.08.2001
- Selenska-Pobell, S.  
Construction of Biological Ceramics with Specific Metal Binding Capacity  
ISME-9  
Amsterdam, Netherlands, 26.-31.08.2001
- Stumpf, S., Stumpf, Th., Fanghänel, Th., Dardenne, K., Klenze, R., Kim, J.I.  
Time-Resolved Laser Fluorescence Spectroscopy (TRLFS): Investigations of the Interaction of Cm(III) with  
Ferrihydrite  
GDCh-Jahrestagung Chemie 2001, FG Nuklearchemie  
Würzburg, Germany, 23.-26.09.2001
- Taut, St., Hübener, S., Eichler, B.  
Halbempirische Berechnung von Metalladsorptionsentropien und –enthalpien, Adsorption von Einsteinium auf  
Titanium, Niob und Tantal  
GDCh-Jahrestagung Chemie 2001, FG Nuklearchemie  
Würzburg, Germany, 23.-26.09.2001
- Vahle, A., Hübener, S., Taut, St., Jäger, E., Schädel, M., Schausten, B., Eichler, B.  
Metalladsorption mit Homologen superschwerer Elemente  
GDCh-Jahrestagung Chemie 2001, FG Nuklearchemie  
Würzburg, Germany, 23.-26.09.2001
- Vulpius, D., Baraniak, L., Geipel, G., Bernhard, G., Fanghänel, Th.  
Komplexierung von Uran(VI) mit Benzoesäure  
GDCh-Jahrestagung Chemie 2001, FG Nuklearchemie  
Würzburg, Germany, 23.-26.09.2001
- Yakushev, A.B., Buklanov, G.V., Chelnokov, M.L., Chepigin, V.I., Dimitriev, S.N., Gorshkov, V.A., Hübener, S.,  
Lebedev, V.Ya., Malyshev, O.N., Oganessian, Yu.Ts., Popeko, A.G., Sokol, E.A., Timokhin, S.N., Türler, A.,  
Vasko, V.M., Yeregin, A.V., Zvara, I.  
First Attempt to Chemically Identify Element 112  
Actinides 2001  
Hayama, Japan, 04.-09.11.2001

### **III. SEMINARS, CONFERENCES AND WORKSHOPS**

## INSTITUTE SEMINARS

C. Bitea  
Forschungszentrum Karlsruhe, Institut für Nukleare Entsorgung  
Zeitaufgelöste Beobachtung der Agglomeration von  $ZrO_2$ -Partikeln  
07.03.2001

Dr. T. Mayerhöfer  
Friedrich-Schiller-Universität Jena, Institut für Physikalische Chemie  
Optische Eigenschaften – Vom Einkristall zum zufällig orientierten, polykristallinen Material  
08.03.2001

Dr. H. Foerstendorf  
Universität Freiburg i.Br., Sektion Biophysik, Institut für Molekulare Medizin und Zellforschung  
Erste Einblicke in die Struktur-Funktionsbeziehungen des Photorezeptors Phytochrom mit Hilfe der lichtinduzierten FTIR-Differenzspektroskopie  
09.03.2001

Dr. C. Kneip  
Procter & Gamble, Frankfurt (Main)  
Sehen mit dem Auge der Pflanze - Resonanz-Raman-Spektroskopische Studien des pflanzlichen Photorezeptors Phytochrom  
12.03.2001

Dr. E. Geidel  
Universität Hamburg, Institut für Physikalische Chemie  
Schwingungsspektroskopische Untersuchungen an Adsorptionskomplexen  
12.03.2001

Dr. W. Hauser  
Forschungszentrum Karlsruhe, Institut für Nukleare Entsorgung  
Online-Quantifizierung von Kolloiden im Felslabor Grimsel mit der Laser-induzierten Breakdown-Detektion  
20.03.2001

Dr. habil. W. Dedek  
ehem. IAR und Universität Leipzig  
100 Jahre Radium-Emanation (Radon)  
02.04.2001

Dr. S. Tsushima  
University of Tokyo, Department of Quantum Engineering and System Science, Japan  
Prediction of the uranium hydroxide solubility from quantum chemical calculations  
02.05.2001; CRG-ROBL, Grenoble, France,

Prof. Dr. G. Büchel  
Friedrich-Schiller-Universität Jena, Institut für Geowissenschaften  
Die prä-Flutungssituation in der ostthüringischen Uranbergbauregion  
08.05.2001

Dr. V. Neck  
Forschungszentrum Karlsruhe, Institut für Nukleare Entsorgung  
Aquatische Chemie tetravalenter Actiniden - Datenbasis und experimentelle Arbeiten am Forschungszentrum Karlsruhe INE  
09.05.2001

Dr. D. Bosbach  
Forschungszentrum Karlsruhe, Institut für Nukleare Entsorgung  
Kristallwachstum und die Reaktivität von Mineraloberflächen  
21.05.2001

Prof. J.D. Navratil, Ph.D.  
Environmental Engineering and Science, Clemson University, Anderson, South Carolina, USA  
Actinide environmental research at Clemson University  
31.05.2001

Dr. T. Pribyl  
Institut für Angewandte Biotechnologie, Leipzig  
Topologie des CzcCBA-Efflux-Komplexes aus *Ralstonia metallidurans* CH34  
19.06.2001

Prof. Dr. J. Bruno  
Quanti Sci, Barcelona, Spain  
Redox Equilibrium and Disequilibrium in Natural Waters  
26.06.2001

PD Dr. M. Floersheimer  
Universität Münster, Physikalisches Institut  
Nichtlineare optische Methoden zur Charakterisierung von Mineral/Elektrolyt-Grenzflächen  
06.07.2001

Dr. J. Tits  
Paul Scherrer Institut Villingen, Schweiz  
Immobilisation of Radionuclides by Cement Phases in the Near-Field of a Low and Intermediate Level Nuclear Waste Repository  
15.10.2001

Prof. Dr. B. Grambow  
SUBATECH, Nantes, France  
Chemie der Mobilisierung und Immobilisierung von langlebigen Radionukliden in geologischen Formationen  
14.11.01

Prof. Dr. R. Köster  
Forschungszentrum Karlsruhe/ITC-WGT und Uni Regensburg  
Zur Immobilisierung von Schwermetallen in Altlasten  
03.12.2001

Prof. Dr. Sh. Nagasaki  
The University of Tokyo, Institute of Environmental Studies, Graduate School of Frontier Sciences  
Fluorescence Spectroscopy of U-HA and Breakdown Spectroscopy for Aerosol and Colloids  
04.12.2001

Dr. K. Gompper  
Forschungszentrum Karlsruhe, Institut für Nukleare Entsorgung  
Partitioning und Transmutation – Ein neuer Weg zur Nuklearen Entsorgung  
05.12.2001

Prof. Dr. M. Sauter  
Universität Jena  
Ansätze zur Modellierung des kurzfristigen und langfristigen Austrags von Uran aus untertägigen gefluteten Grubengebäuden  
12.12.2001

### **INTERNAL SEMINARS** (open for the public)

Dr. C. Hennig  
Bestimmung von Schweratom-Kristallstrukturen mit EXAFS und XRD am Beispiel von Uranylarsenaten  
16.01.2001

Dipl.-Biol. J. Raff  
Das Hüllprotein des *Bacillus sphaericus* Haldenisolats JG-A12 und seine Wechselwirkungen mit Metallen  
24.01.2001

Dr. G. Geipel  
Laserspektroskopie mit ultrakurzen Pulsen – Systemänderungen und neue Ergebnisse  
26.03.2001

Dr. A. Koban  
Komplexierung des Urans mit phosphathaltigen, organischen Liganden  
19.04.2001

Dipl.-Ing. (FH) D. Vulpus  
Bestimmung von Komplexbildungskonstanten von organischen Uran(VI)-Komplexen durch Potentiometrie und Fluoreszenzspektroskopie  
19.04.2001

Dr. A. Merroun  
Spectroscopic characterization of uranium complexes formed at the cell surfaces of *Acidithiobacillus ferrooxidans* types  
10.05.2001

Dr. H. Moll  
Komplexierung des Urans(VI) mit alpha-substituierten Carbonsäuren  
10.05.2001

Dr. K. Schmeide  
Bestimmung von Strukturparametern von Actinid-Humat-Komplexen mittels XAFS-Spektroskopie  
17.05.2001

Dr. A. Günther  
Arbeiten zur Identifizierung und Charakterisierung von Komplexbildungsprodukten des U(VI) in Pflanzen  
17.05.2001

Dipl.-Min. M. Walter  
EXAFS-Spektroskopie von Uranylkomplexen an Mineraloberflächen  
21.06.2001

Dr. S. Sachs  
Synthese <sup>14</sup>C-markierter und modifizierter Huminsäuren und Untersuchungen zur Np(V)-Komplexierung modifizierter Huminsäuren  
21.06.2001

Dr. T. Arnold  
Sorption von U(VI) an Muskovit (Zusammenhang der Modellierung von Oberflächenkomplexen und spektroskopischen und mikroskopischen Ergebnissen)  
28.06.2001

Dipl.-Biol. J. Raff  
Charakterisierung des Hüllproteins des Haldenisolats *Bacillus sphaericus* JG-A12 unter besonderer Berücksichtigung der Wechselwirkungen mit Metallen  
28.06.2001

Dipl.-Chem. A. Roßberg, Dipl.-Math. E. Müller  
Anwenderseminar Faktorenanalyse: Softwarecodes zur Analyse von spektroskopischen Daten mehrkomponentiger Systeme  
20. 12. 2001

## **CONFERENCES / WORKSHOPS** (organized by Institute of Radiochemistry)

*Workshop: Speziesanalytik in Umweltproben*  
Rossendorf, Germany, 01.03.2001

Forschungszentrum Rossendorf, Institut für Radiochemie (FZR),  
Friedrich-Schiller-Universität Jena, Institut für Ernährungswissenschaften (FSU/E),  
Friedrich-Schiller-Universität Jena, Institut für Geowissenschaften (FSU/G),  
Thüringer Landesanstalt für Landwirtschaft (TLL)

Bernhard, G. (FZR)  
Vorstellung des Instituts und seiner Forschungsschwerpunkte

Krawczyk-Bärsch, E. (FZR)  
Uran-Sorption an Gesteinen und Mineralen

Günther, A. (FZR)  
Uran-Speziation in Pflanzen

Geipel, G. (FZR)

Speziesanalytik mittels Laser-induzierter Spektroskopie

Bergmann, H. (FSU/E)

Schwermetalle/Radionuklide und ihre Pflanzenverfügbarkeit

Leiterer, M. (TLL)

Anorganische Spurenanalytik in landwirtschaftlichen und biologischen Proben

Merten, D. (FSU/G)

Wismut-spezifische Anwendung der ICP-MS bezüglich Stoffpfadkartierung mittels Mustererkennung von Seltenen Erden

Schönbuchner, H. (FSU/G)

Spezielle Ergebnisse von Testfeldern auf Wismuthalden

Büchel, G. (FSU/G)

Projekt "Gessenbach"

*Workshop Forschungsvorhaben "Abtrennung von Uranylionen aus Sicker- und Grundwässern mit uranophilen Calixarenen – Integrierter Umweltschutz in der Textilindustrie"*

Rosendorf, Germany, 21.08.2001

Forschungszentrum Rosendorf, Institut für Radiochemie (FZR)

Deutsches Textilforschungszentrum Nord-West, Krefeld (DTNW)

SynTec Gesellschaft für Chemie und Technologie der Informationsaufzeichnung mbH, Wolfen (SynTec)

Thomas Josef Heimbach GmbH & Co., Düren

Schmeide, K. (FZR)

Abtrennung von Uran aus wässriger Lösung durch Calixarene

Jansen, K. (DTNW)

Textile Anbindung von Calixarenen auf Polyestervliesen

Keil, D. (SynTec)

4-tert-Butyl-calix[6]arene und Derivate: Synthese und Charakterisierung.

*ACTAF Meeting*

Rosendorf, Germany, 01.-02.10.2001

Geipel, G., Bernhard, G., Fanghänel, Th.

Studies of Interactions of Actinides with Organic Ligands using Femtosecond-Laser-Induced Spectroscopy

## **IV. PERSONNEL**

## PERSONNEL

### Director

Prof. Dr. Th. Fanghänel

### Administrative Staff

G. Kreusel

H. Pospischil

### Scientific Staff

Dr. T. Arnold\*  
Dr. L. Baraniak\*  
Prof. Dr. G. Bernhard  
DC D. Birnstein  
Dr. V. Brendler  
Dr. H.-J. Engelmann  
Dr. H. Foerstendorf  
Dr. H. Funke  
Dr. G. Geipel  
Dr. A. Günther\*  
Dr. K.H. Heise

Dr. C. Hennig\*  
Dr. S. Hübener  
Dr. A. Koban\*  
Dr. E. Krawczyk-Bärsch\*  
Dr. K. Krogner  
Dr. P. Merker  
Dr. M. Merroun\*  
Dr. J. Mibus\*  
Dr. H. Moll\*  
DC C. Nebelung

Dr. T. Reich  
Dr. D. Rettig\*  
Dr. W. Richter  
Dr. S. Sachs\*  
Dr. S. Selenska-Pobell  
Dr. K. Schmeide\*  
Dr. T. Stumpf\*  
Dr. S. Taut\*  
Dr. A. Vahle\*  
Dr. H. Zänker

### Technical Staff

DI(FH) B. Barz\*  
DI(FH) C. Eckardt  
DBC K. Flemming  
J. Falkenberg  
DI(FH) H. Friedrich  
Ch. Fröhlich  
DI(FH) G. Grambole  
S. Heller\*

DI(FH) K. Henkel  
B. Heschel  
H. Heyne  
B. Hiller  
DI(FH) G. Hüttig  
DI(FH) R. Jander  
P. Kluge  
M. Leckelt\*

DI(FH) M. Meyer  
Ch. Müller  
H. Neubert  
DI(FH) K. Nicolai\*  
DI(FH) R. Nicolai\*  
A. Rumpel  
R. Ruske  
DI(FH) U. Schaefer

### Graduate Students

DC S. Amayri  
DB J. Raff

DC A. Roßberg  
DI(FH) D. Vulpius

DM M. Walter

### Trainee

Bergmann, J.  
Birk, T.  
Brockmann, S.  
Buste, M.  
Dombrowski, C.  
Effenberg, K.

Geisler, A.  
Großmann, K.  
Schröter, D.  
Schubert, R.  
Schubert, S.

Smuda, Ch.  
Stange, A.  
Thiele, M.  
Tokpa, G.  
Westphal, D.

\* post doc

\* term contract

DC: Dipl.-Chem.

DI: Dipl.-Ing.

DBC: Dipl.-Biochem.

DB: Dipl.-Biol.

DM: Dipl.-Min.

## Guest Scientists

Prof. Dr. A. Alian	Atomic Energy Authority, Cairo, Egypt
Prof. Dr. Yu.A. Babanov	Institute of Metal Physics, Russian Academy of Sciences, Ekaterinburg, Russia
Dr. D. Bosbach	Institut für Nukleare Entsorgung, Forschungszentrum Karlsruhe, Germany
Dr. J. Lützenkirchen	Institut für Nukleare Entsorgung, Forschungszentrum Karlsruhe, Germany
Dr. V. Marti	Laboratori de Gestió de Residus, Centre Tecnològic de Mansera, Barcelona, Spain
Prof. Dr. S. Nagasaki	Institute of Environmental Studies, Graduate School of Frontier Sciences, The University of Tokyo, Japan
Dr. G. Radeva	Institute of Molecular Biology, Bulgarian Academy of Sciences, Sofia, Bulgaria
Dipl.-Biol. G. Satchanska	Institute of Molecular Biology, Bulgarian Academy of Sciences, Sofia, Bulgaria
Dipl.-Chem. S. Stumpf	Institut für Nukleare Entsorgung, Forschungszentrum Karlsruhe, Germany
Dr. J. Tits	Paul Scherrer Institut Villigen, Switzerland
Dr. S. Tsushima	The University of Tokyo, Department of Quantum Engineering and System Science, Tokyo, Japan
Dr. M. Tshoukalina	Institute of Microelectronics Technology, Russian Academy of Science, Chernogolovka, Russia
Dipl.-Biol. I. Tzvetkova	University of Sofia, Dept. of Microbiology, Sofia, Bulgaria
Dipl.-Biol. Tz. Tzvetkova	University of Sofia, Dept. of Microbiology, Sofia, Bulgaria
Dr. C. Walther	Institut für Nukleare Entsorgung, Forschungszentrum Karlsruhe, Germany
Dipl.-Phys. T.Ye. Zayarnaya	Institute of Metal Physics, Russian Academy of Sciences, Ekaterinburg, Russia

## **V. ACKNOWLEDGMENTS**

## ACKNOWLEDGMENT OF FINANCIAL SUPPORT

The Institute is part of the Forschungszentrum Rossendorf e.V., which is financed in equal parts by the Federal Republic of Germany and the Free State of Saxony.

Eight projects were supported by the Bundesministerium für Bildung und Forschung (BMBF) and by the Bundesministerium für Wirtschaft (BMW):

- Entwicklung einer mineralspezifischen Sorptionsdatenbank für Oberflächenkomplexierungsmodelle  
Contract No.: BMWi 02 E 9471
- Wechselwirkung von Actiniden mit dominanten Bakterien des Äspö-Grundwasserleiters  
Contract No.: BMBF 02 E 9491
- Diversity of Bacteria in Bulgarian and German Uranium Waste Piles – a Comparative Analysis  
Contract No.: DRL-IB/BGR 99/011
- Biocere auf Basis bakterieller Membranproteine für Schwermetall bindende Filter zur Behandlung von industriellen Abwässern und kontaminiertem Grundwasser  
Contract No.: InnoRegio 03I4004B
- Stilllegung und Rückbau: Schnelles Freimeßverfahren für  $\alpha$ -aktive Nuklide in Bauschutt durch Direktmessung von großflächigen dünnen Meßpräparaten - Automatisierung des Verfahrens -  
Contract No.: BMBF 02 S 7768/6
- Entwicklung eines Verfahrens zur Restsalzmessung mittels Laseranregung  
- Optische Funktionseinheit und Messverfahren -  
Projektförderung durch BMWi - AIF  
Contract No.: KF 0249402K WZ1
- Integrierter Umweltschutz in der Textilindustrie: Abtrennung von Uranylionen aus Sicker- und Grundwässern mit uranophilen Calixarenen (Verbundprojekt)  
Contract No.: BMBF 0339917/3
- Untersuchungen über die Komplexierung und die Migration von Actiniden und nichtradioaktiven Stoffen mit Huminsäuren unter geogenen Bedingungen - Komplexierung von Huminsäuren mit Actiniden in der Oxidationsstufe IV Th, U, Np (Verbundprojekt)  
Projektförderung durch BMWi  
Contract No.: 02E9299

The Commission of the European Communities supported five projects:

- Building confidence in deep disposal: the BOREhole Injection Sites at Krasnoyarsk-26 and Tomsk-7 (BORIS)  
In collaboration with:  
Galson Sciences Limited, United Kingdom; United Kingdom Nirex Limited, Nirex Safety Assessment Research Program, United Kingdom; FZ Karlsruhe, Institut für Nukleare Entsorgungstechnik, Germany; Studiecetrum voor Kernenergie / Centre d'Étude de L'Énergie Nucléaire, Waste & Disposal Department / SCK-CEN, Belgium; Institut de Protection et de Sûreté Nucléaire, France; All-Russian Designing and Research Institute of Production Engineering, VNIPIPT, Laboratory for Liquid industrial waste underground disposal, Russia; The Environment Agency, EA, National Centre for Risk Analysis and Options Appraisal, United Kingdom; AEA Technology plc, United Kingdom; Universitat Politècnica de Catalunya, Spain  
Contract No.: FIKW-CT 2000-00105
- ACTAF - Aquatic Chemistry and Thermodynamics of Actinides and Fission Products Relevant to Nuclear Waste Disposal  
In collaboration with:  
FZ Karlsruhe, Germany; Paul Scherrer Institut Villigen, Switzerland; Kungl. Tekniska Högskolan Stockholm, Sweden; Universitat Politècnica Catalunya Barcelona, Spain; Københavns Universitet Copenhagen, Denmark; Enterpris Ltd. Reading, United Kingdom; CIEMAT Madrid, Spain  
Contract No.: FILW-CT-2000-00035
- Humic Substances in Performance Assessment of Nuclear Waste Disposal: Actinide and Iodine Migration in the Far-Field [HUPA]  
In collaboration with:  
FZ Karlsruhe, Institut für Nukleare Entsorgung, Germany; GSF-FZ für Umwelt und Gesundheit, Institut für Hydrologie, Germany; Commissariat à l'Énergie Atomique, Department of Physico-Chemistry, Saclay, France; Université de Nantes, Laboratory of Biochemistry and Radiochemistry, Nantes, France; University of

Manchester, Department of Chemistry, Great Britain; Technical University of Prague, Czech Republic; Fodor Jozsef National Center of Public Health, Frederic Joliot-Curie National Research Institute for Radiobiology and Radiohygiene, Hungary  
Contract No.: FIKW-CT-2001-00128

- Structure, Bonding and Thermodynamics in Binary and Ternary Dioxouranium Complexes  
Marie Curie Individual Fellowship within the Fifth Framework Program of the European Union  
Contract No.: HPMF-CT-1999-00342
- Infrared Microspectroscopy on Environmental Samples  
Support for experimental studies at LURE, Orsay, France  
Project No.: LURE IC 008-01

The Sächsisches Staatsministerium für Wissenschaft und Kunst provided support for the following projects:

- Charakterisierung und Klassifizierung von Bakterien aus uranhaltigen Halden mit Hinblick auf Bioremediation: Bakterielle Diversität, Populationsdynamik und Bioakkumulation von Uran und ausgewählten Radionukliden durch Bakterien  
Contract No.: SMWK 4-7531.50-03-FZR/607
- Biologische Synthese von Metallclutern an Proteinen und deren technischer Nutzung  
Contract No.: SMWK 4-7531.50-03-370-01/
- Konstruktion und Analyse einer Archaeal-Klonbibliothek für die Gittersee/Coschütz Mill Tailings Mittel- und Osteuropa Gastprogramm  
Contract No.: SMWK 4-7531-04-844/01/10
- Konstruktion und Analyse einer Bakterien-Klonbibliothek für die Gittersee/Coschütz Mill Tailings Mittel- und Osteuropa Gastprogramm  
Contract No.: SMWK 4-7531-04-844/01/11
- Chemische Konvertierung der Altbestände Kohlenstoff-14-markierter Verbindungen zu [<sup>14</sup>C]- Bariumcarbonat. Förderung im Rahmen des Vorhabens ‚Nukleare Entsorgung des Forschungsstandorts Rossendorf‘ Altlastenfonds 2001 des SMWK

Six projects were supported by Deutsche Forschungsgemeinschaft (DFG):

- Identifizierung und Charakterisierung von Komplexbildungsprodukten des U(VI) in Pflanzen.  
Contract No.: DFG BE 2234/1-1; DFG BE 2234/1-2
- Komplexbildung von Uranyl- und Neptunylionen mit phenolischen Monomeren des natürlichen Ligninabbaus als Grundlage für die Beschreibung der Radionuklidverbreitung  
Contract No.: DFG BE 2234/3-1
- Biocere mit spezifischer Metallbindungsaktivität  
Contract No.: DFG SE 671/7-1
- Heterogene Reaktionsmechanismen und deren Kinetik an Schichtsilikatoberflächen  
Contract No.: DFG BE 2234/4-2
- Charakterisierung der Kolloidpartikel in den Wasserfließsystemen stillgelegter sächsischer Bergwerke  
Contract No.: DFG ZA 238/1-4
- Untersuchung der Sorptionsmechanismen von Uran(VI) auf Gesteins- und Mineraloberflächen mit spektroskopischen und mikroskopischen Verfahren.  
Contract No.: DFG NI 210/6-1; DFG NI 210/6-2

One project was supported by the BfS:

- Sorptionsexperimente im Deckgebirge des Endlagers für radioaktive Abfälle Morsleben (ERAM)  
BfS-Projekt No.: 9M 212230-62